EVALUATION AND ANALYSIS OF SEASAT-A SCANNING MULTICHANNEL MICROWAVE RADIOMETER (SMMR) ANTENNA PATTERN CORRECTION (APC) ALGORITHM

FINAL REPORT FOR SUB-TASK 4: INTERIM MODE T_B VS. CROSS AND NOMINAL MODE T_B

Prepared under JPL contract number 955368 by:

J. L. Kitzis
S. N. Kitzis

Environmental Sensing Algorithm Development Company

8238 Fenwick Street
Sunland, California 91040

July 27, 1979

This work was performed for the Jet Propulsion Laboratory, California Institute of Technology sponsored by the National Aeronautics and Space Administration under Contract NAS7-100.

ABSTRACT

This report presents a "snapshot" of the work completed to date towards evaluating the brightness temperature data produced by the SMMR Antenna Pattern Correction (APC) algorithm. As the algorithm evolves, further evaluation will be performed. The current evaluation consists of 1) a direct comparison of the outputs of the interim, cross, and nominal APC modes, 2) a refinement of the previously determined cos β estimates, and 3) a comparison of the world brightness temperature (T_B) map with actual SMMR measurements. The results obtained from these investigations are the subject of this report.

CONTENTS

CONTENTS (CONTINUED)

CONTENTS (CONTINUED)

FIGURE

CONTENTS (CONTINUED)

FIGURE

CONTENTS (CONTINUED)

FIGURE

CONTENTS (CONTINUED)

FIGURE

1.0 SUMMARY

This report presents a "snapshot" of the work completed to date towards evaluating the brightness temperature data produced by the SMMR Antenna Pattern Correction (APC) algorithm. As the algorithm evolves, further evaluation will be performed. The current evaluation consists of 1) a direct comparison of the outputs of the interim, cross, and nominal APC modes, 2) a refinement of the previously determined cos β estimates, and 3) a comparison of the world brightness temperature (T_B) map with actual SMMR measurements.

The more important conclusions of the study are:

(1) It appears that the sidelobe corrections applied by both the cross and nominal APC modes are introducing significant cross-track gradients into the 6.6, 10.7, and 18 GHz T_B data. The 21 and 37 GHz channels do not show these effects.

(2) The nominal mode T_B data exhibits sidelobe over- and under-compensation effects when the SMMR swath crosses or is adjacent to land. In contrast, the cross mode data does not exhibit these effects.

(3) The cos β corrections appear to be correctly implemented in the APC software. In addition, the current cos β values account for the major cross-track gradient discrepancies previously observed in interim mode output.

(4) The world T_B map appears to be in fairly good agreement with SMMR clear weather T_B measurements. It appears that the map will be significantly in error only when heavy clouds and/or rain are present.

2.0 INTRODUCTION

This report summarizes the most recent work completed in the ongoing evaluation of the final APC algorithm. The current work is a continuation of that previously described in reference 1. Much of this work is primarily concerned with the evaluation of the sidelobe corrections performed by the final APC. This evaluation is most effectively carried out by producing two sets of brightness temperatures from a single set of spacecraft data. The first set of T_B values is corrected for sidelobe contributions, whereas the second set is not. Comparisons of these two data sets should reveal differences due solely to the sidelobe correction software.

This simple picture is complicated by the fact that several sidelobe correction procedures are currently being considered. Two of these

procedures are evaluated in the context of this report. Thus, three modes of the final APC are compared with each other:

(1) Interim mode - In this mode of the final APC, no sidelobe corrections are applied for radiation from the earth's surface. In all other respects, the interim mode is equivalent to those modes involving sidelobe corrections.

(2) Nominal mode - In this mode of the final APC, sidelobe corrections are applied using the actual antenna pattern coefficients. For a given cell, these corrections are made for all cells outside the cell being corrected.

(3) Cross mode - This mode is identical to the nominal mode except that sidelobe corrections are not applied for the four cells immediately adjacent to the cell being corrected. The gains for these four cells are added to that of the center cell and then are artificially set equal to zero. Although this method reduces the effective spatial resolution of the final APC, it also reduces the T_B noise resulting from the amplification of small errors in the nearest cells.

In contrast to the final APC evaluated in reference 1, the sidelobe corrections applied in the nominal and cross modes use the actual antenna pattern coefficients rather than Gaussian approximations. In addition, the data for all three modes has been corrected for the cos β effects previously discussed in reference 1 (see section 3.2 for further discussion). However, as in reference 1, the final APC evaluated here does not contain corrections for Faraday rotation or non-nominal spacecraft attitude. These corrections as well as additional sidelobe correction procedures will be evaluated in the near future.

The current evaluation consists of several parallel efforts:

(1) The brightness temperature outputs of the interim, cross, and nominal modes are compared to evaluate the effects of the different sidelobe correction procedures.

(2) The previously determined estimates of cos β (see reference 1) are further refined.

(3) Brightness temperature values predicted by the world T_B map used within the final APC are compared with actual SMMR measurements.

The results obtained from these investigations will be discussed in the following sections of this report. Many of the techniques used in the present evaluation were initially developed during our previous work. The software tools thus inherited will not be described here as they are already documented in previous study reports.

3.0 TECHNICAL DISCUSSION

3.1 Comparison of Interim, Cross, and Nominal Modes. The comparisons presented here are a continuation of the work previously discussed in section 3.1 of reference 1. Several software analysis tools have been used to facilitate these comparisons.

One of these tools produces plots of brightness temperatures versus latitude for two modes of the APC. Typically, these plots display interim mode data along with either nominal or cross mode data. Examples of these plots are shown in figures 1.1 through 1.10. For all plots presented here, the symbol "I" represents interim mode data, while "F" represents either cross or nominal mode data, as indicated in the plot title.

A second analysis tool produces plots of T_B cross-track gradients versus latitude. These gradients are calculated by fitting a straight line to each row of T_B data cells. The gradients are plotted in units of degrees Kelvin per grid cell. Examples of these plots are shown in figures 7.1 through 7.5. In each plot, the symbol "V" represents gradients for the vertical polarization and "H" represents gradients for the horizontal polarization for the frequency indicated in the plot title.

The comparisons presented here have been performed for the purpose of evaluating the effects of the different sidelobe correction procedures. The following results are expected from these types of comparisons:

(1) All three modes of the APC should produce generally similar results over open ocean, in terms of both mean T_B levels and any gradients which may exist in the data. However, the nominal mode is expected to exhibit more point-to-point variation than the interim mode, with the cross mode being intermediate between the two.

(2) When crossing a land-sea interface, the sharpest transition is expected for the nominal mode, a somewhat less sharp transition for the cross mode, and the smoothest transition for the interim mode. The cross mode is expected to remove the ringing phenomena observed in the nominal mode and discussed in reference 1.

(3) When paralleling a coastline, the nominal mode should be least sensitive, the cross mode slightly more sensitive, and the interim mode most sensitive to the nearby land.

Section 3.1.1 contains the results of a direct comparison of interim mode data with nominal and cross mode data from the APC. Separate comparisons are made for the open ocean, land-crossing, and land-paralleling cases listed above. Section 3.1.2 contains the results

of a comparison of the cross-track gradients observed for the different modes of the APC. Comparisons are made for both actual SMMR data and simulated SMMR data produced by E. Njoku.

3.1.1 Direct Comparison of APC Modes

3.1.1.1 Open Ocean Case. For the open ocean case, we have analyzed data from two Seasat passes over the Gulf of Alaska, orbits 1178 and 1212. For each pass, we have plotted data from three columns of cells corresponding to the left edge, right edge, and center of the SMMR swath. The plots contain data for all three APC modes. A representative subset of these 120 plots is given in figures 1.1 through 1.10 for the nominal and interim modes and in figures 2.1 through 2.10 for the cross and interim modes.

The full set of plots is summarized in Tables 1 and 2. These tables contain estimated mean differences observed between the interim mode and the two sidelobe-corrected modes for the three positions within the SMMR swath.

Observations regarding this set of data are listed below.

(1) Weather conditions for orbit 1178 are generally worse than those for orbit 1212. This is reflected in the fact that the general T_B level for orbit 1178 is higher than that for orbit 1212.

(2) As expected, the nominal mode data exhibits more point-to-point variation (i.e. noise) than does the interim data. The cross mode noise is similar to that of the interim mode.

(3) In general, the nominal and cross mode data are lower in value than the interim mode data. For a given channel, the difference between the nominal and interim modes is about the same as that between the cross and interim modes. This suggests that the sidelobe corrections applied in both the nominal and cross modes may be too large.

(4) The tabulated differences between the interim mode and either sidelobe-corrected mode are greater for orbit 1212 than for orbit 1178. This means that the sidelobe corrections applied for orbit 1212 are larger than those applied for orbit 1178. The larger sidelobe corrections for orbit 1212 may be related to the lower overall T_B level for this orbit.

(5) For orbit 1212, the tabulated differences between the nominal and interim modes tend to be larger at the edges of the swath than they are in the center. This means that the nominal mode sidelobe corrections applied for these edge cells are larger

than those applied in the center. This suggests that the edge cells may be over-corrected for sidelobe contributions from outside the SMMR swath. The fact that this phenomenon is not observed in the data from orbit 1178 suggests that this effect becomes evident only for relatively low T_B levels (i.e. clear weather conditions).

(6) Since the differences shown in Tables 1 and 2 vary with position across the swath, it appears that the sidelobe corrections are introducing gradients not present in the interim mode values. In some cases, these modifications are in opposite directions for the vertical and horizontal polarizations of a single frequency. For example, in Table 1, the differences between the interim and nominal modes increase across the swath from -1° to 3°K for 10.7 V and decrease from 4° to -1°K for 10.7 H. These gradient modifications will be discussed further in section 3.1.2.

3.1.1.2 Coastline Crossing Case. We have chosen orbit 1178 as an example of the SMMR swath's crossing of a coastline. We have produced expanded scale plots for the left edge, right edge, and center of the SMMR swath for a small portion of this orbit near the point of the crossing (~58°N.). As an example of these plots, figures 3.1 through 3.10 display nominal and interim mode values for the left edge of the swath, while figures 4.1 through 4.10 display cross and interim mode values for the same data.

For orbit 1178, the left edge of the swath leaves the Alaskan mainland near Juneau and then successively crosses a bay, the tip of a peninsula near 58.4°N, a small inlet, and finally Chichagof Island near 57.7°N before reaching the open ocean. These features can be most clearly discerned in figure 4.9. The following observations are made regarding figures 3 and 4:

(1) The cross mode data appears very similar to the interim mode data. It does not exhibit more noise than the interim mode nor does it exhibit better spatial resolution than the interim. The cross mode values are offset from the interim values by a nearly constant amount over ocean and by a different amount over land. In addition the cross mode data does not exhibit any sign of the ringing phenomenon previously discussed in reference 1.

(2) The nominal mode data exhibits more point-to-point variation (i.e. noise) than either of the other two modes. This is particularly true for the higher frequencies. In addition, the nominal mode does exhibit ringing effects at interface crossings, being anomalously low on the ocean side and high on the land side. It does not appear that the nominal mode provides significantly better resolution than the other modes, although it does vary over wider ranges of brightness temperatures due to the ringing effects.

(3) Nominal mode ringing appears to be more severe for the horizontal channels than for the vertical channels. Normally, the ringing effects are evident in only those cells immediately adjacent to the interface. However, the ringing for the 37 GHz channels (figures 3.9 and 3.10) sometimes extends two cells away from the interface. The best example of this is found in figure 3.10, where the nominal mode point at 57.0° is significantly higher than the interim and the point at 57.2° is significantly lower than the interim mode, with the interface occurring with the next point at 57.4°.

(4) Whereas the sidelobe-corrected data consistently appears to be lower than the interim mode data over ocean, this is not always the case over land. For the lower frequency channels, the nominal and cross mode data tends to be higher than the interim mode data when over land. For the higher frequency channels, the situation is confused with some channels being higher and some lower than the interim mode data.

3.1.1.3 Paralleling Coastline Case. We have chosen orbit 1212 as an example of the SMMR swath following a course parallel and extremely close to land. The right hand edge of the swath runs parallel to the California coastline and comes within 50 kilometers of San Francisco. There are two points of closest approach to land, one at 38.5° and the other at 40° north latitude. Figures 5.1 through 5.10 display nominal and interim mode data for the right hand edge of the swath, while figures 6.1 through 6.10 display cross and interim values for the same data.

Several observations are made regarding these plots:

(1) As noted before, the cross mode mimics the interim mode very closely, except that it is consistently lower than the interim by about 5°K.

(2) The effects of the adjacent land on the cross and interim modes can be seen as a rise in T_B values occurring between 38° and 40° north latitude. As discussed previously in reference 1, the horizontal channels show larger sidelobe effects than the vertical channels. In fact, the 18 V and 21 V channels (figures 6.5 and 6.7) show hardly any response to the nearby land.

(3) It does not appear that the cross mode removes sidelobe effects caused by nearby land appreciably better than the interim mode. In fact, the cross mode for 10.7 H (figure 6.4) appears to overcompensate for sidelobe effects at 37.2°N and undercompensate at 38.8°N.

(4) As noted before, the nominal mode exhibits more noise than the other two modes. In addition, the difference between the interim and nominal modes appears to be greater than the difference between the interim and cross modes. This is shown not only in figures 5 and 6, but also in the Table 2 differences listed for the right hand side of the swath. Since this is systematically observed only in the differences for the right hand side of the orbit 1212 swath, this effect is probably due to the nearness of land. The magnitudes of these differences suggest that the nominal mode may be overcompensating somewhat for land which is outside the swath but within the horizon.

(5) The nominal mode appears to alternately overcompensate and undercompensate for land within one cell-width of the swath. This effect is analogous to the ringing effect observed for coastline crossings. The clearest example is shown for the 18 H channel in figure 5.6. In this figure, the nominal values are ordinarily 5 to 10°K below the interim values. However, at 38.8°N and 39.8°N, the difference diminishes to only 3°K, while at 39.3°N, the difference increases to 25°K. Effects of similar magnitude may be seen for the 6.6 H and 10.7 H channels. Note that the cross mode is generally immune to this effect with the possible exception of the 10.7 H channel.

3.1.2 Cross-Track Gradient Comparison

3.1.2.1 Comparison Using Spacecraft Data. As mentioned previously, in the case of open ocean the three modes of the APC should generally exhibit similar gradients in the T_B values. That is, the application of sidelobe corrections should not significantly alter any gradients present in the interim mode data. However, our initial observations of cross-track gradients for the three modes indicate that these gradients are appreciably different in the different modes.

Figures 7, 8, and 9 respectively display plots of cross-track gradients observed in the interim, cross, and nominal mode outputs for orbit 1178. As can be seen from the plots, the gradients for the 6.6, 10.7, and 18 GHz channels change significantly from mode to mode. For example, figure 7.2 shows that only very small gradients are present in the 10.7 interim mode data between 30°N and 40°N. Figure 8.2 shows that the cross mode has introduced large opposing cross-track gradients in the 10.7 V and H channels. Figure 9.2 shows that this effect is further enhanced in the nominal mode. Similar gradient changes can be observed in the plots for the 6.6 and 18 GHz channels.

In order to quantify what we have observed in the cross-track gradient plots, we have produced average gradient values for portions of orbits 1178 and 1212. These average gradients for each mode are contained in the first three columns of Table 3. The last two columns

contain the gradient differences observed between the interim mode and the two sidelobe corrected modes. The gradient differences observed in orbits 1178 and 1212 have been averaged together and displayed in the first two columns of Table 4. The second two columns of this table contain these average differences scaled to represent a total variation across the swath.

As shown in the last two columns of Table 4, the cross and nominal modes both significantly alter the gradients originally present in the interim mode for the 6.6, 10.7, and 18 GHz channels. The gradient differences are generally larger for the nominal mode than for the cross mode. Changes in the gradients for the 21 and 37 GHz channels are not as severe.

3.1.2.2 Comparison Using Simulated Data. E. Njoku has provided us with interim and nominal mode APC output produced from simulated antenna temperature data. The antenna temperatures are simulated by integrating the antenna patterns over a constant brightness temperature scene. The T_B level for each channel is that given by the world brightness temperature map for 30° north latitude. These T_B values may be found in Table 8.2. Since the original T_B scene is a constant for each channel, we would expect the resulting APC output to also be constant for each channel. However, our analysis of the outputs has shown that this is not the case.

Table 5 displays the gradients observed in the interim and nominal mode outputs produced from the simulated antenna temperatures. These gradients are the result of performing a linear curve fit to individual rows of T_B values. The R^2 terms in the first column of the table are the squared correlation coefficients for these fits, where a correlation of 1.00 indicates a perfectly linear relationship.

E. Njoku suspects that the gradients observed in the interim mode output are attributable to an inaccuracy in the method by which cos β effects are introduced into the generation of the antenna temperatures. Note that the interim mode gradients are generally small in magnitude, and are very smooth as evidenced by the high correlation coefficients. In addition, these gradient values qualitatively correspond with the cos β values used in the simulation.

Several observations are made regarding the gradients in Table 5:

(1) As shown by the correlation coefficients, the nominal mode data does not exhibit the smooth, linear variation across the swath which is observed in the interim mode data. This agrees with the earlier observation that the nominal mode data exhibits more noise than the interim mode data.

(2) The gradients observed in the nominal mode output for the 6.6, 10.7, and 18 GHz channels are much larger in magnitude than those observed for the interim mode, while the nominal mode gradients for the 21 and 37 GHz channels are comparable to the corresponding interim mode values.

(3) For the three lower frequencies, the nominal mode gradients for the V and H channels of a single frequency are generally of similar magnitude and opposite in sign. In addition, the nominal mode gradients are lower in value for the vertical channels and higher in value for the horizontal channels than the corresponding interim mode gradients. The nominal mode gradients are not simply an amplification of the interim mode gradients. For example, the 10.7 V interim mode gradient is 0.03 degrees per cell, while the corresponding nominal mode gradient is -0.43 degrees per cell.

(4) Simple calculations involving the slopes and intercepts for the two modes show that the nominal mode values tend to be lower than the corresponding interim mode values. This agrees with earlier observations that the sidelobe corrected T_B values are generally lower than interim mode values.

A small analysis has been performed to try to relate the nominal mode gradients seen for the simulated data to those observed in the actual spacecraft data. Since the actual data contains gradients due to weather, we have compared the differences between H and V gradients for the two data sets. These H-V gradient differences for both the spacecraft and simulated data sets are displayed in Table 6.

The H-V gradient differences for the 6.6, 10.7, and 37 GHz channels correlate quite well between the spacecraft and simulation data sets. However, there is little correlation evident for the 18 and 21 GHz channels. Perhaps further evaluation using spacecraft data having better weather conditions could clarify why the 18 and 21 GHz channels correlate so poorly.

3.2 Refining of cos β Estimates.

3.2.1 Evaluation of Initial cos β Estimates. The work presented in this section is a continuation of that discussed in section 3.2 of reference 1. Reference 1 documents the derivation of an initial set of cos β estimates. These estimates are reproduced in the first column of Table 7.

Corrections based on these estimates have now been implemented in the APC software, and we have evaluated the effects of these corrections by producing plots of cross-track gradients versus latitude. Plots are

produced for interim mode data both before and after the cos β corrections are applied. By comparing these before and after plots, we have found that the implemented corrections remove all obvious problems such as opposing V and H gradients (i.e. gradients of opposite sign) for the 10.7, 18, 21, and 37 GHz channels. The corrections for the 6.6 GHz channels remove most, but not all, of the observed discrepancies. The residual errors in the 6.6 GHz data are attributable to the fact that no attempt was made to account for Faraday rotation effects in the initial determination of cos β values.

A portion of orbit 1463 has been used to determine Faraday-free cos β estimates for the 6.6 GHz channels. This orbit segment is a local night pass and thus contains minimal Faraday rotation effects since ionospheric activity is minimized during the night. The revised cos β estimates are displayed in the second column of Table 7. Since orbit 1463 has been used to update only the 6.6 GHz estimates, the estimates for the other channels are unchanged from column 1. Note that the cos β corrections currently implemented in the APC are based on the values in column 2.

Figures 10.1 through 10.5 display cross-track gradient plots produced for interim mode data from orbit 1463. The gradients shown are those present before the application of cos β corrections. Figures 11.1 through 11.5 display similar plots for the same data after the application of cos β corrections based on the values given in column 2 of Table 7. The following observations are made regarding figures 10 and 11:

(1) As evidenced by figures 10.2 and 10.5, the 10.7 and 37 GHz data do not exhibit anomalous gradients before the application of cos β corrections. Figures 11.2 and 11.5 show that the cos β corrections do not appreciably change the gradients for these frequencies.

(2) There are large opposing cross track gradients in the first set of plots for the 6.6 and 18 GHz data (figures 10.1 and 10.3). These opposing cross track gradients are almost completely removed in the second set of plots (figures 11.1 and 11.3).

(3) Figure 10.4 contains many cases of a 21 V gradient being larger in magnitude than the corresponding 21 H gradient (e.g. 15°N). This is geophysically unrealistic since the 21 H channel is more sensitive to most geophysical phenomena than the 21 V channel. Figure 11.4 shows that these unrealistic gradients have been corrected (e.g. 15°N).

3.2.2 Determination of Final cos β Estimates. Concurrent with our work, E. Christensen and B. Wind have carried on a parallel effort to determine cos β values. This section documents our contribution to their efforts. The approach followed by E. Christensen involves the use of a least squares batch filter. A brief description of this filter follows.

Let Y_{obs} represent the vector of measured antenna temperatures. Let X_k represent the estimate at the kth iteration step of the brightness temperatures and cos β values corresponding to Y_{obs}. Then, the linearized model equation may be written as

$$(Y_{obs} - Y_{comp}) = \left[\frac{\partial y}{\partial x}\right] (X_{k+1} - X_k) + \varepsilon \qquad (1)$$

where

Y_{comp} = vector of antenna temperatures computed from X_k, using the narrow beam antenna pattern equations (see reference 1).

ε = randomly distributed "white" noise.

$\left[\frac{\partial y}{\partial x}\right]$ = matrix of partial derivatives calculated from X_k, again using the narrow beam antenna pattern equations.

Equation (1) may be re-written as

$$\tilde{Y} = A \tilde{X} + \varepsilon \qquad (2)$$

where

$\tilde{Y} = Y_{obs} - Y_{comp}$, the vector of differences between the measured and calculated antenna temparatures.

$A = \left[\frac{\partial y}{\partial x}\right]$, the matrix of partial derivatives computed from X_k.

$\tilde{X} = X_{k+1} - X_k$, the vector of differences between the estimates for step k and step k+1.

At each iteration step, the A matrix is updated, and the new estimate X_{k+1} is calculated as

$$X_{k+1} = X_k + \tilde{X} \qquad (3)$$

where

$$\tilde{X} = (A^T A)^{-1} A^T \tilde{Y} \qquad (4)$$

The matrix A^TA has dimension n x n, where n is the number of parameters to be estimated. For a given frequency, the estimated parameters include two cos β values (for V and H), and p x q brightness temperatures, where p is the number of T_B cells per grid row for the given frequency, and q is the number of grid rows processed in the batch. Since a minimum of five blocks of data are needed to remove weather effects from the cosβ estimates, the A^TA matrix quickly becomes very large. For example, the A^TA matrix for five blocks of 6.6 GHz data has dimension 162 x 162, or 26,244 elements. Similarly, there are 242,064 matrix elements for the 10.7 GHz data; 1,468,944 elements for 18 and 21 GHz; and 23,444,964 elements for 37 GHz. Needless to say, the brute force storage and inversion of the A^TA matrix for the higher frequencies would tax the capacity of any machine.

Part of our contribution to this parallel effort has involved the development of a subroutine which allows the efficient inversion of the A^TA matrix. This is possible because most of the elements of the matrix are zero. By taking advantage of this sparseness, it is possible to partition the A^TA matrix into seven sub-matrices, five of which are diagonal. This partitioning allows the calculation of $(A^TA)^{-1}$ on an element by element basis without the necessity of storing the full array at any one time. As each element is calculated, it can be multiplied by the appropriate element of $A^T\tilde{Y}$ and added to a running sum in order to build up the components of $\tilde{X}$ one at a time.

Our subroutine accepts the non-zero elements of the A^TA matrix and the elements of $A^T\tilde{Y}$, and returns $\tilde{X}$. It requires no core other than that needed to store its inputs. For the 6.6 GHz case, 562 words of storage are required rather than the 26,244 needed previously for the full array. In addition, the inversion procedure requires much less CPU time than that required for a brute force inversion. The major benefit of this subroutine is that it allows the determination of cos β estimates for the higher frequency channels. Only 1717 words are required for 10.7 GHz; 4,237 for 18 and 21 GHz; and 16,942 for 37 GHz.

A final set of cos β estimates has been determined using the batch filter technique. These estimates are given in the third column of Table 7. Note that these estimates are generally within one standard deviation of the column 2 values. The standard deviations calculated by the batch filter program for the final cos β estimates are given in column 4 of Table 7. The corresponding uncertainties in total T_B cross-track variation appear in the last column of the table. These values are calculated by multiplying the cos β uncertainties (column 4) by the partials relating cross-track variation to the cos β terms.

The final cos β values for the 6.6 GHz V and H channels are derived from local night data which minimizes Faraday rotation effects. The final cos β values for the other eight channels are derived from equal amounts of local night (descending) and local day (ascending) data. These final values have not yet been implemented in the APC software, and so there has been no opportunity to assess how they compare with the prior values. Their implementation and evaluation will take place in the near future.

3.3 Comparison of World T_B Map to SMMR T_B Values. The APC uses a world brightness temperature map in order to perform sidelobe corrections for radiation received from the earth's surface outside the SMMR swath. The map T_B values corresponding to ocean regions are derived from a geophysical model which assumes latitudinally varying sea surface temperature and water vapor content, no winds, and no clouds. Thus, these map values should approximate those values measured by the SMMR during clear weather, low wind speed conditions. The map values corresponding to land are constant for each channel, and represent an average over different land scenes such as forests, deserts, etc.

When the actual conditions being observed do not correspond to those assumed in the world T_B map, the APC algorithm may over- or undercompensate for radiation received from outside the SMMR swath. When the world T_B map values are higher than those actually present, the resulting sidelobe corrections will be too large, and the SMMR corrected brightness temperatures will tend to be too low. The opposite situation will occur when the map values are lower than those actually present. Generally, however, less than 10% of the total radiation received for any given cell is from outside the SMMR swath. Therefore, sidelobe correction errors will not normally be larger than 10% of any errors in the world T_B map. Errors for cells which are not on the edge of the swath are even smaller since these cells receive even less radiation from outside the swath.

Table 8.1 contains interim mode brightness temperature values measured by the SMMR under relatively clear weather conditions. The table entries for each latitude range are the lowest observed values from selected portions of orbits 1178, 1206, 1212, and 1255. Note that the entries for land consist only of measurements from Alaska. Due to the limited nature of the data set, the errors for each entry could be as large as 15°K. A larger data set would be needed to reduce these errors.

Table 8.2 contains ocean T_B values from the world brightness temperature map for different latitudes and land values which are constant with respect to latitude. Table 8.3 contains differences between the world T_B map and the SMMR measured T_B values of Table 8.1. With a few exceptions, these differences are too small to cause significant sidelobe correction errors. The exceptions occur over ocean near the

equator for the 18, 21, and 37 GHz channels; and overland for the 6.6 and 37 GHz channels. However, even these exceptions would result in sidelobe correction errors of less than 4°K, which would be the maximum error for the 21 H channel at the equator.

An interesting point to observe is that the Table 8.3 differences for each channel are always positive at low latitudes and decrease with increasing latitude, particularly for the higher frequency channels. This seems to imply that the map values assume too much variation in water vapor content from the equator to higher latitudes, even though the global mean water vapor content appears correct.

Tables 8.1 through 8.3 show that the world T_B map does not significantly disagree with those SMMR T_B values measured during clear weather conditions. However, Table 9 shows that SMMR measured brightness temperatures sometimes vary greatly from their baseline clear weather levels. Table 9 contains the T_B variations caused for each channel by a dense cloud feature encountered during orbit 1212. It is not known whether rain was present. When severe weather conditions such as these occur outside the SMMR swath, the APC algorithm may be undercorrecting for sidelobe contributions by as much as 10% of the Table 9 entries (e.g. 10°K for 37 H). However, errors of this magnitude are unlikely in light of the fact that such conditions do not often occur over large extended areas.

4.0 CONCLUSIONS

Several conclusions may be drawn from the results discussed in the previous section 3.0:

(1) It appears that the sidelobe corrections applied by both the cross and nominal APC modes are adding significant cross-track gradients to the 6.6, 10.7, and 18 GHz T_B data. The added gradients are different for each channel, tending to be negative for the vertical channels and positive for the horizontal channels. For the three lower frequencies, the gradients added to the V and H channels are similar in magnitude, although opposite in sign. The 21 and 37 GHz data do not exhibit significant gradient changes between the interim and sidelobe-corrected modes. These results are reproduced quite well for the 6.6, 10.7, and 37 GHz data in a SMMR simulation produced by E. Njoku. The source of these gradient changes is not clear at the present time.

(2) It appears that the T_B data produced by the nominal and cross modes tends to be consistently lower in value than data produced by the interim mode. This effect is especially pronounced for clear weather conditions, in which the overall T_B level is relatively low. This T_B lowering may be attributable to the

sidelobe corrections derived from the world T_B map being too large, thereby lowering the corrected brightness temperatures. This explanation is supported by examples from orbit 1212 in which the edge cells are lower than the center cells. However, this T_B lowering may also be related to the gradient changes discussed above. The nominal mode gradients seen in the SMMR simulation tend to produce T_B values which are lower than the corresponding interim mode values. The actual cause of the T_B lowering probably involves some combination of both of these possibilities.

(3) The nominal mode T_B data exhibits ringing effects when crossing a land-sea interface. In addition, the nominal mode data exhibits alternating over- and under-compensation for sidelobe contributions from land when the SMMR swath is paralleling a coastline. In contrast, the cross mode data does not exhibit either of these two effects. Instead, it strongly mimics the behavior of the interim mode.

(4) The nominal mode T_B data appears to be noisier than the interim mode data. It also tends to provide somewhat better spatial resolution. The cross mode T_B data does not exhibit appreciably more noise than the interim mode, nor does it appear to provide increased spatial resolution. In general, the only difference between the cross and interim modes seems to be a bias which varies across the swath.

(5) The world T_B map appears to be in fairly good agreement with SMMR clear weather T_B measurements. However, the SMMR clear weather measurements seem to exhibit less variation with latitude than do the world map values. It appears that the world T_B map will be significantly in error only when heavy clouds and/or rain are present.

(6) The cos β corrections appear to be correctly implemented in the APC software. In addition, the current cos β values account for the major cross-track gradient discrepancies previously observed in interim mode output.

5.0 RECOMMENDATIONS

As a result of this study, we feel that the following recommendations are appropriate:

(1) At the present time, the source of the cross-track gradients introduced by the sidelobe correction procedure is unknown. These gradients should be investigated and removed if possible. Probably the best means of quantifying this effect consists of re-running the SMMR simulation, setting cos β values to zero, and producing interim, cross, and nominal mode APC outputs.

(2) At present, the ringing phenomena and the over- and under-compensation effects near land are not completely understood. Unless a final decision is made to discard the nominal mode, these effects should be further investigated with the intention of minimizing them. Perhaps these effects can best be studied by simulating a brightness temperature scene which is half ocean and half land.

(3) The final set of cos β values should be implemented in the APC software and their effects should be evaluated.

(4) The possibility of refining the world brightness temperature map should be considered. The best values to be included in the map should be determined by examining a large set of SMMR T_B data so as to obtain accurate clear weather ocean values and average land values.

6.0 NEW TECHNOLOGY

No new technology has been developed in the course of this study.

7.0 REFERENCES

1. Kitzis, J. L. and Kitzis, S. N., "Evaluation and Analysis of SEASAT-A SMMR APC Algorithm: Interim T_B vs. Final T_B with Gaussian Coefficients", May 25, 1979.

Table 1. Estimated Mean T_B Differences Between APC Modes, Orbit 1178, 30°N to 50°N

1. Interim minus Nominal

Channel	Left	Center	Right
6.6 V	0	0	2
6.6 H	0	0	-1
10.7 V	-1	0	3
10.7 H	4	2	-1
18 V	-1	0	3
18 H	5	5	0
21 V	3	2	0
21 H	0	3	2
37 V	5	3	2
37 H	0	2	0

2. Interim minus Cross

Channel	Left	Center	Right
6.6 V	0	1	1
6.6 H	1	1	1
10.7 V	0	2	2
10.7 H	4	2	1
18 V	1	1	3
18 H	6	4	2
21 V	4	2	1
21 H	1	3	4
37 V	4	3	3
37 H	3	2	3

Notes:

1. Data for each channel is taken from its best grid.
2. All differences are in degrees Kelvin.
3. "Left" indicates data from the extreme left cells of all grids (columns 1, 1, 1, 1 of grids 1, 2, 3, 4 respectively).
4. "Right" indicates data from the extreme right cells of all grids (columns 4, 7, 11, 22)
5. "Center" indicates data from columns 3, 4, 6, 12 of grids 1, 2, 3, 4 respectively.
6. Accuracy (3σ) for 6.6 and 10.7 GHz entries is estimated to be 1°K.
7. Accuracy (3σ) for 18, 31, and 37 GHz entries is estimated to be 3°K.

Table 2. Estimated Mean T_B Differences Between APC Modes, Orbit 1212, 30°N to 45°N

1. Interim minus Nominal

Channel	Left	Center	Right
6.6 V	1	2	7
6.6 H	2	0	2
10.7 V	2	2	4
10.7 H	6	4	6
18 V	5	2	6
18 H	7	6	5
21 V	6	3	5
21 H	2	4	6
37 V	6	4	6
37 H	7	4	5

2. Interim minus Cross

Channel	Left	Center	Right
6.6 V	1	2	4
6.6 H	2	2	3
10.7 V	2	3	3
10.7 H	6	4	5
18 V	2	2	5
18 H	7	6	4
21 V	6	3	3
21 H	3	4	5
37 V	4	4	5
37 H	5	3	4

Notes:

1. Data for each channel is taken from its best grid.
2. All differences are in degrees Kelvin.
3. "Left" indicates data from the extreme left cells of all grids (columns 1, 1, 1, 1 of grids 1, 2, 3, 4 respectively).
4. "Right" indicates data from the extreme right cells of all grids (columns 4, 7, 11, 22).
5. "Center" indicates data from columns 3, 4, 6, 12 of grids 1, 2, 3, 4 respectively.
6. Accuracy (3σ) for 6.6 and 10.7 GHz entries is estimated to be 1°K.
7. Accuracy (3σ) for 18 and 37 GHz entries is estimated to be 3°K.
8. Accuracy (3σ) for 21 GHz entries is estimated to be 5°K.

Figure 1.1. Open Ocean, Nominal and Interim

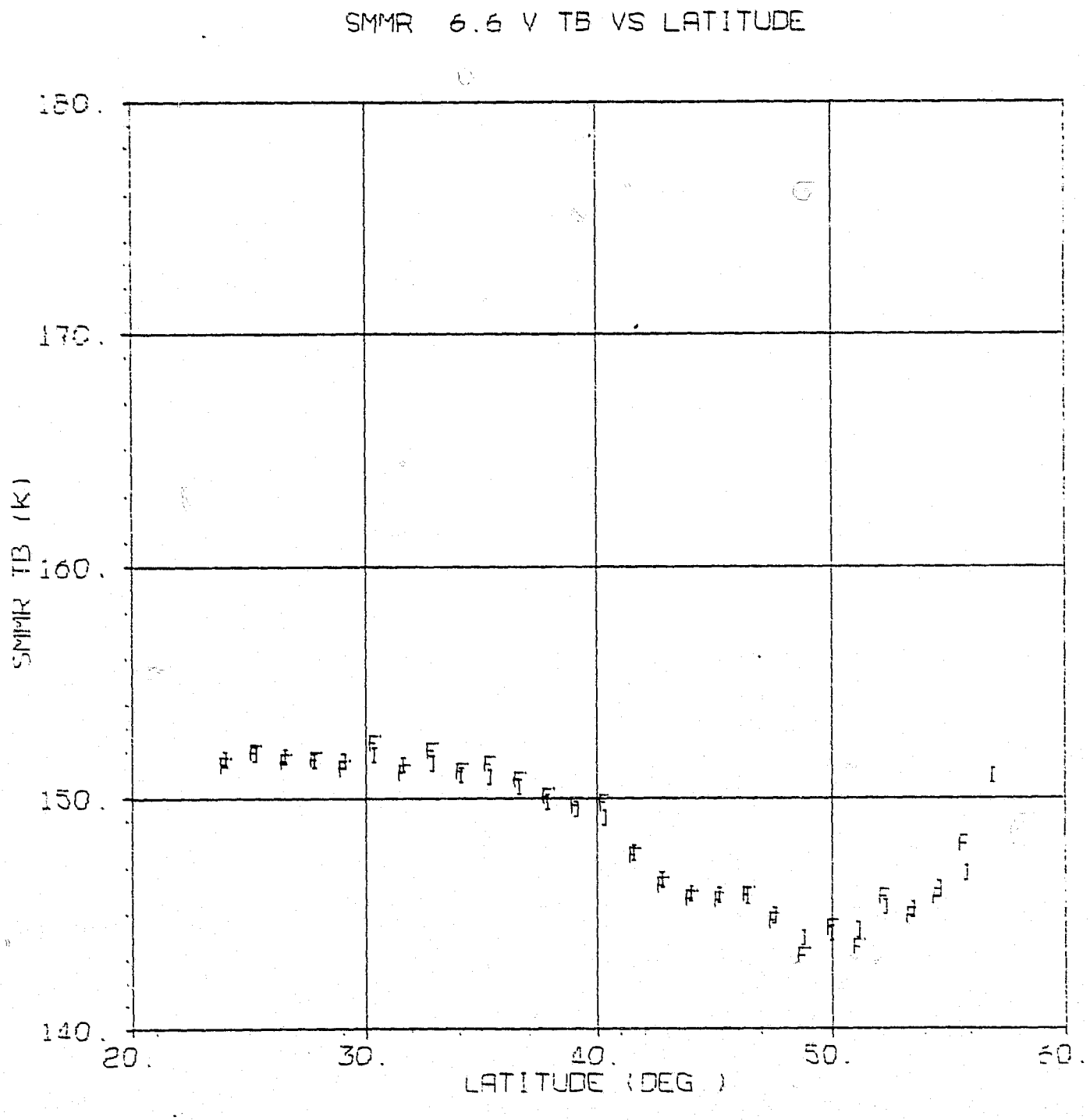

Orbit 1178, Grid 1, Column 1

Figure 1.2. Open Ocean, Nominal and Interim

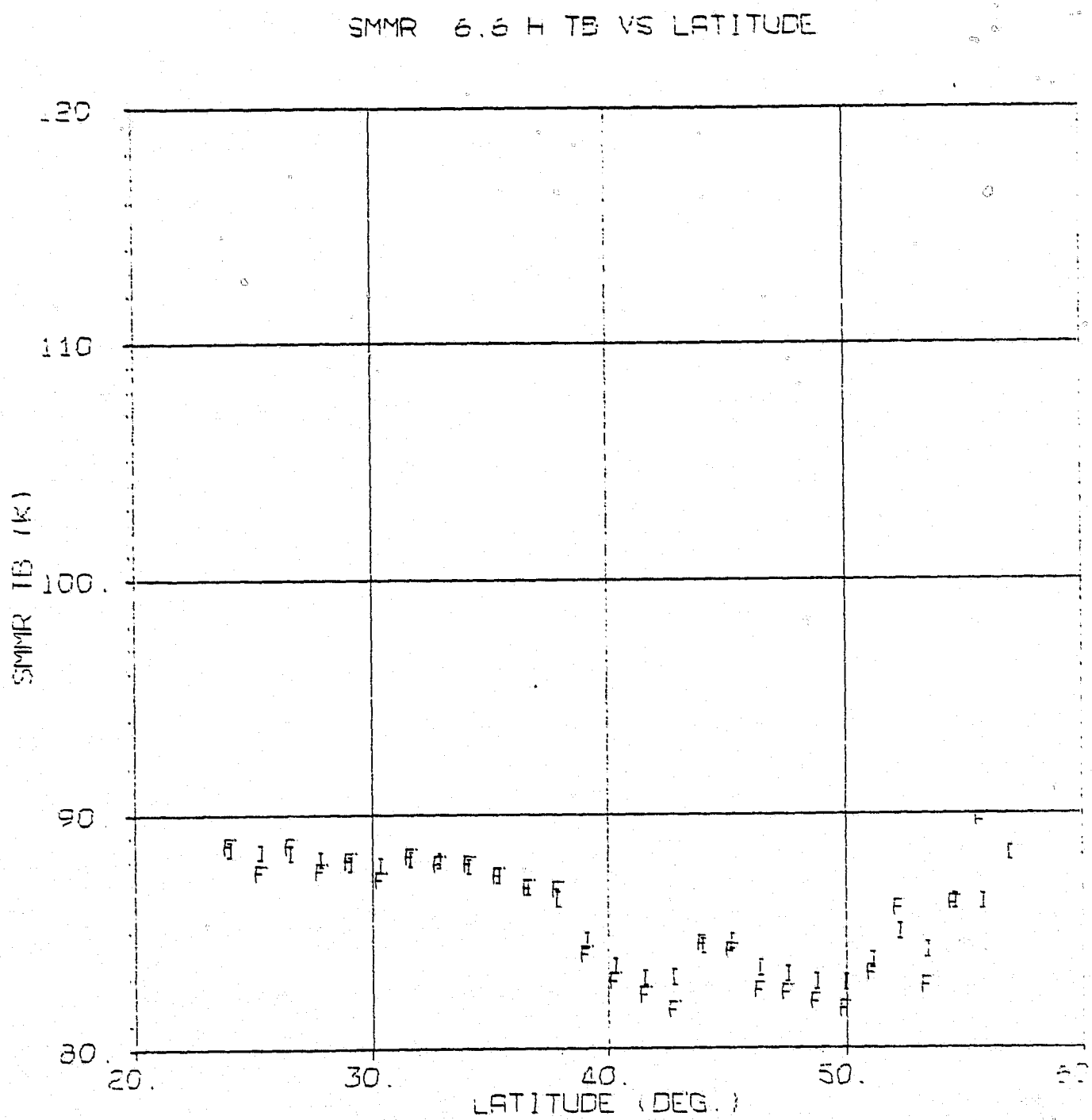

Orbit 1178, Grid 1, Column 1

Figure 1.3. Open Ocean, Nominal and Interim

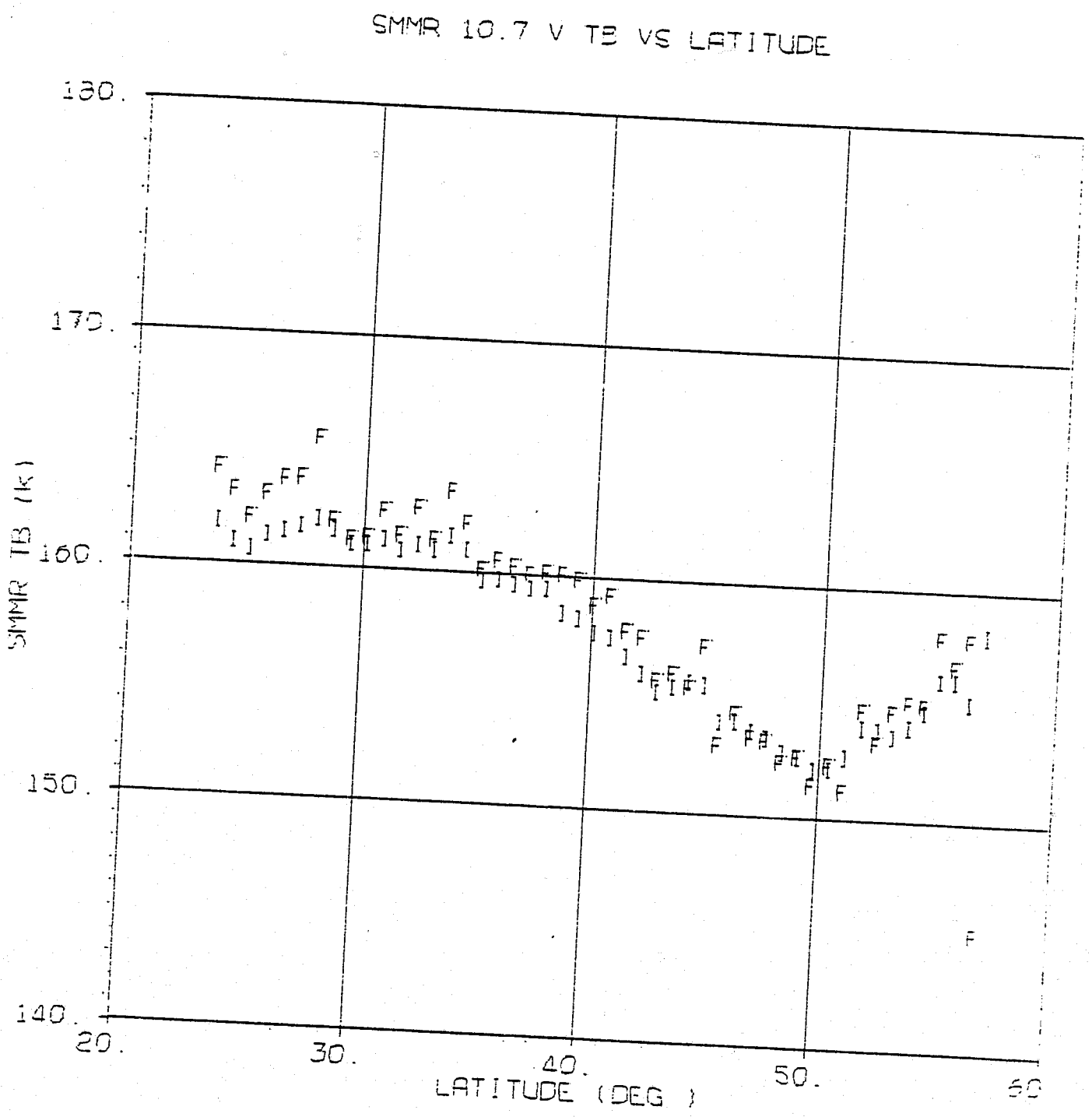

Orbit 1178, Grid 2, Column 1

Figure 1.4. Open Ocean, Nominal and Interim

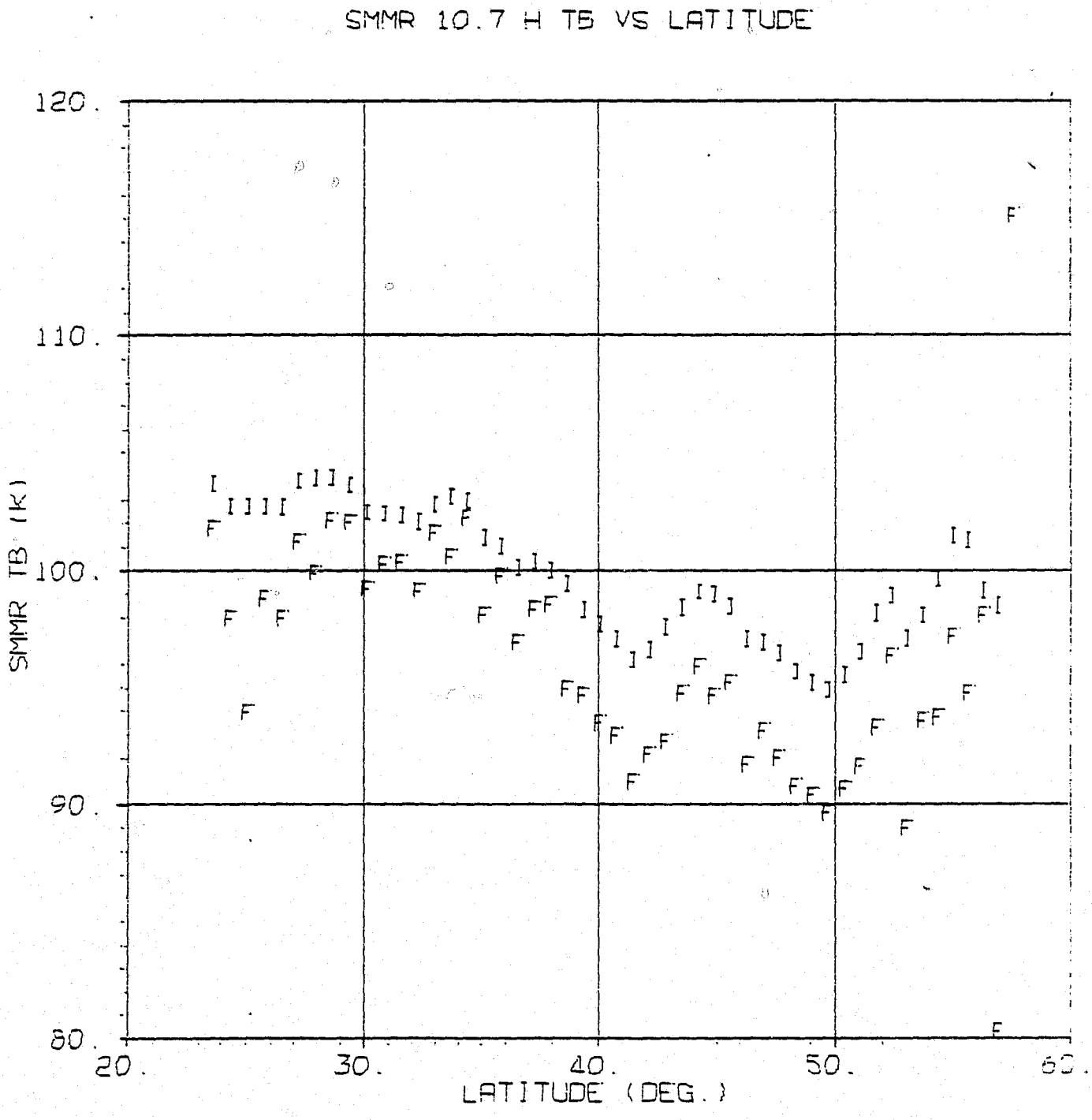

Orbit 1178, Grid 2, Column 1

Figure 1.5. Open Ocean, Nominal and Interim

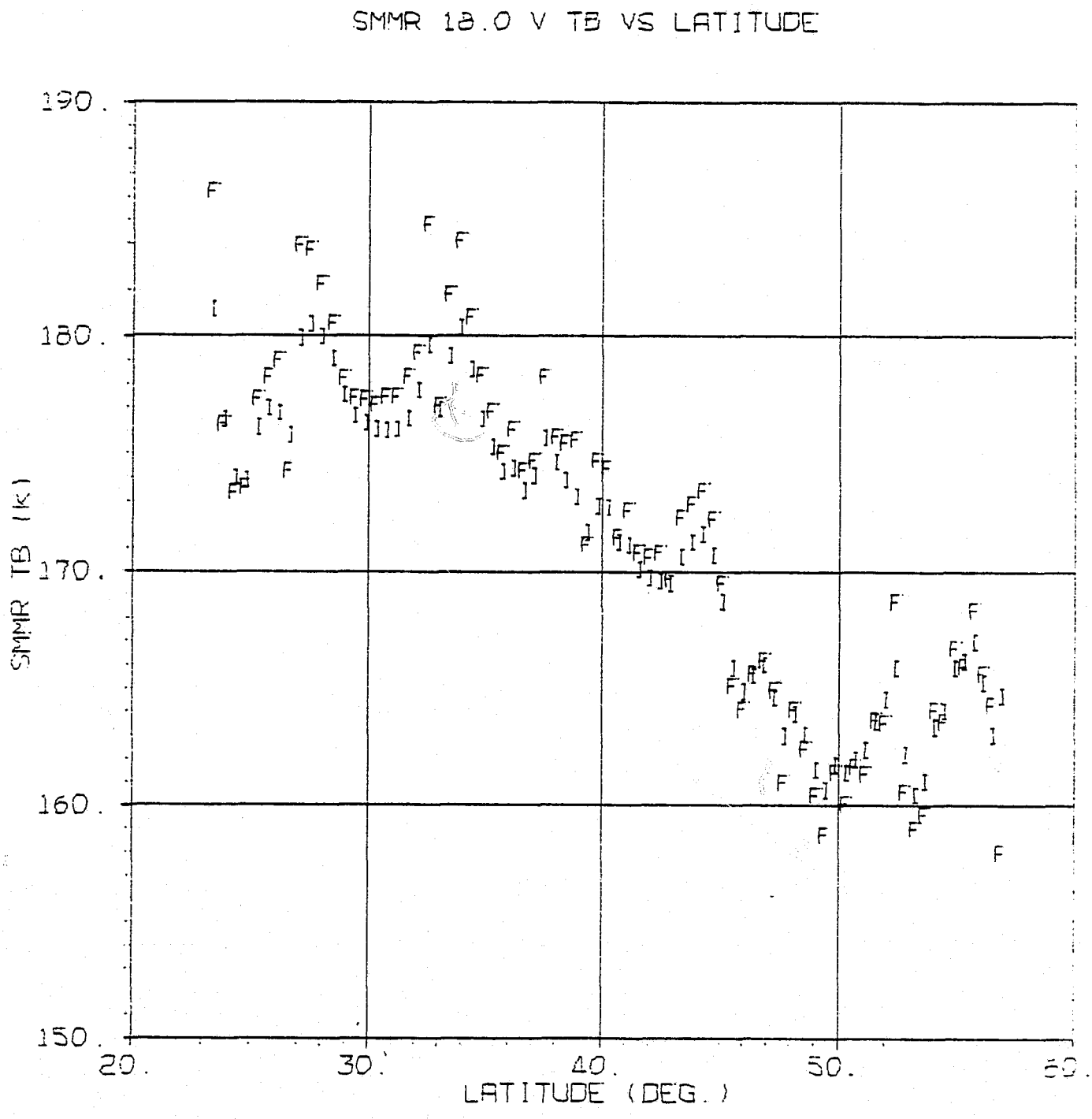

Orbit 1178, Grid 3, Column 1

Figure 1.6. Open Ocean, Nominal and Interim

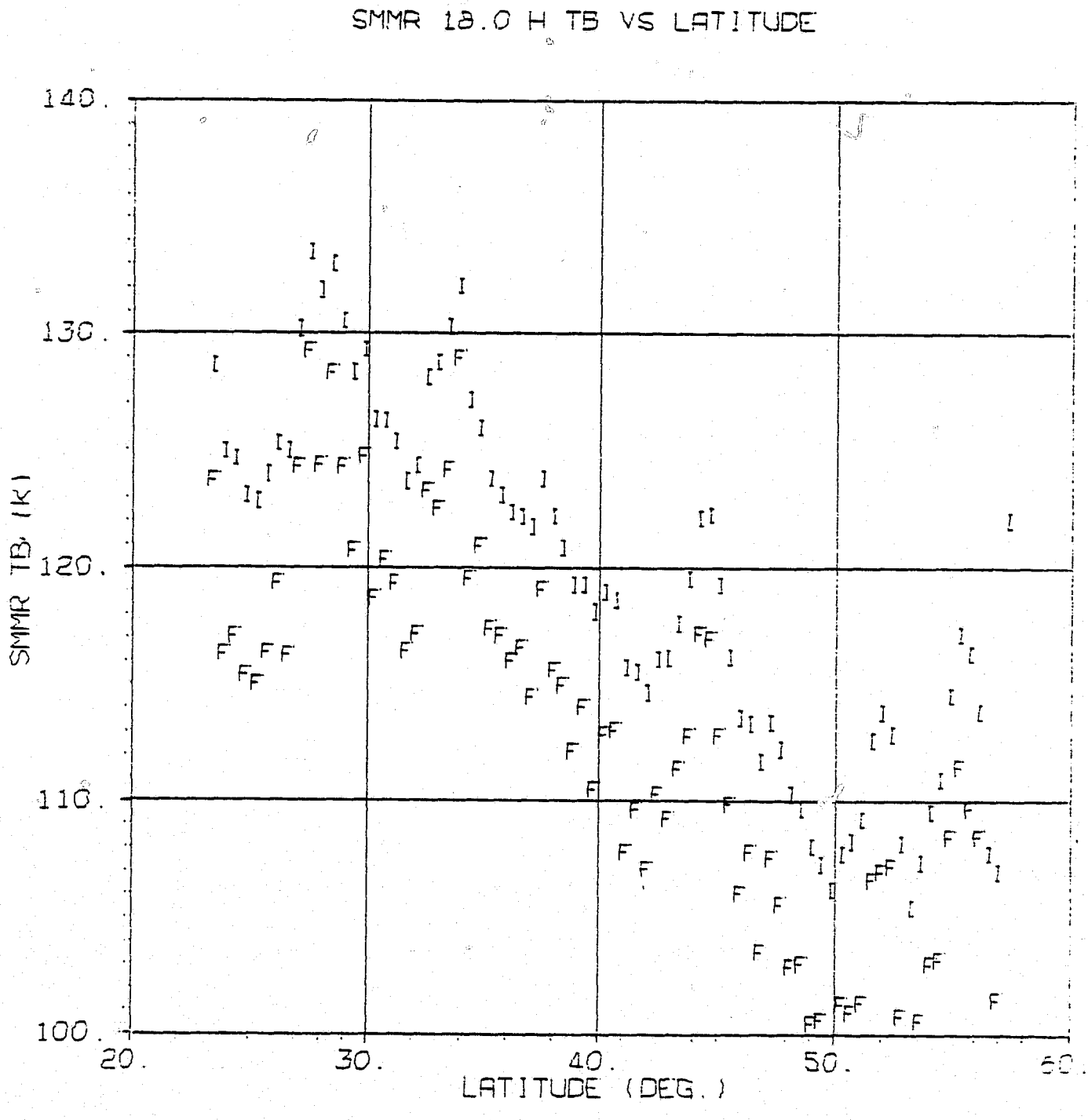

Orbit 1178, Grid 3, Column 1

Figure 1.7. Open Ocean, Nominal and Interim

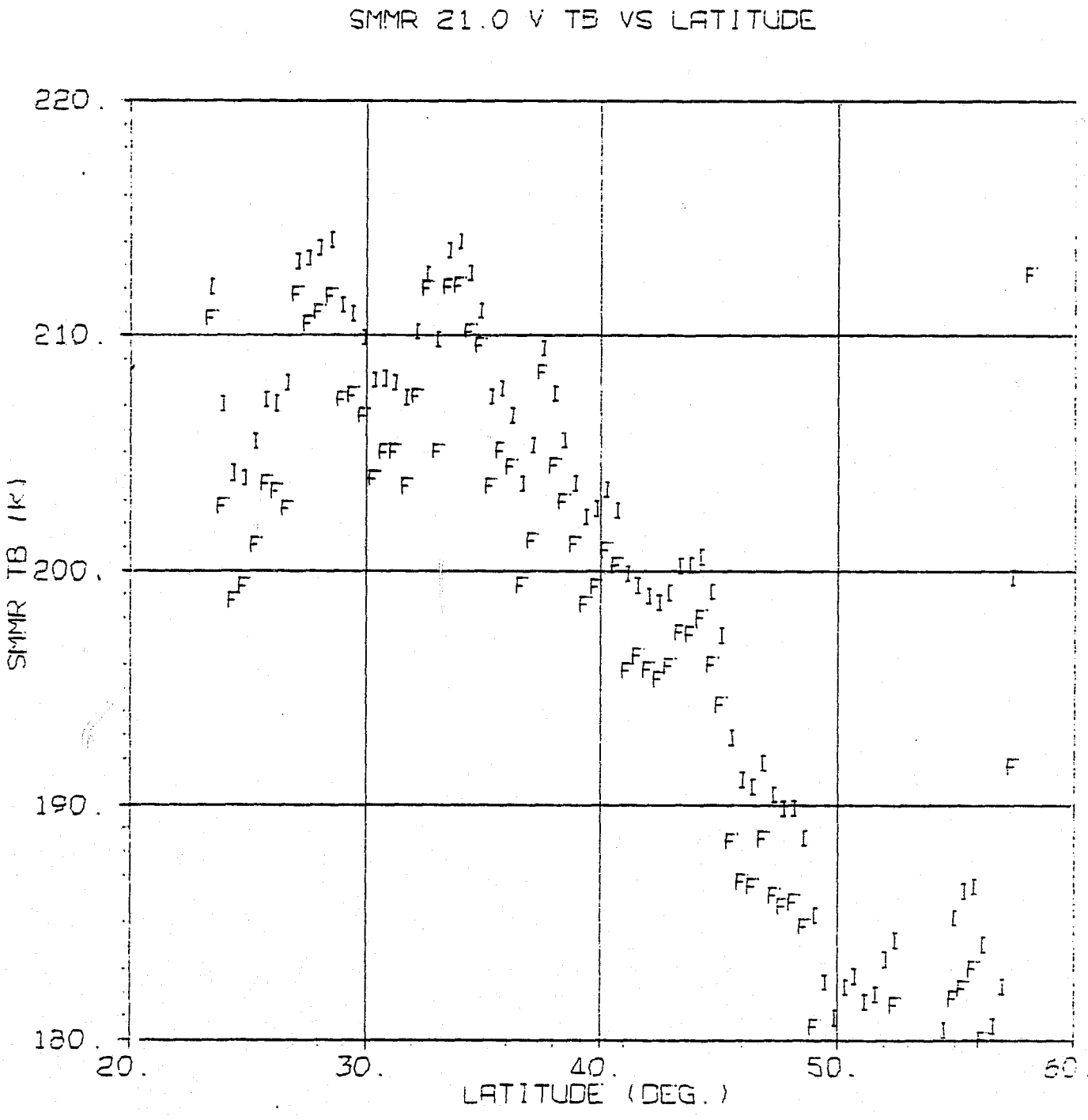

Orbit 1178, Grid 3, Column 1

Figure 1.8. Open Ocean, Nominal and Interim

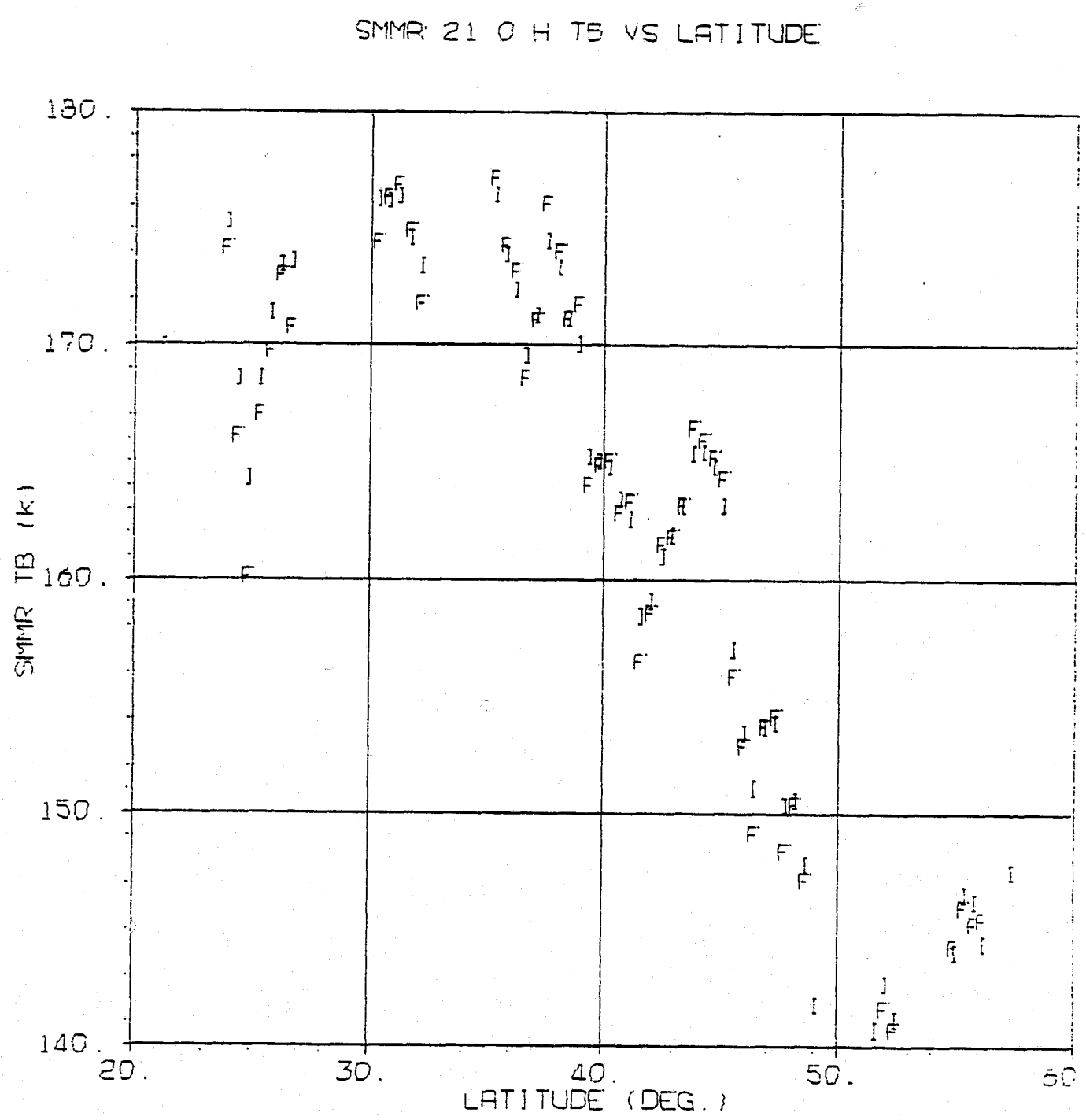

Orbit 1178, Grid 3, Column 1

Figure 1.9. Open Ocean, Nominal and Interim

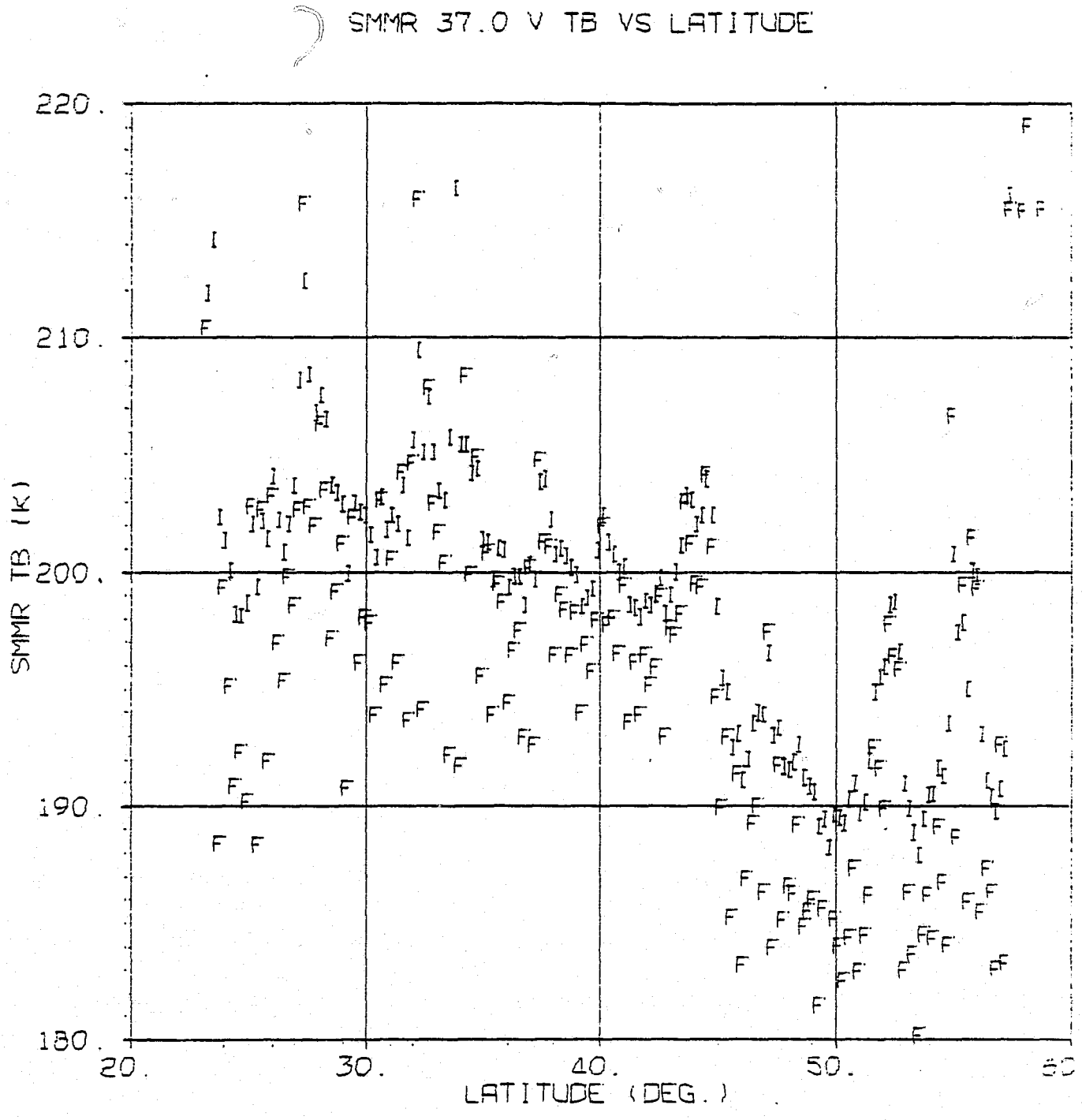

Orbit 1178, Grid 4, Column 1

Figure 1.10. Open Ocean, Nominal and Interim

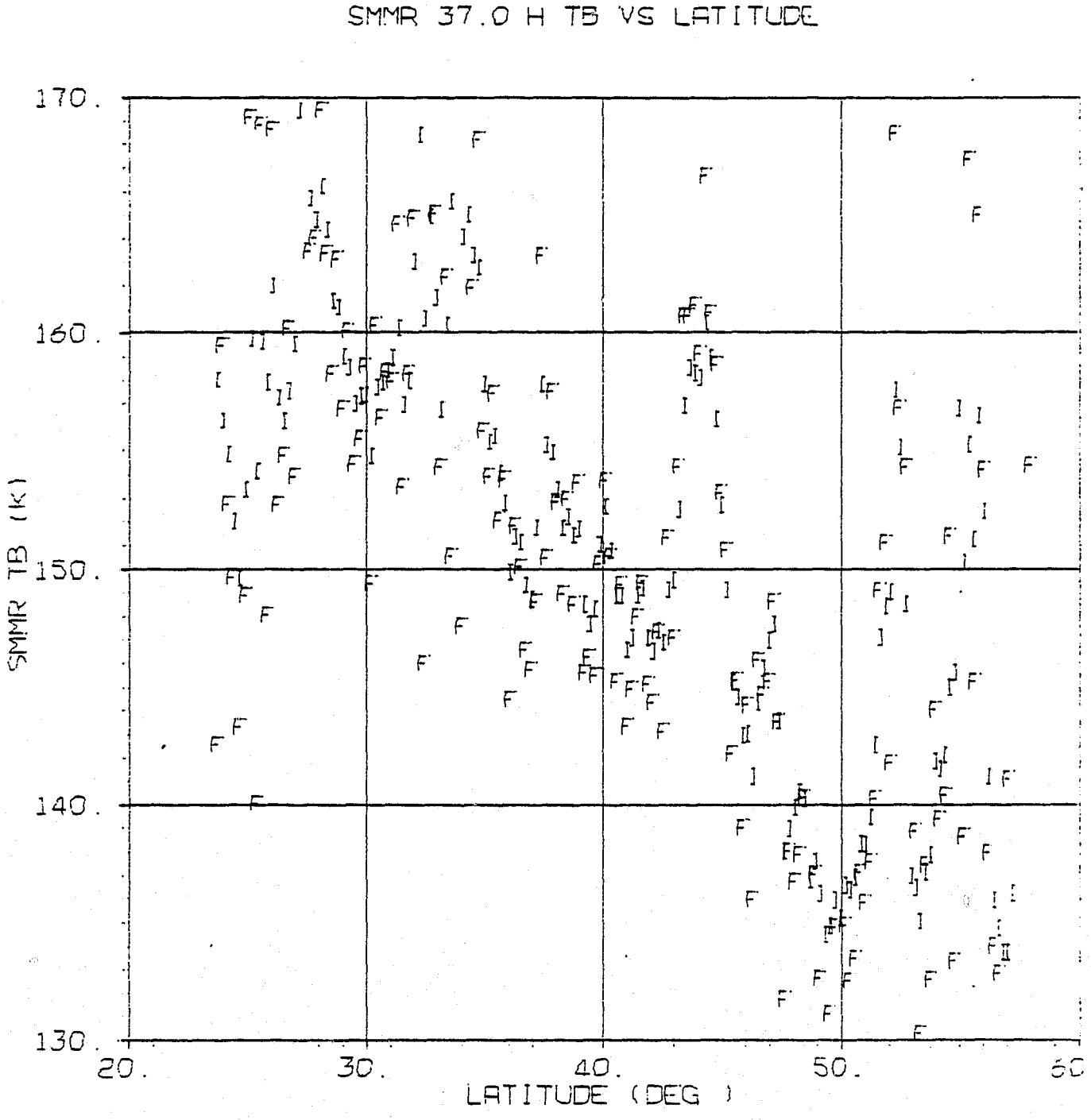

Orbit 1178, Grid 4, Column 1

Figure 2.1. Open Ocean, Cross and Interim

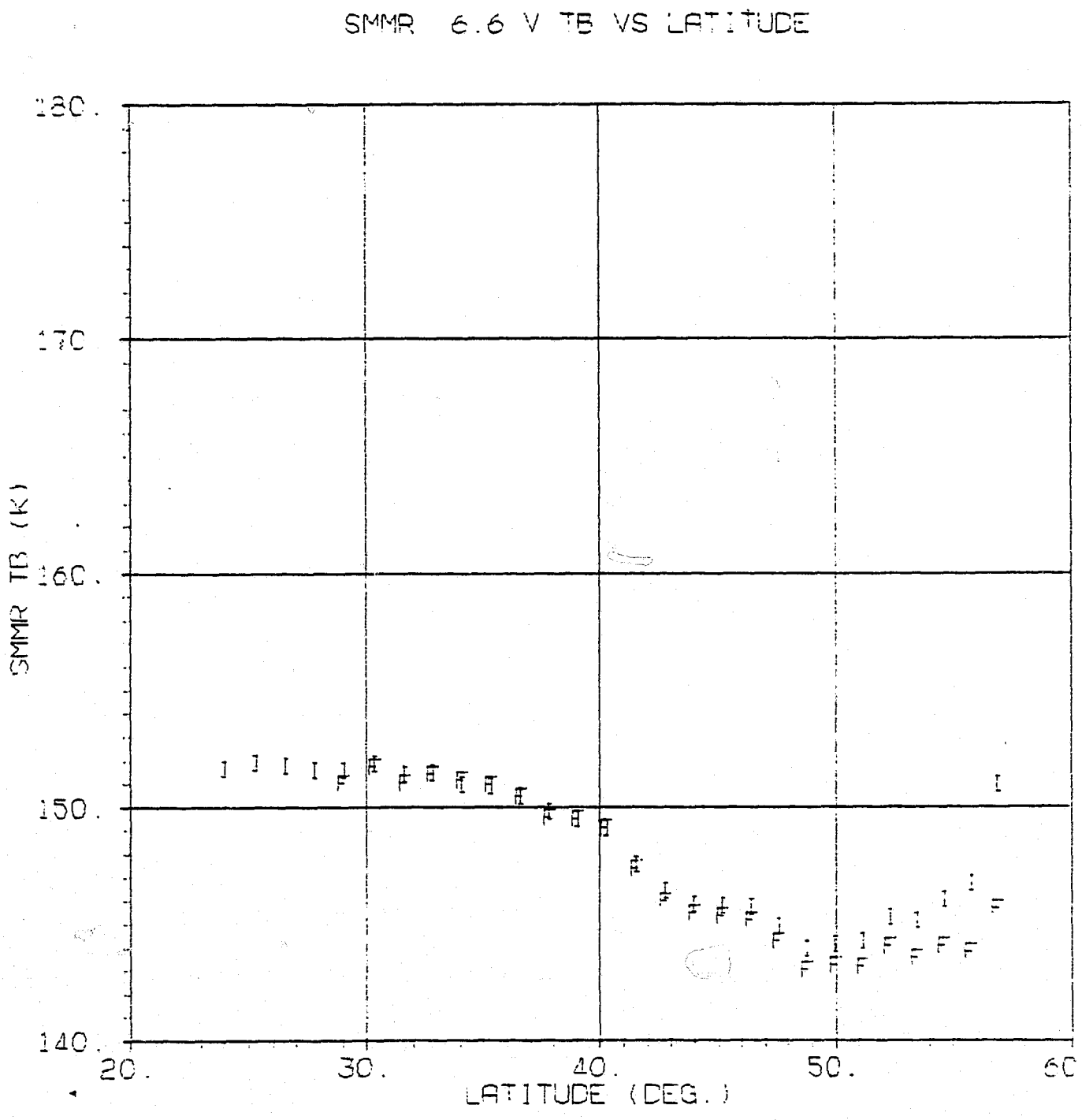

Orbit 1178, Grid 1, Column 1

Figure 2.2. Open Ocean, Cross and Interim

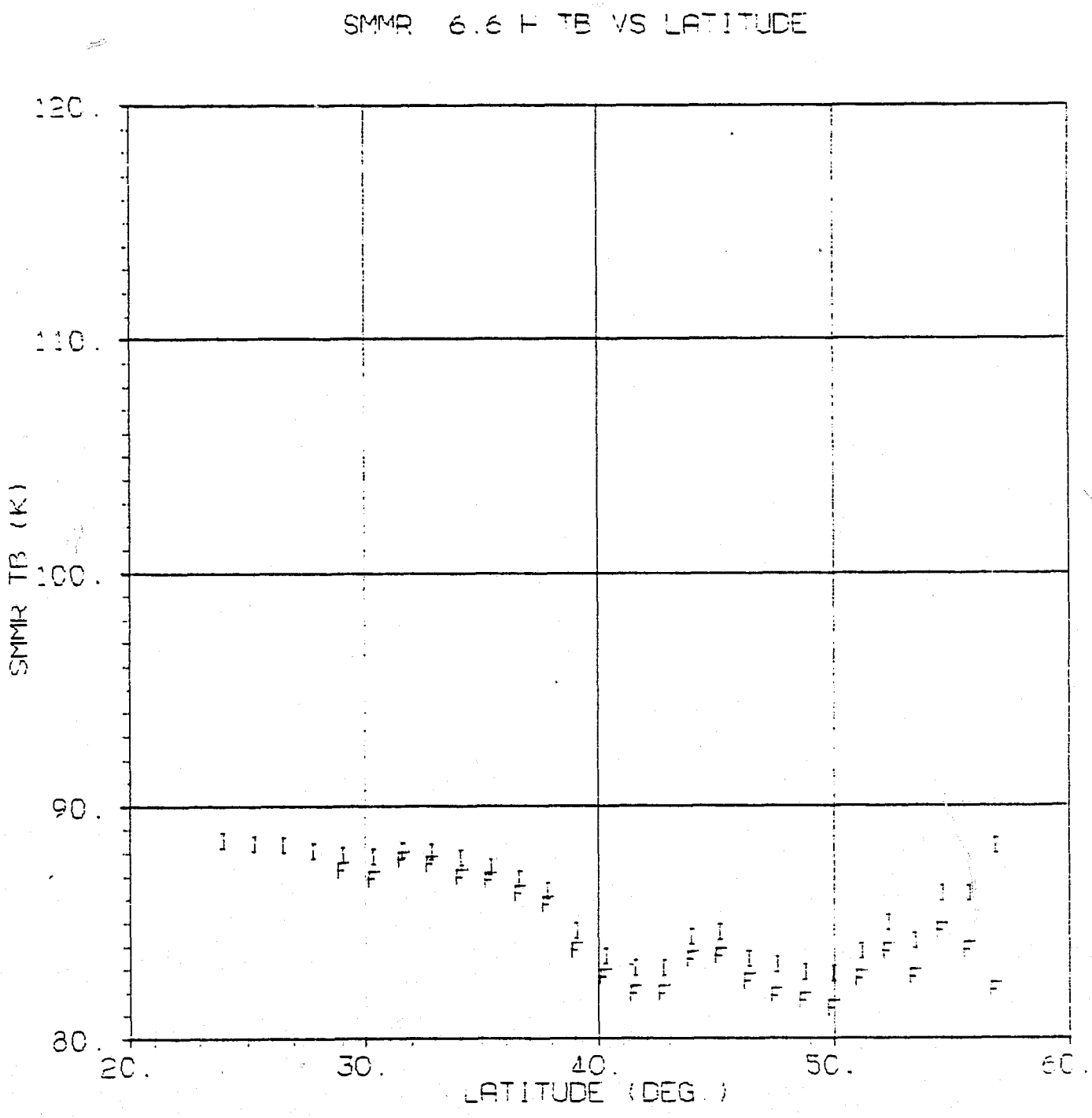

Orbit 1178, Grid 1, Column 1

Figure 2.3. Open Ocean, Cross and Interim

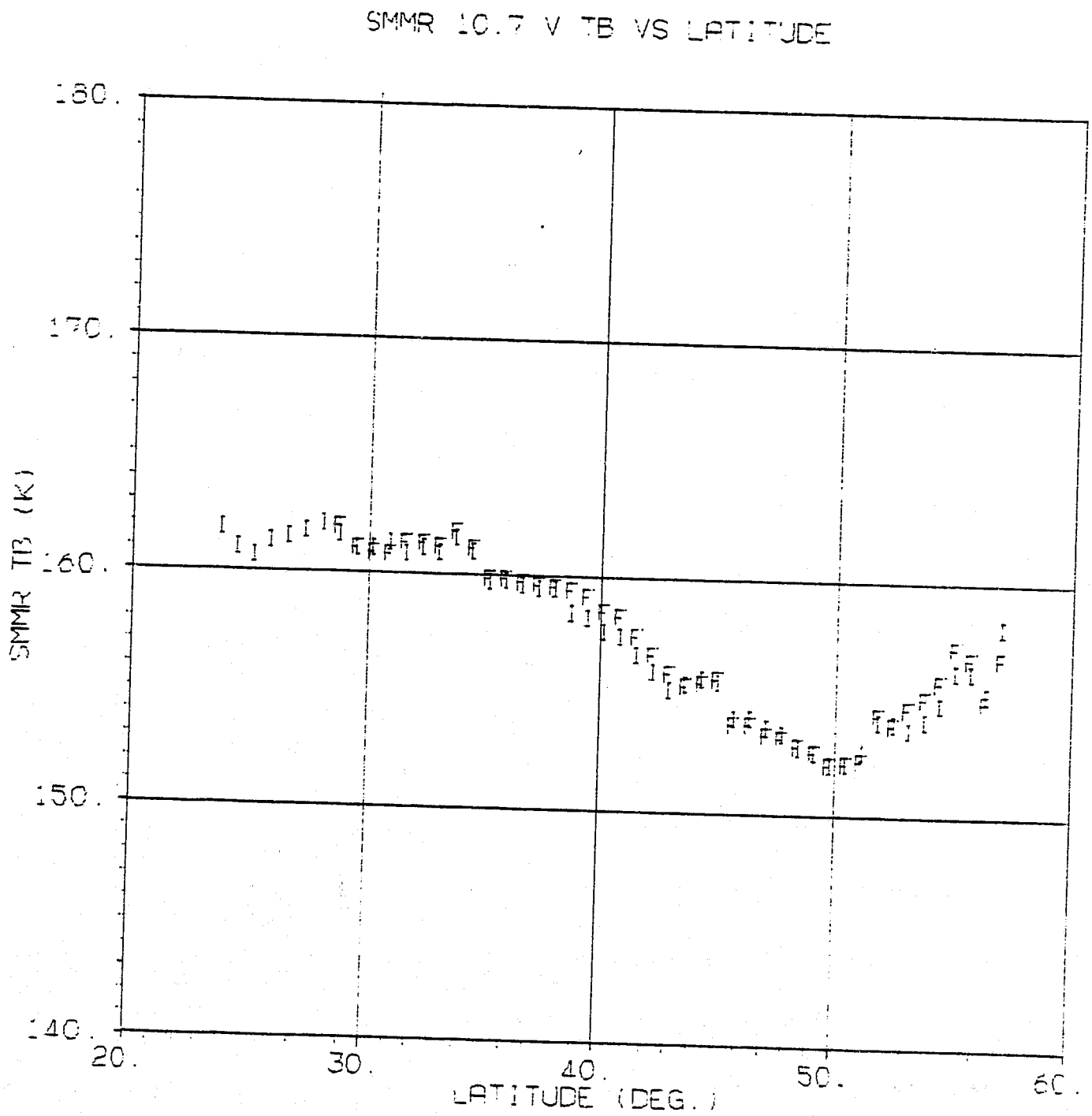

Orbit 1178, Grid 2, Column 1

Figure 2.4. Open Ocean, Cross and Interim

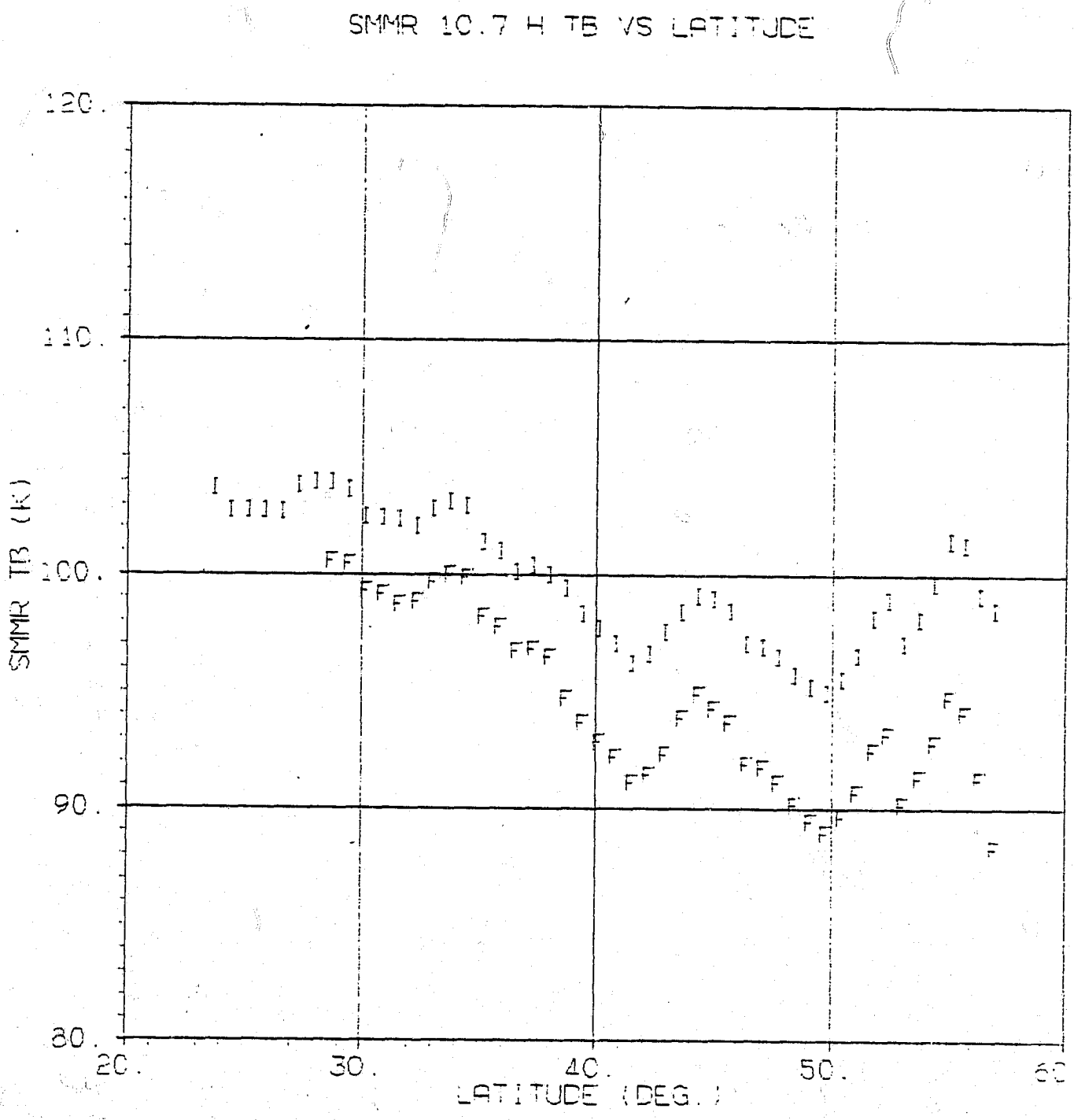

Orbit 1178, Grid 2, Column 1

Figure 2.5. Open Ocean, Cross and Interim

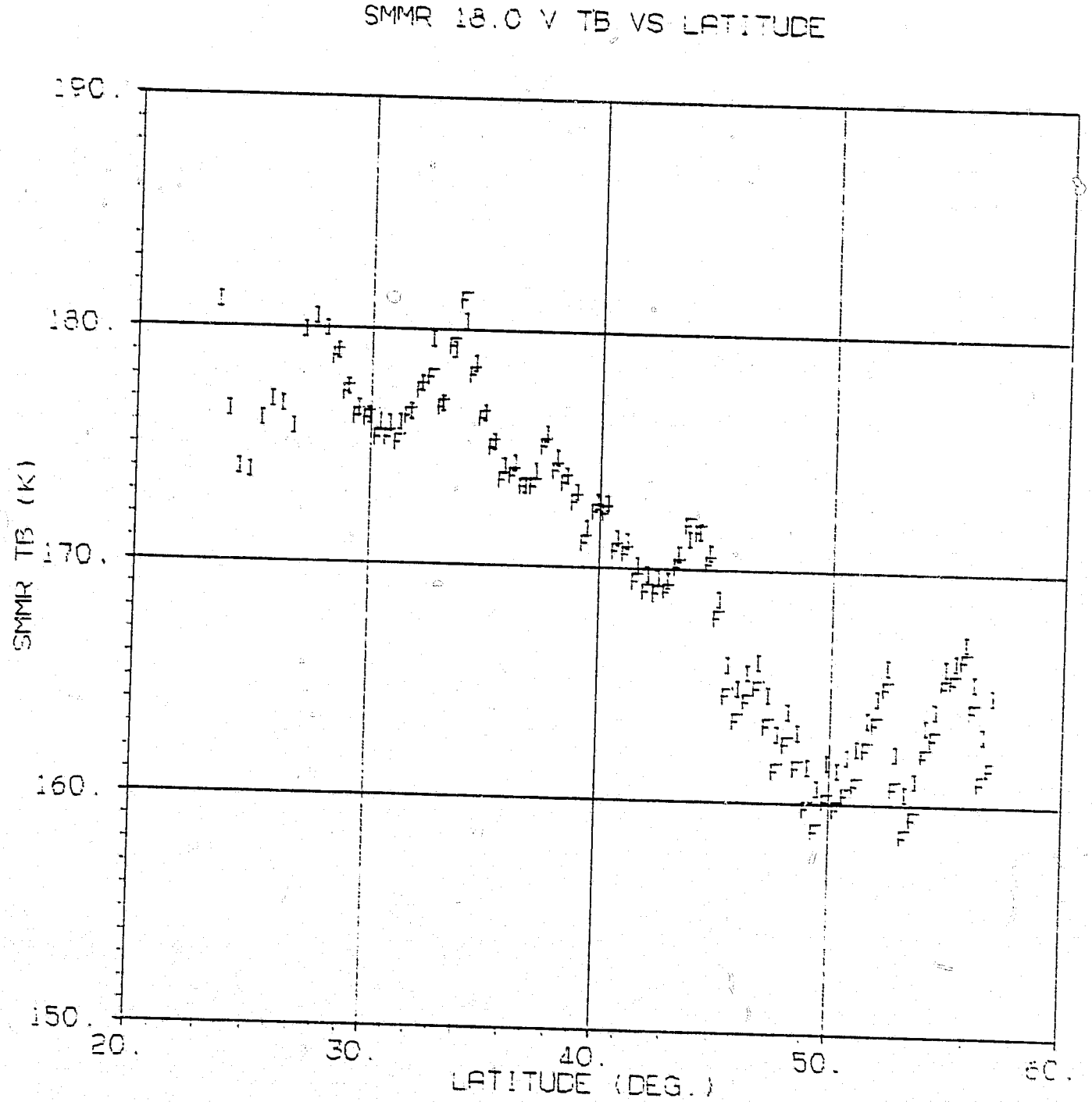

Orbit 1178, Grid 3, Column 1

Figure 2.6. Open Ocean, Cross and Interim

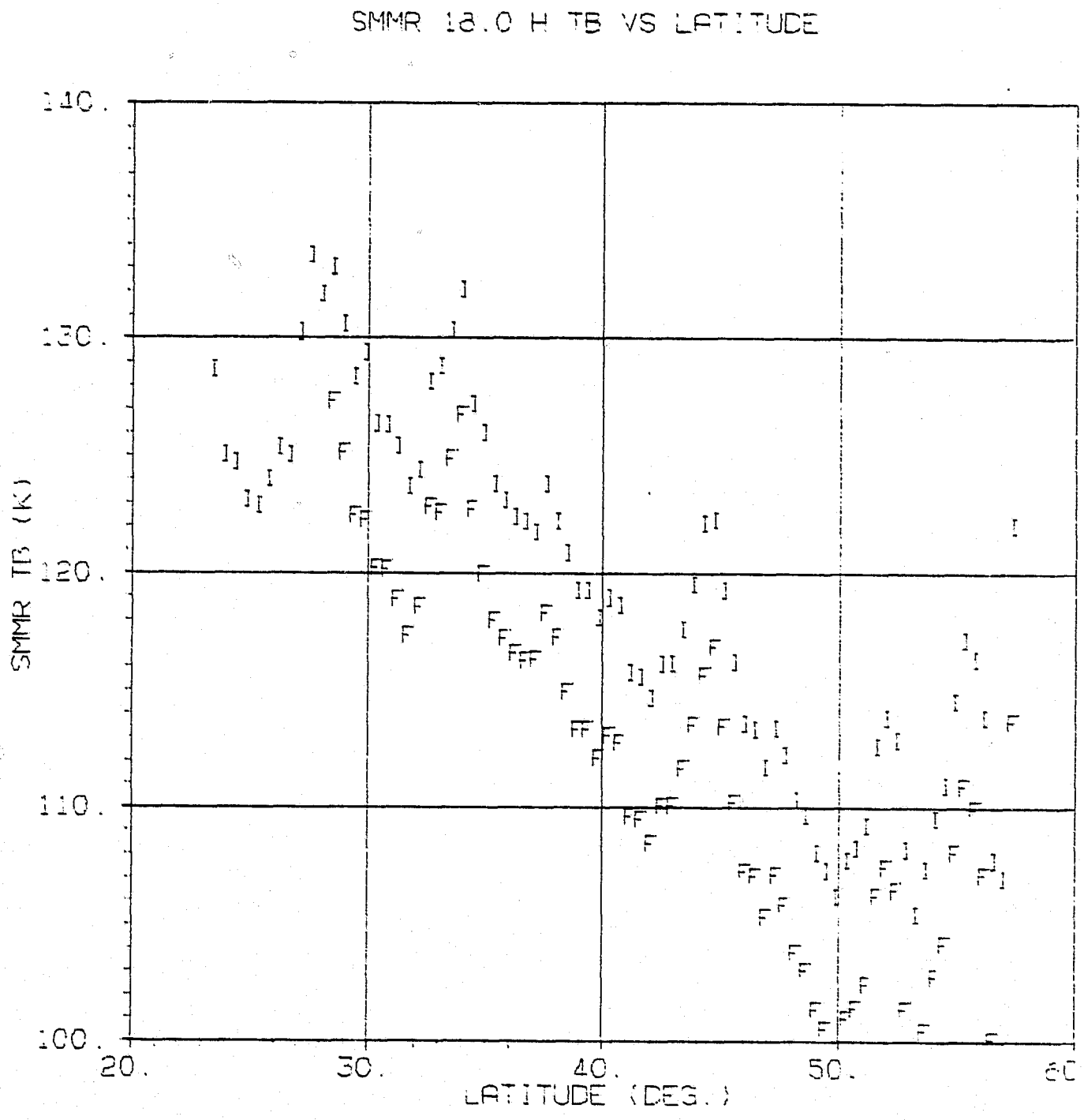

Orbit 1178, Grid 3, Column 1

Figure 2.7. Open Ocean, Cross and Interim

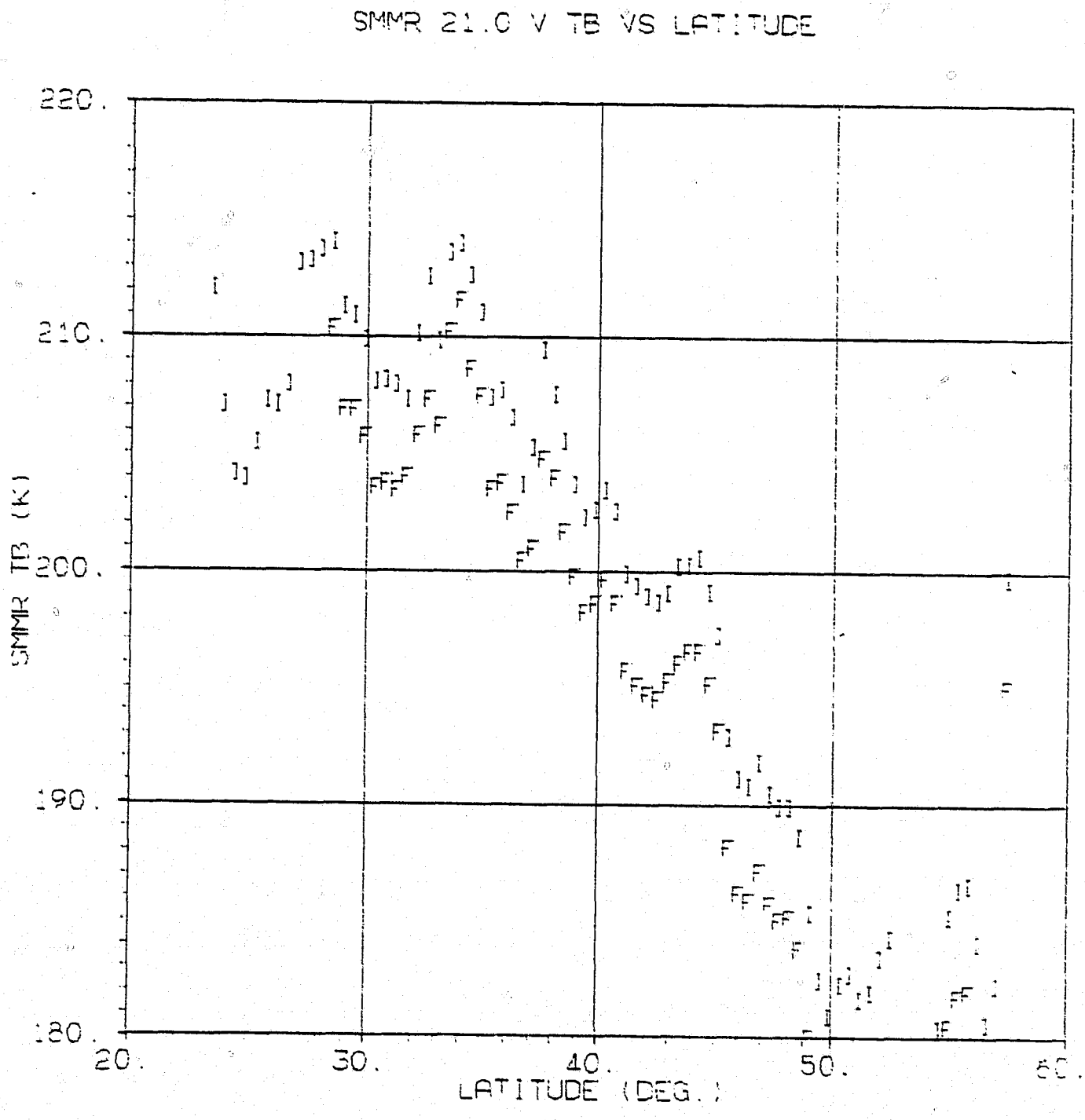

Orbit 1178, Grid 3, Column 1

Figure 2.8. Open Ocean, Cross and Interim

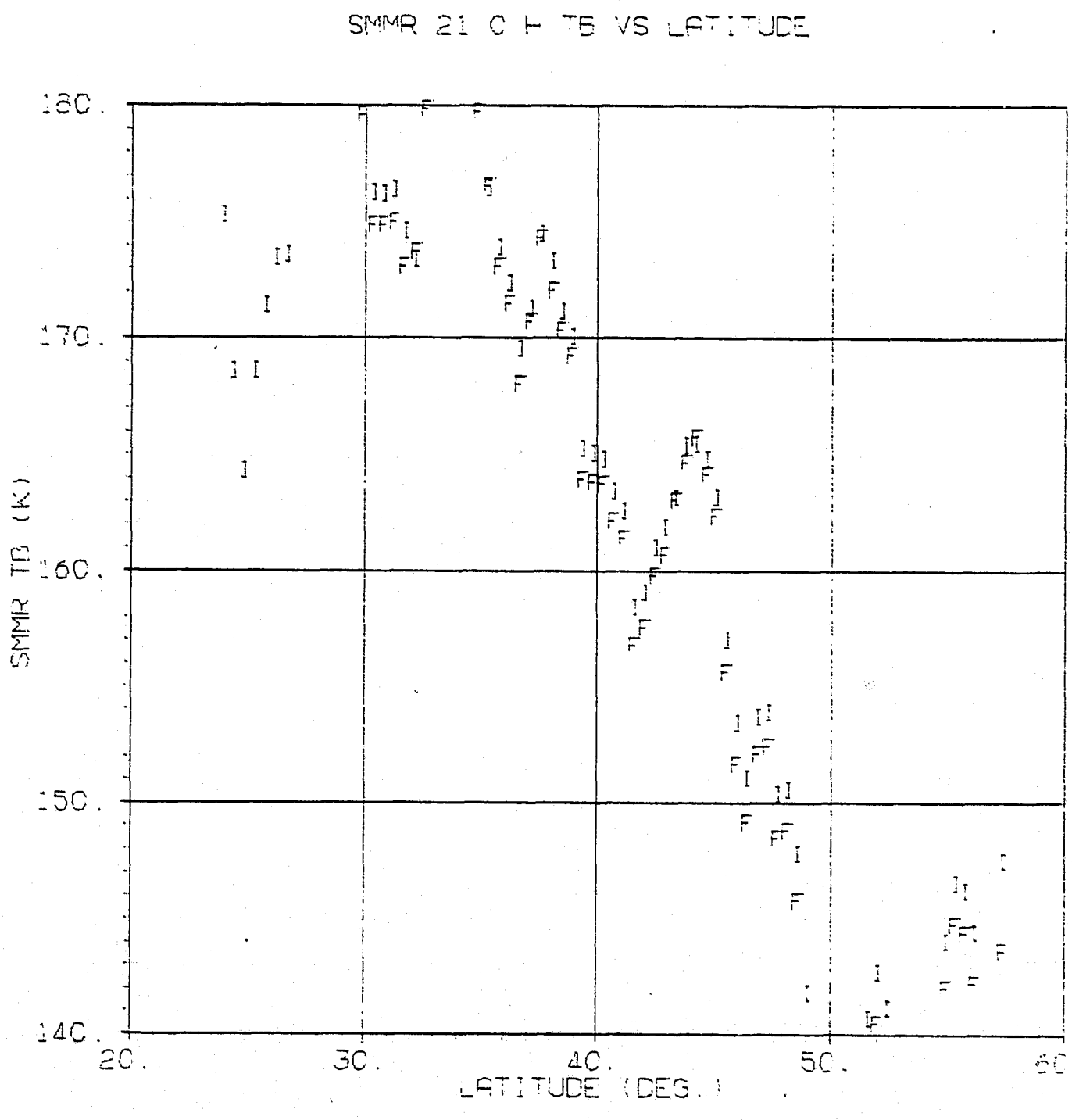

Orbit 1178, Grid 3, Column 1

Figure 2.9. Open Ocean, Cross and Interim

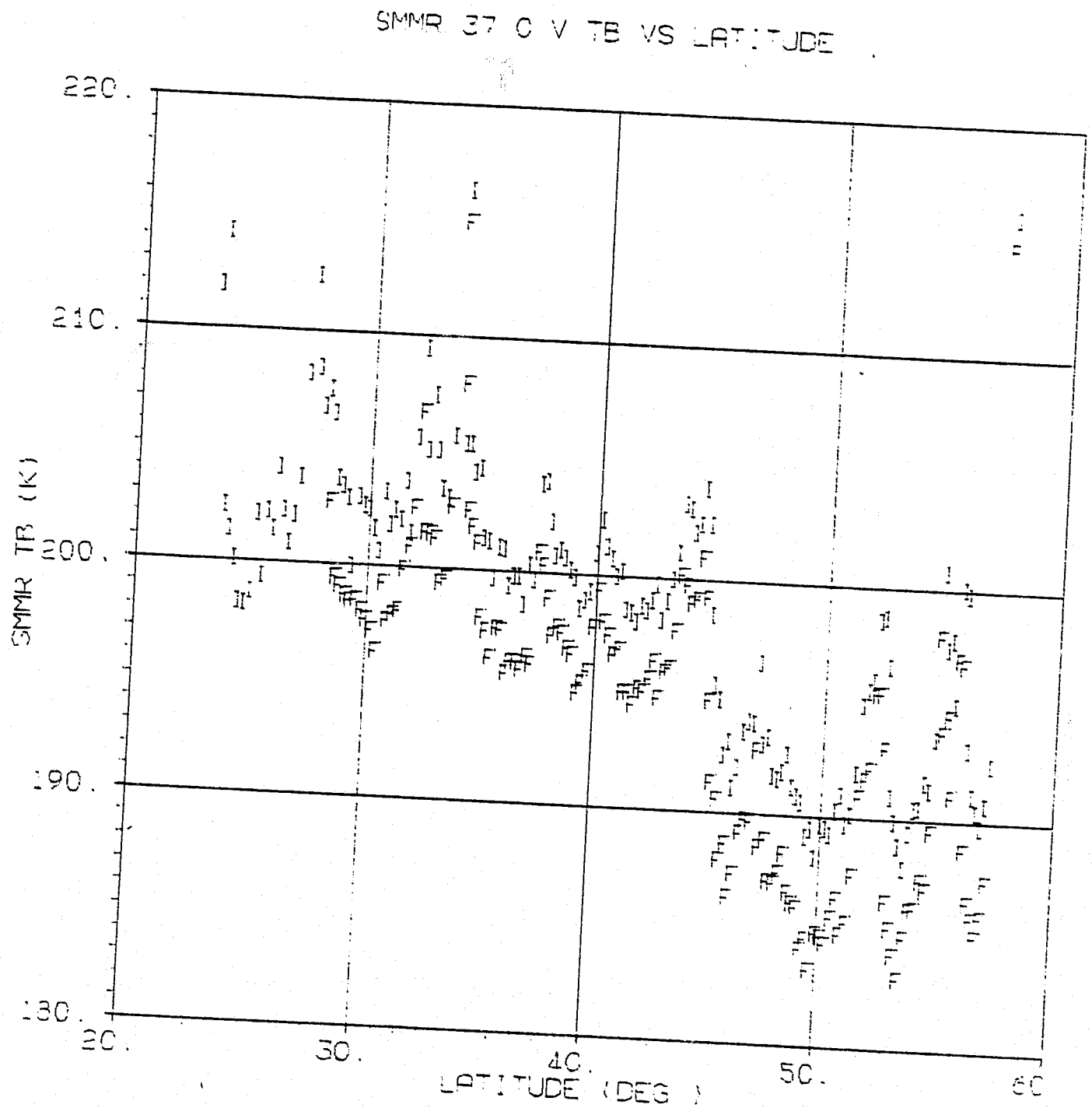

Orbit 1178, Grid 4, Column 1

Figure 2.10. Open Ocean, Cross and Interim

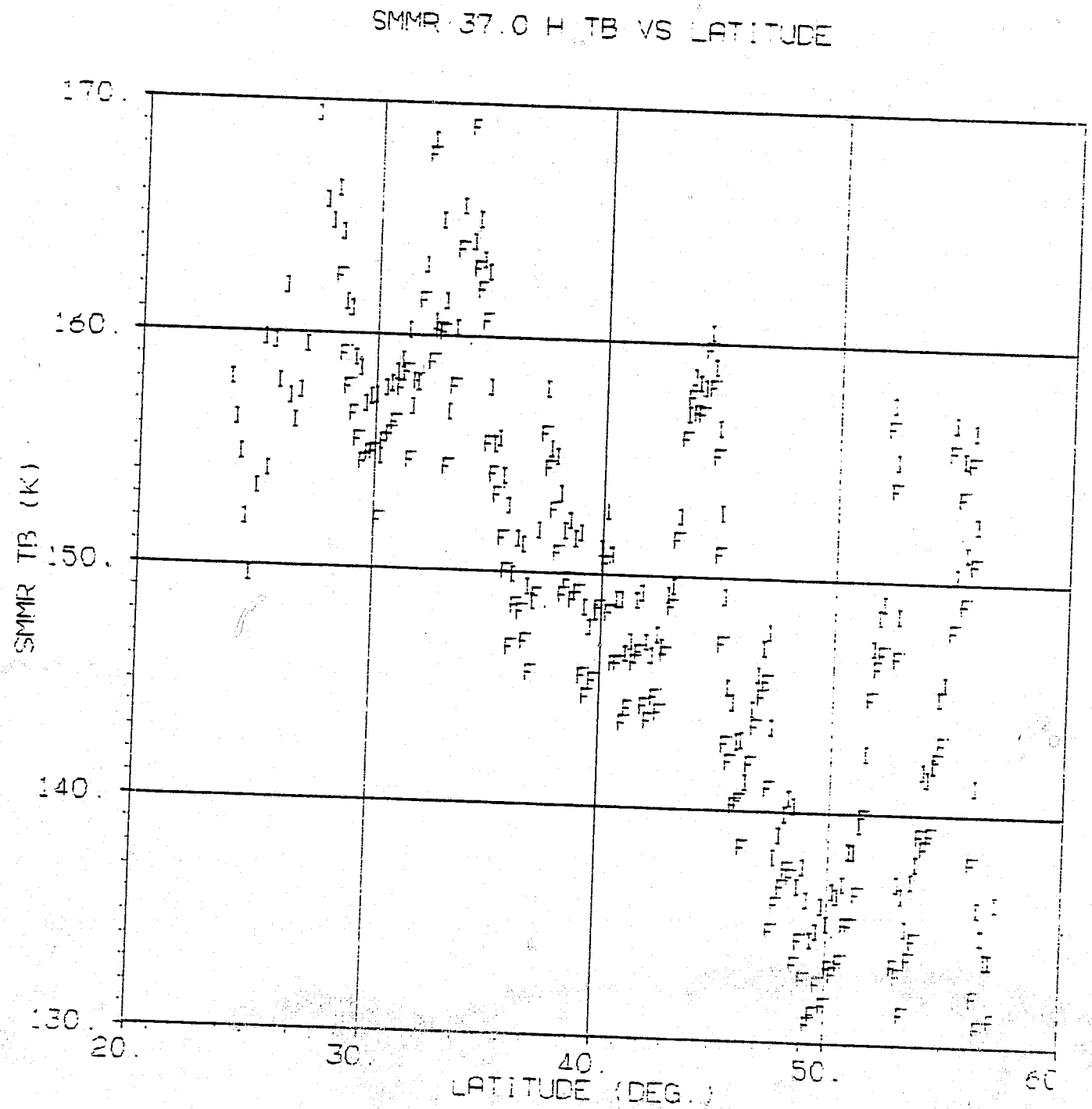

Orbit 1178, Grid 4, Column 1

Figure 3.1. Coastline Crossing, Nominal and Interim

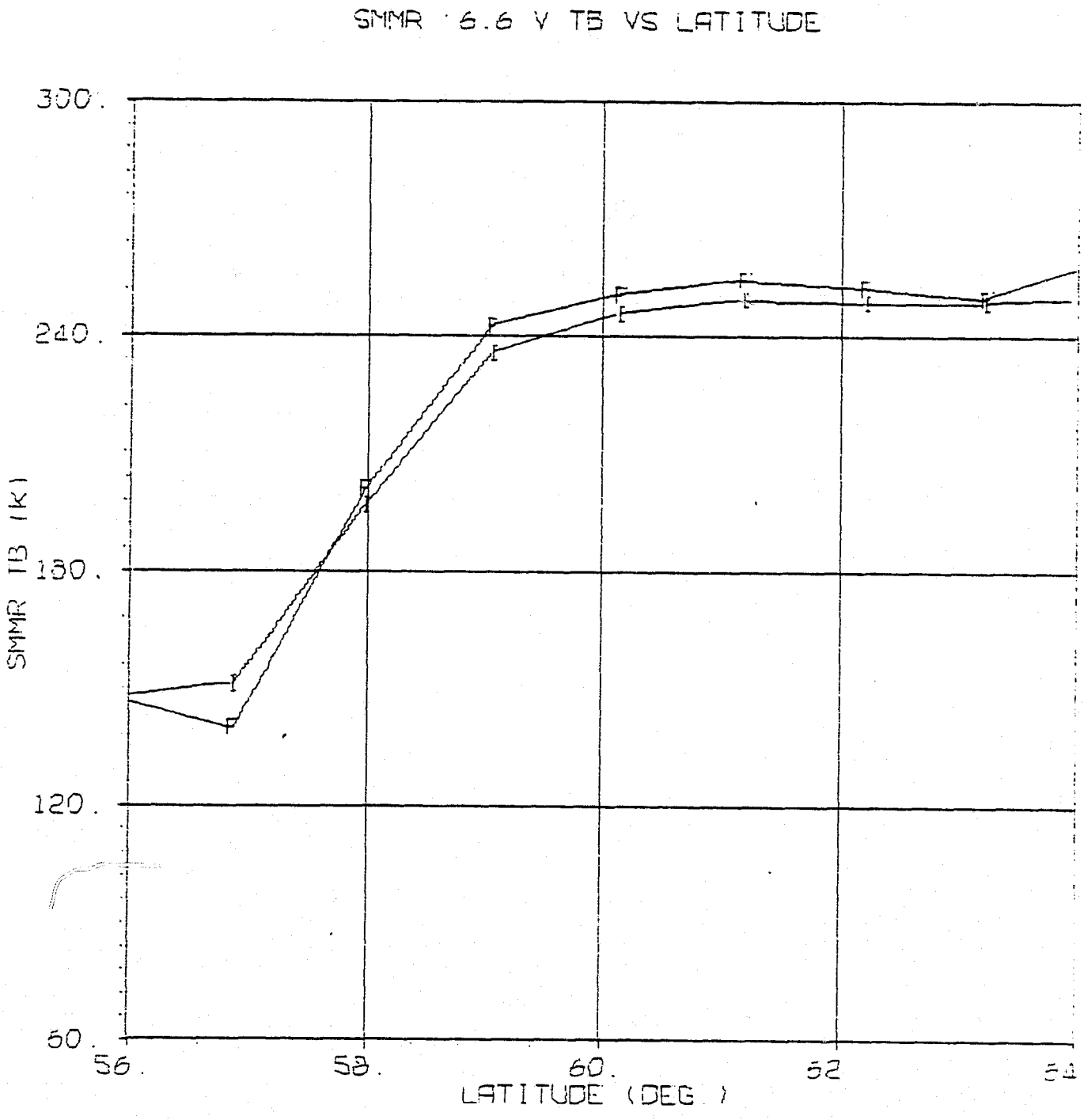

Orbit 1178, Grid 1, Column 1

Figure 3.2. Coastline Crossing, Nominal and Interim

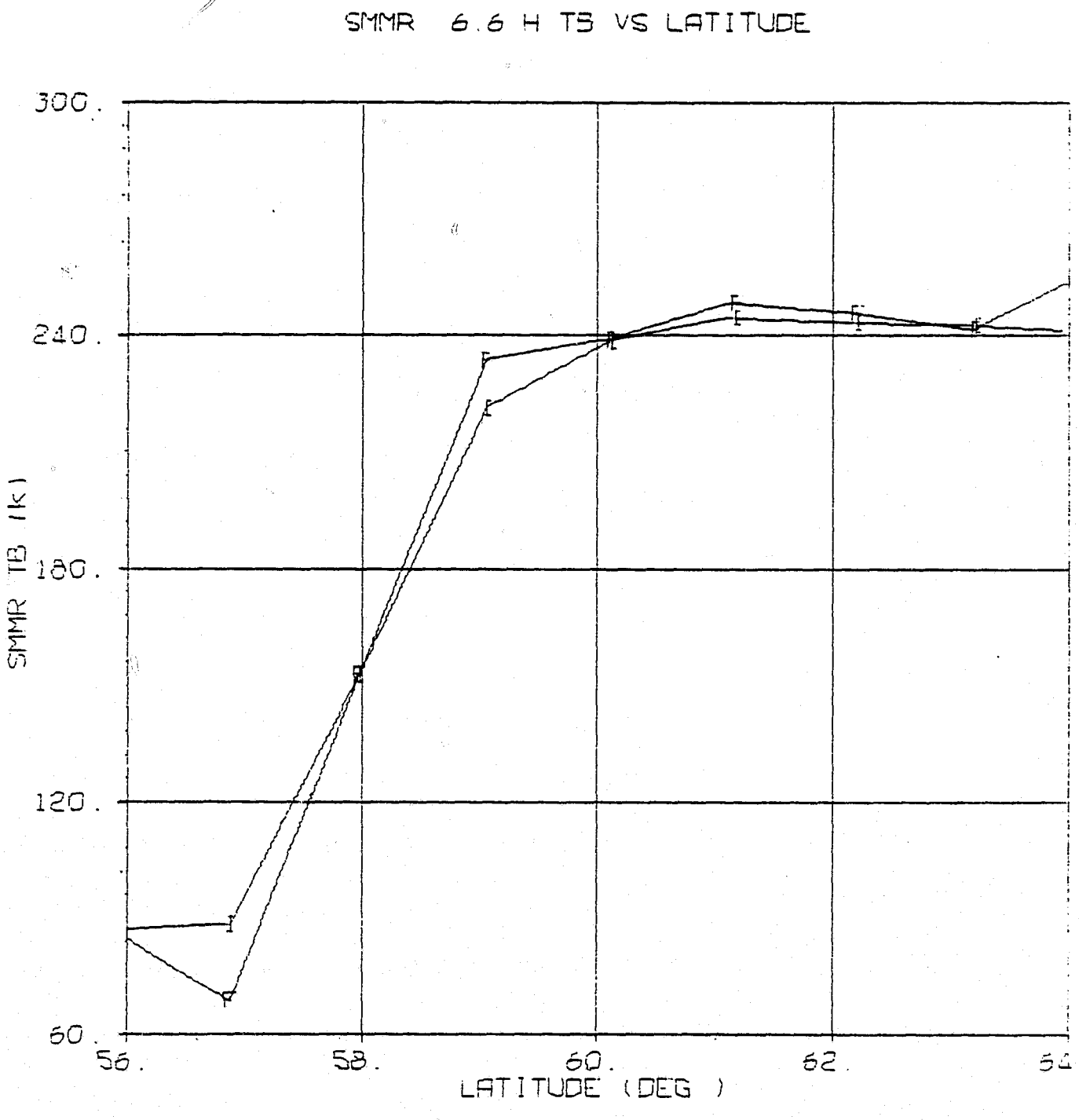

Orbit 1178, Grid 1, Column 1

Figure 3.3. Coastline Crossing, Nominal and Interim

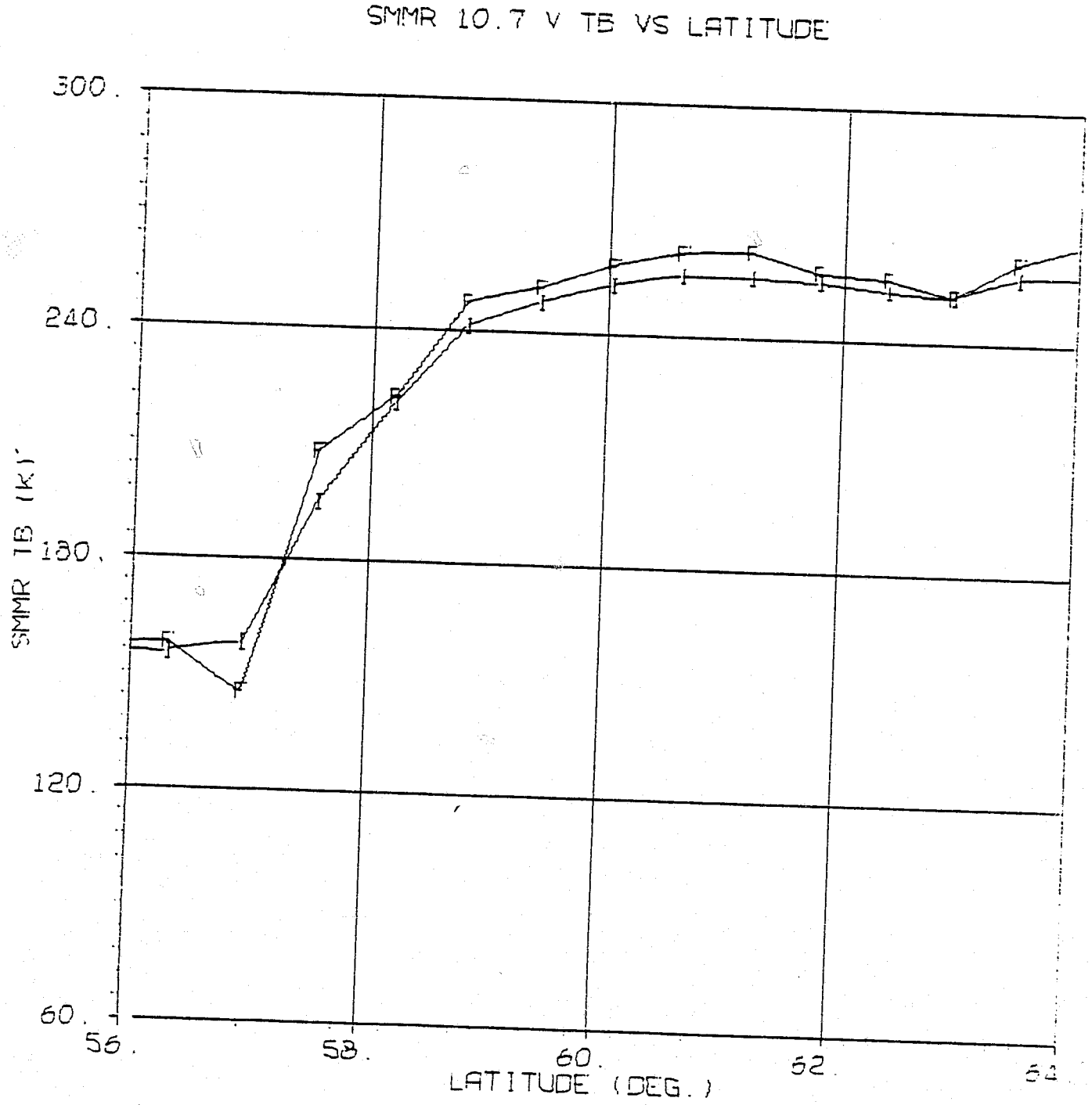

Orbit 1178, Grid 2, Column 1

Figure 3.4. Coastline Crossing, Nominal and Interim

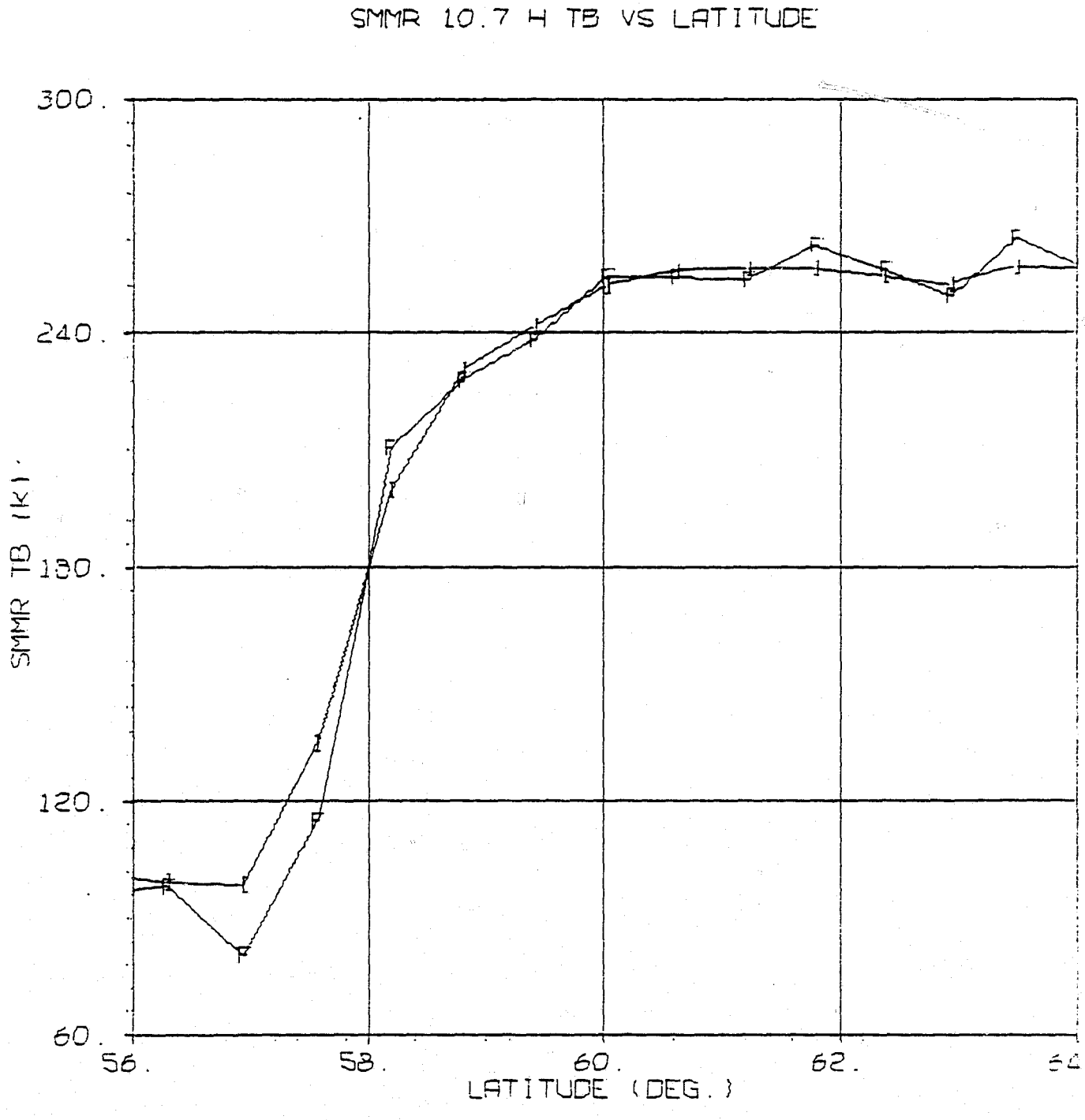

Orbit 1178, Grid 2, Column 1

Figure 3.5. Coastline Crossing, Nominal and Interim

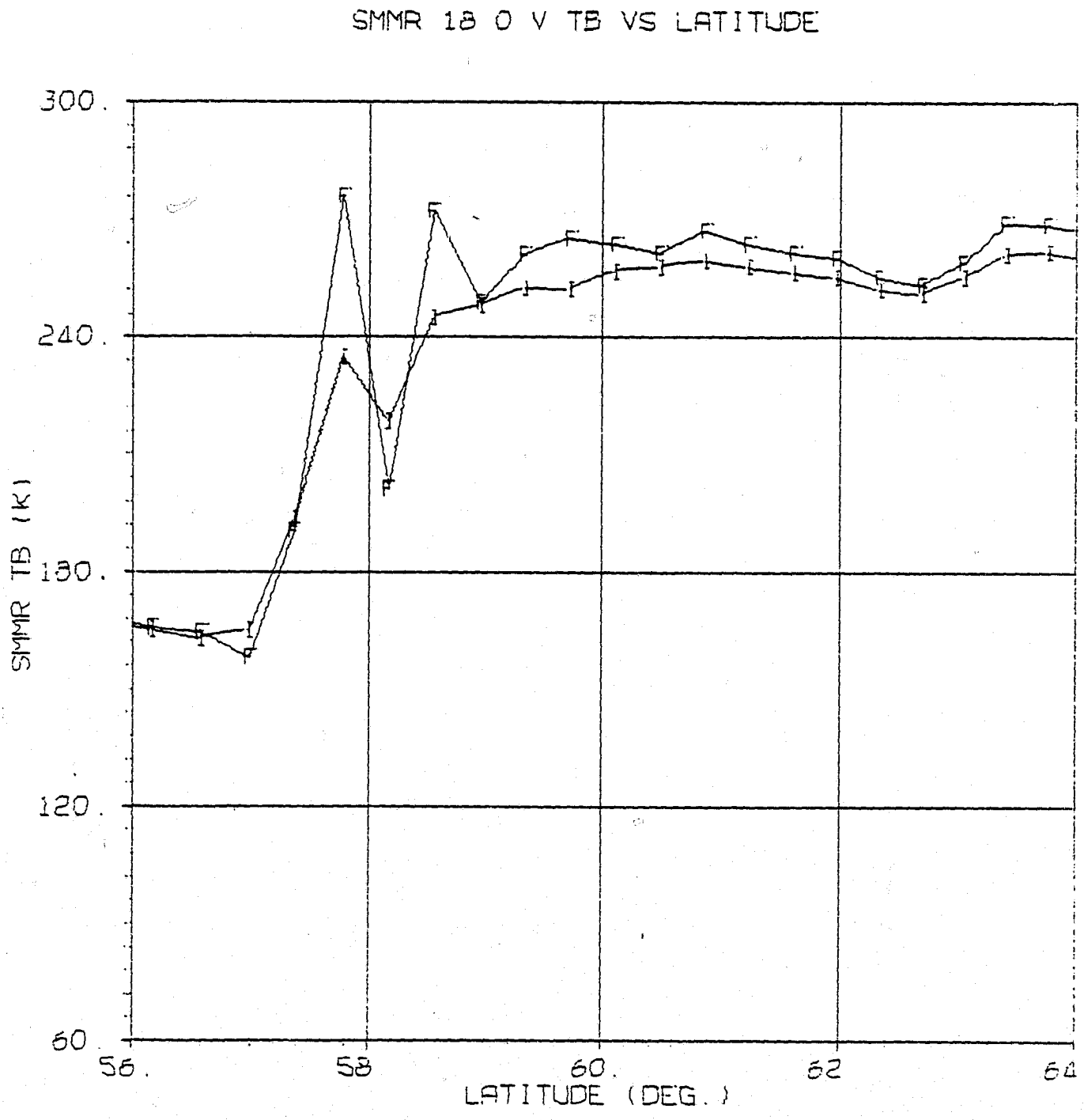

Orbit 1178, Grid 3, Column 1

Figure 3.6. Coastline Crossing, Nominal and Interim

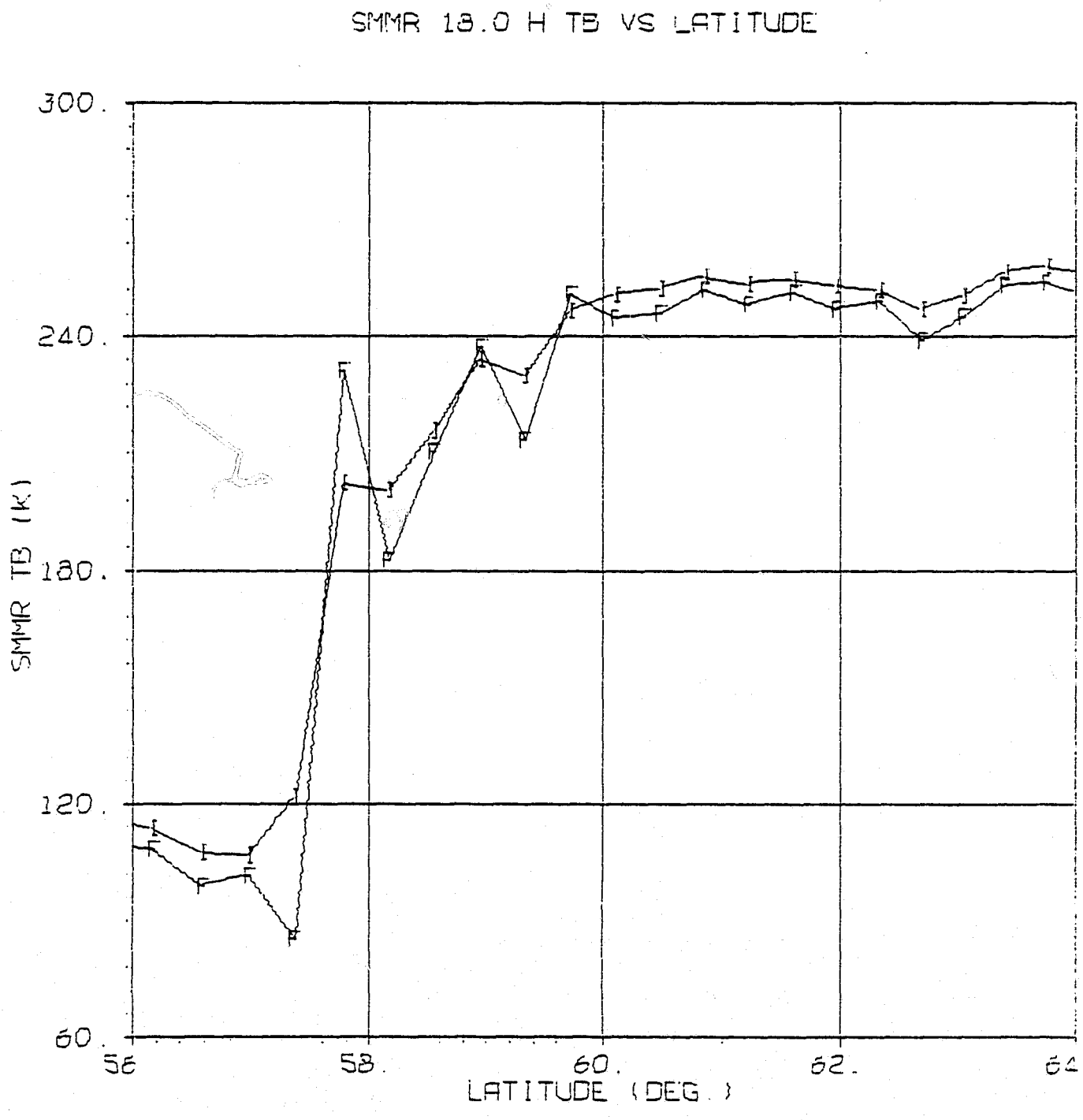

Orbit 1178, Grid 3, Column 1

Figure 3.7. Coastline Crossing, Nominal and Interim

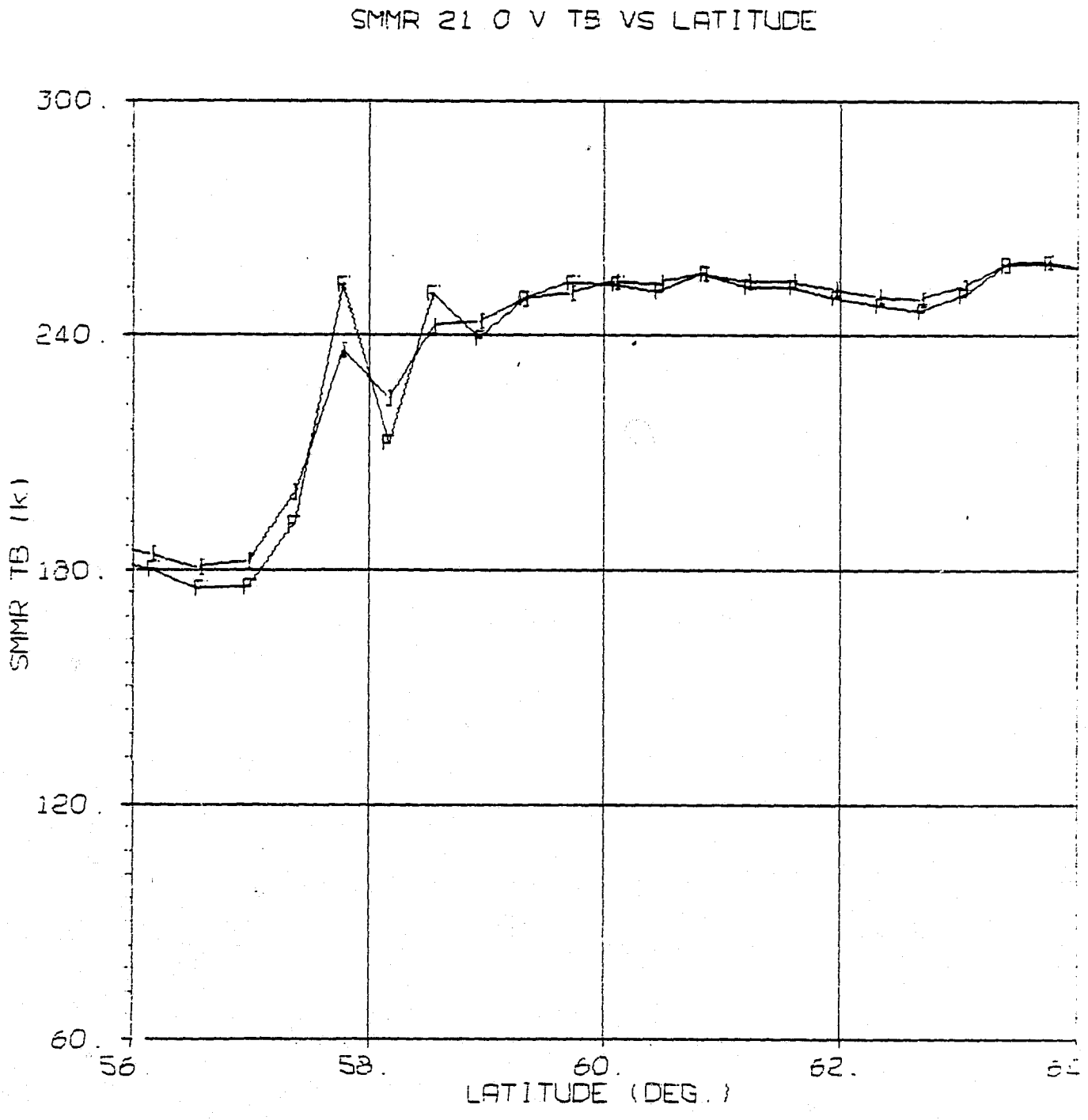

Orbit 1178, Grid 3, Column 1

Figure 3.8. Coastline Crossing, Nominal and Interim

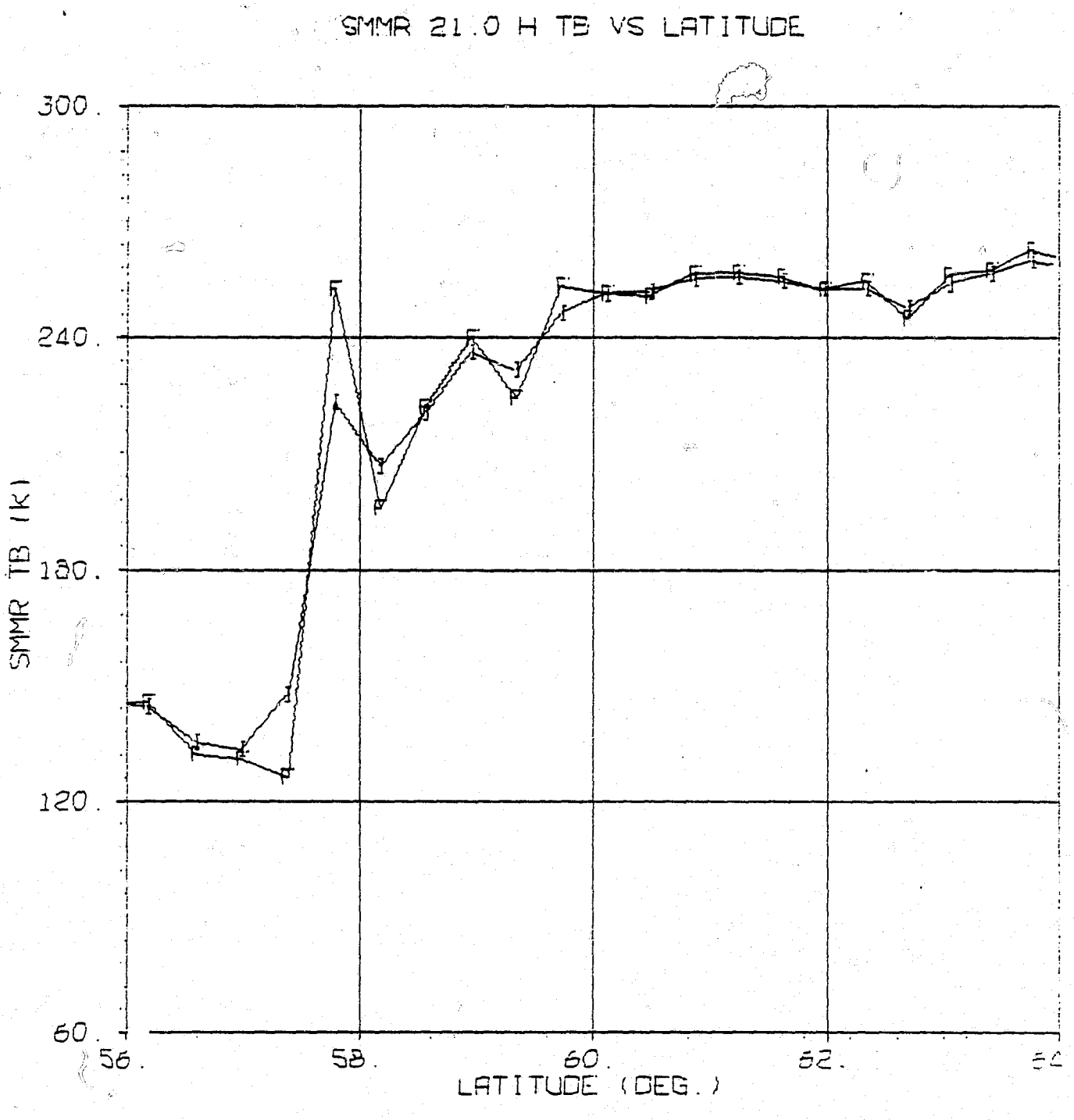

Orbit 1178, Grid 3, Column 1

Figure 3.9. Coastline Crossing, Nominal and Interim

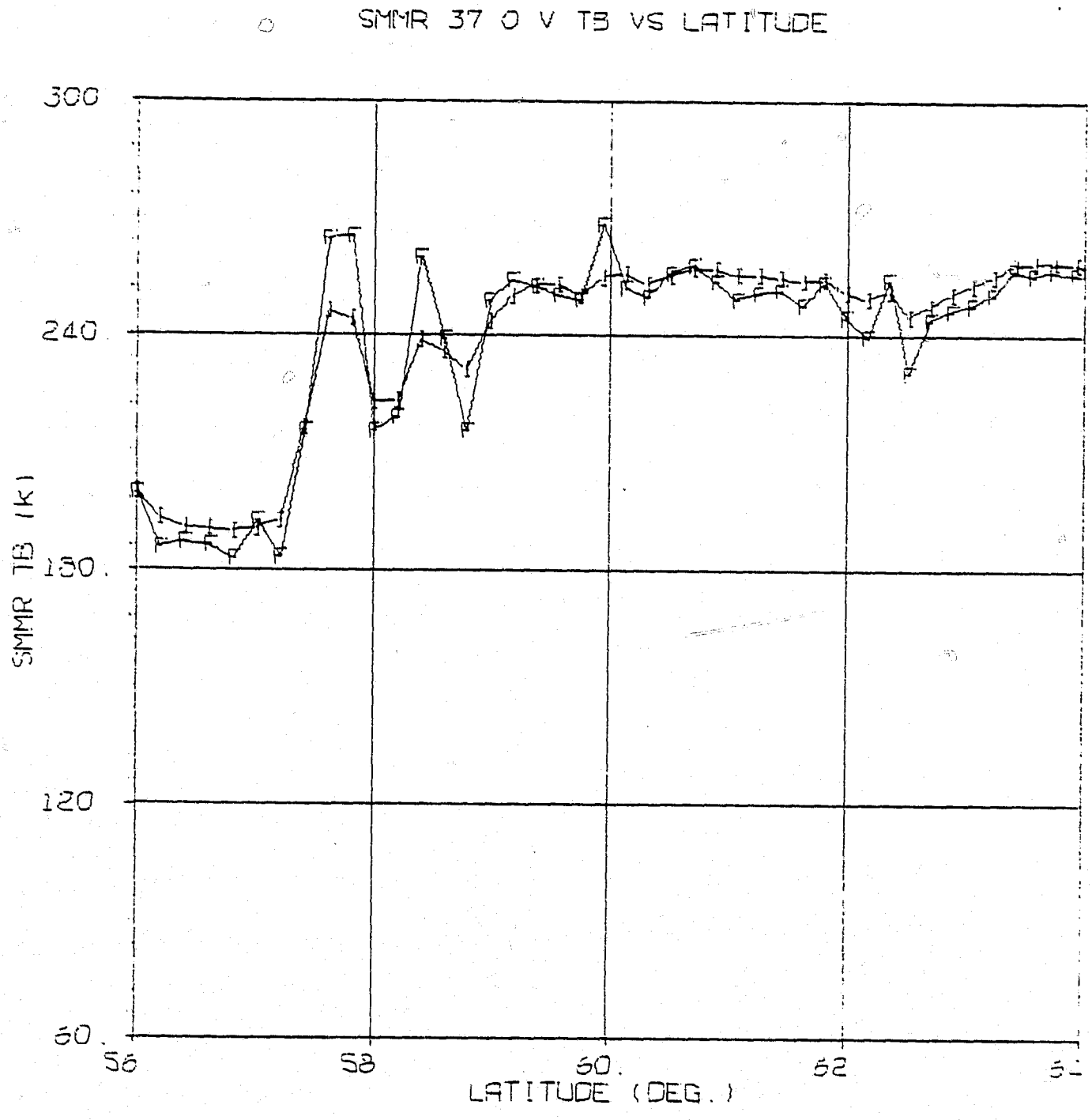

Orbit 1178, Grid 4, Column 1

Figure 3.10. Coastline Crossing, Nominal and Interim

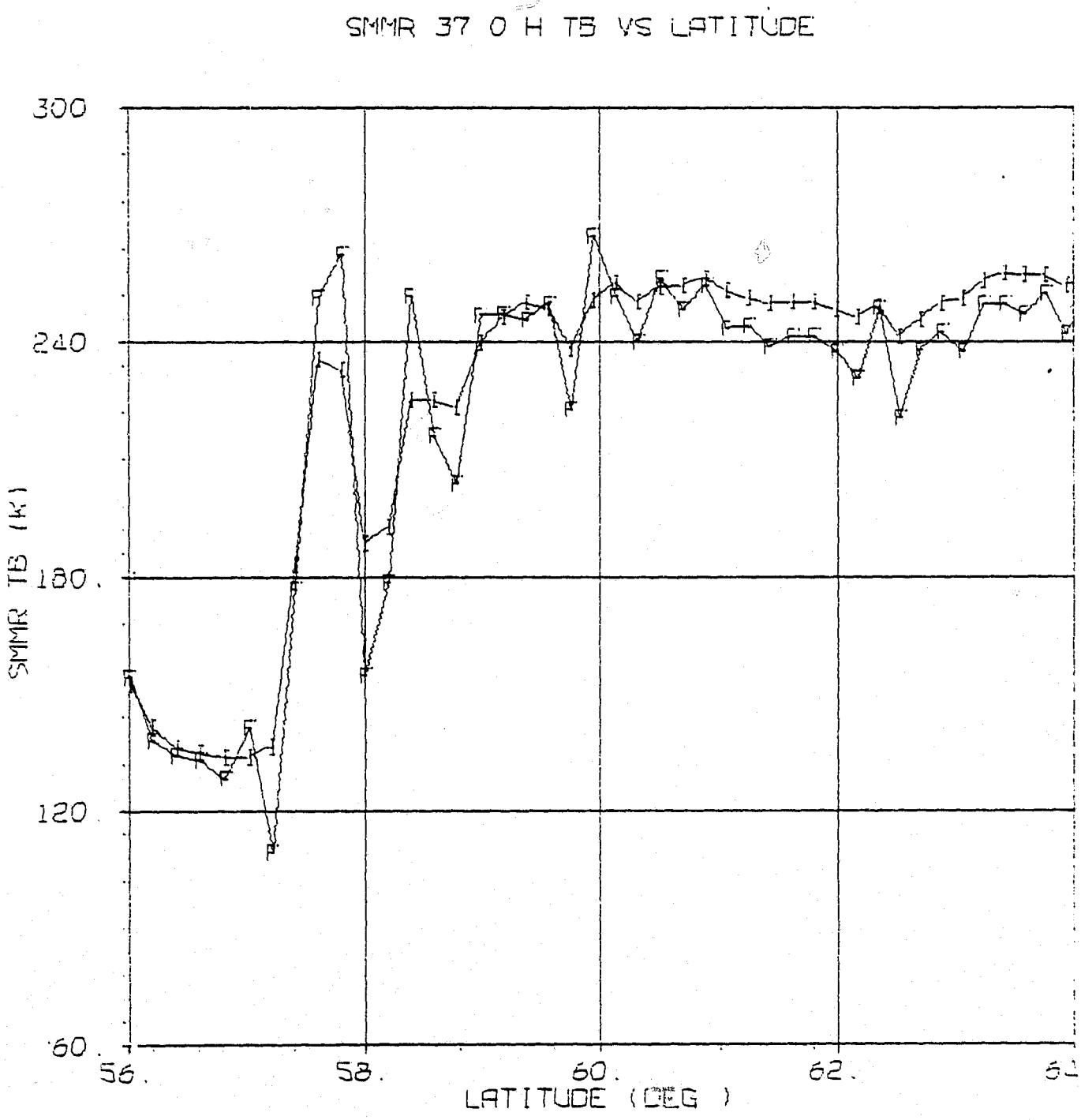

Orbit 1178, Grid 4, Column 1

Figure 4.1. Coastline Crossing, Cross and Interim

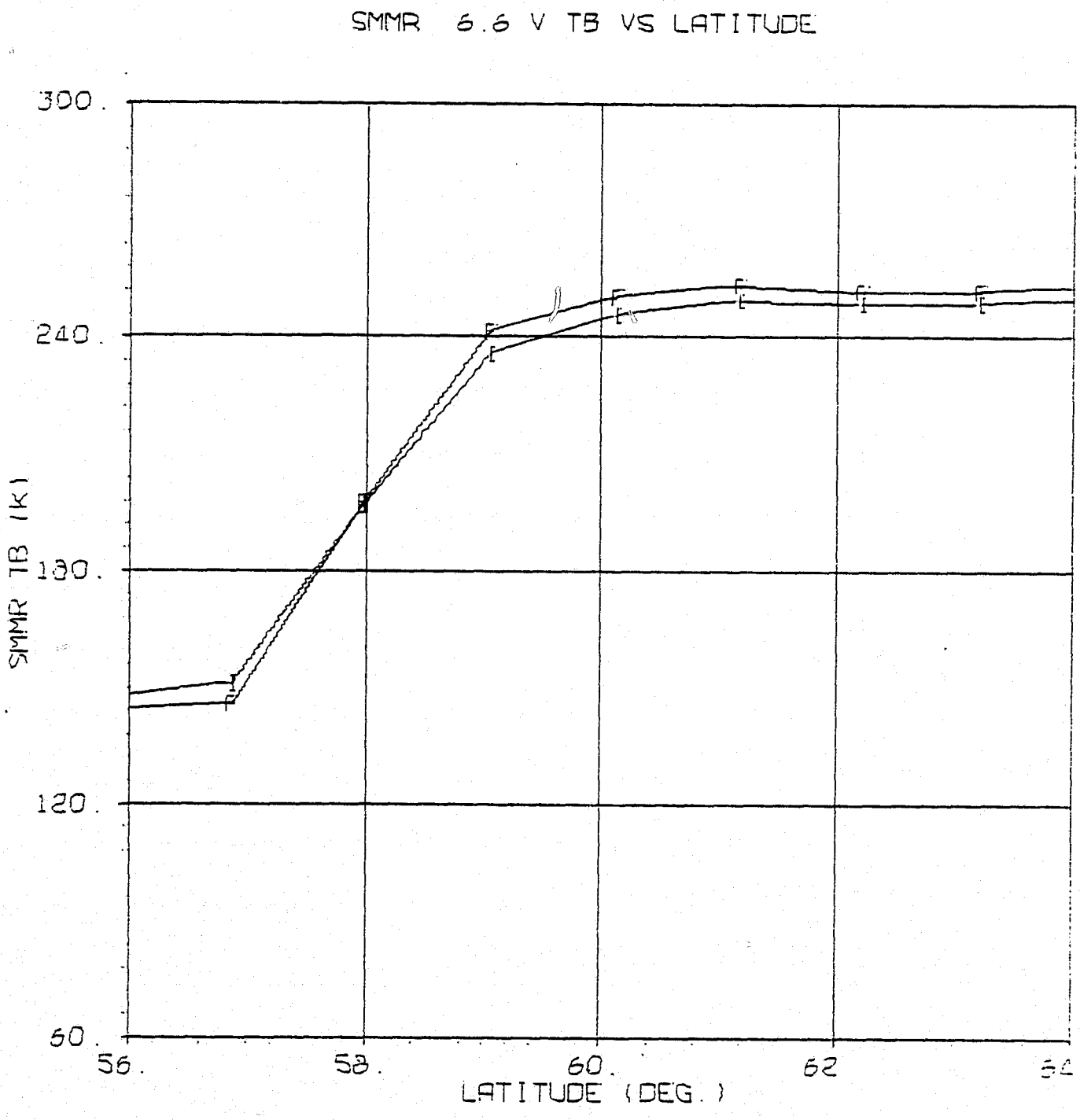

Orbit 1178, Grid 1, Column 1

Figure 4.2. Coastline Crossing, Cross and Interim

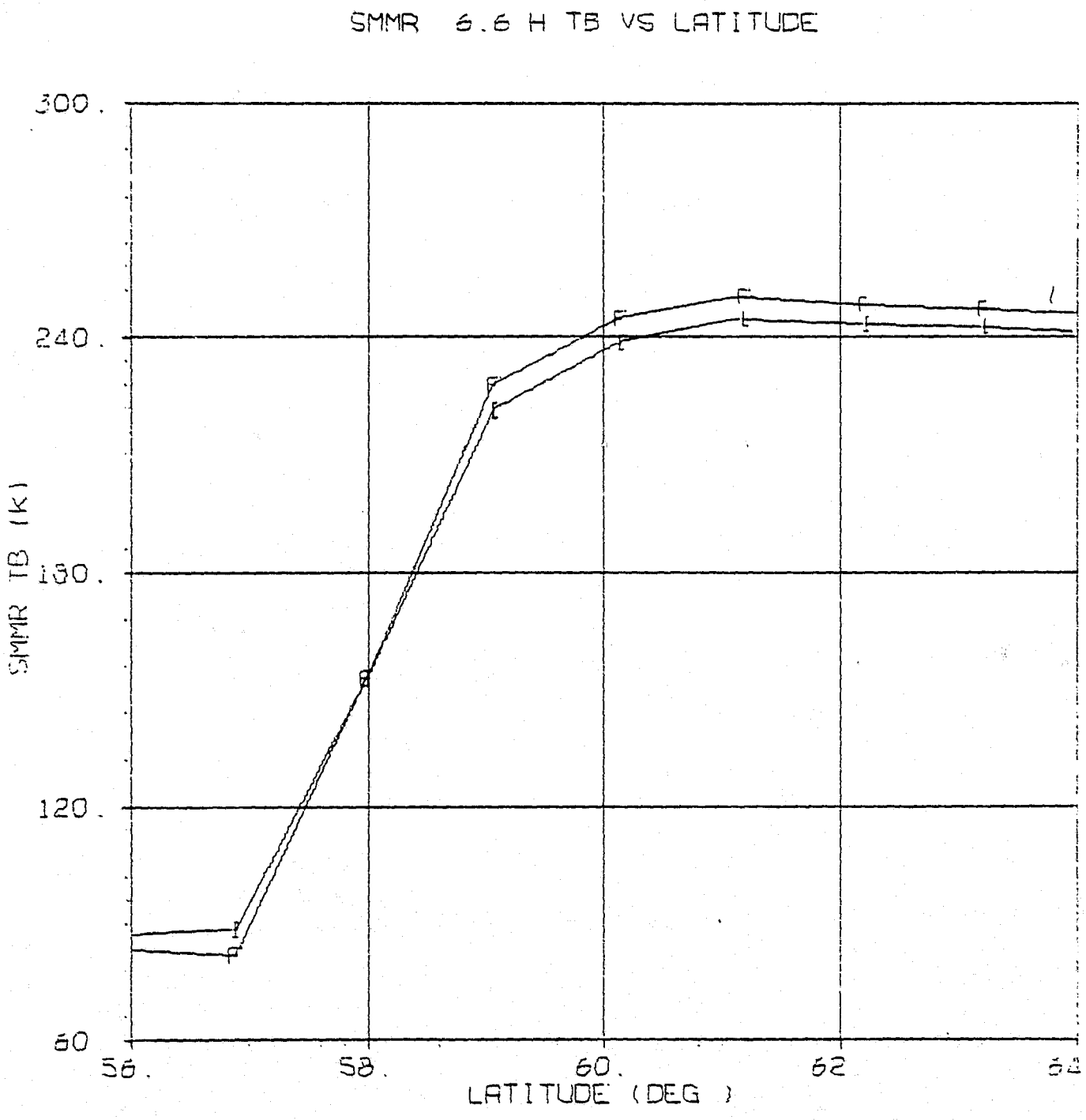

Orbit 1178, Grid 1, Column 1

Figure 4.3. Coastline Crossing, Cross and Interim

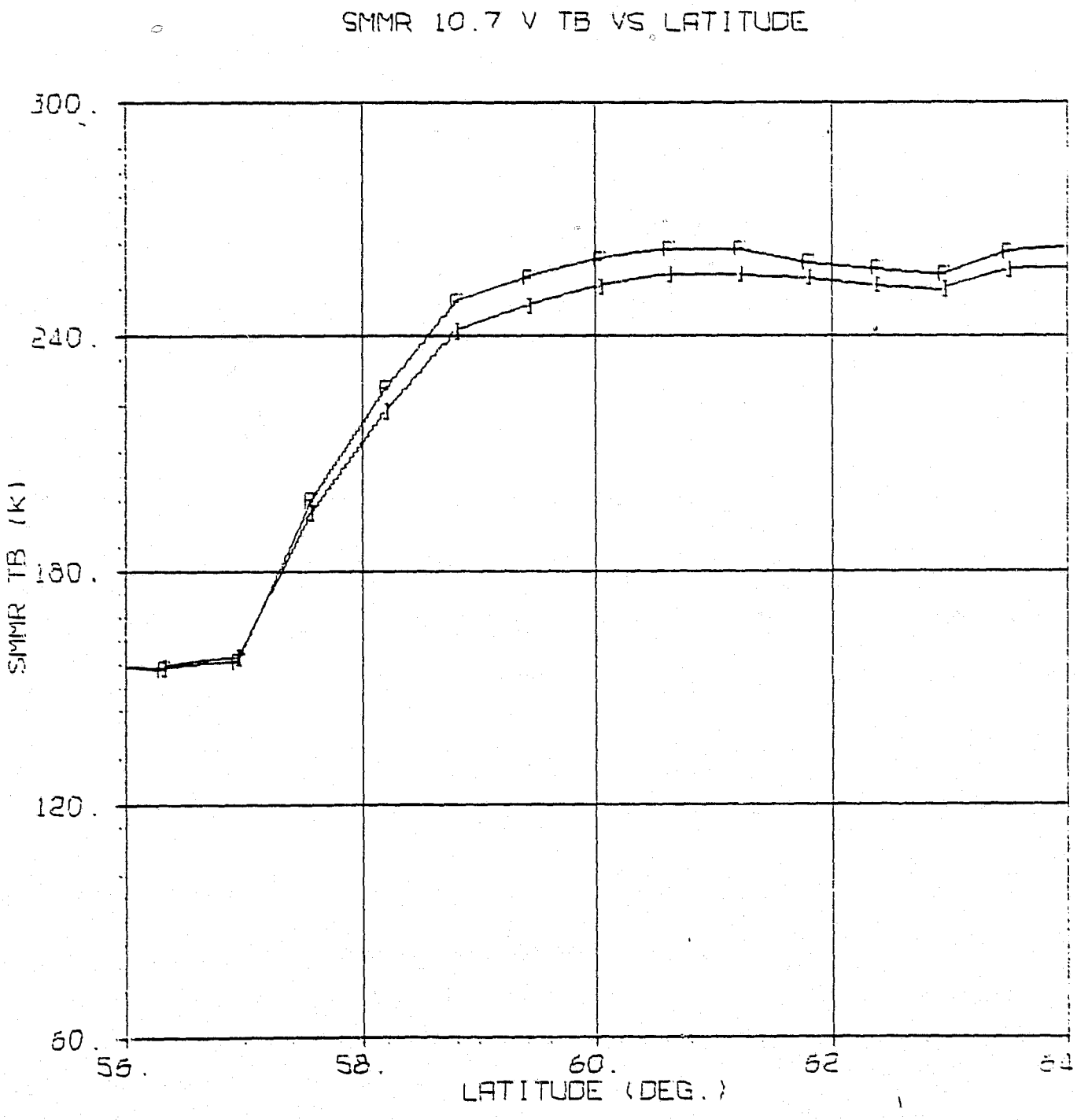

Orbit 1178, Grid 2, Column 1

Figure 4.4. Coastline Crossing, Cross and Interim

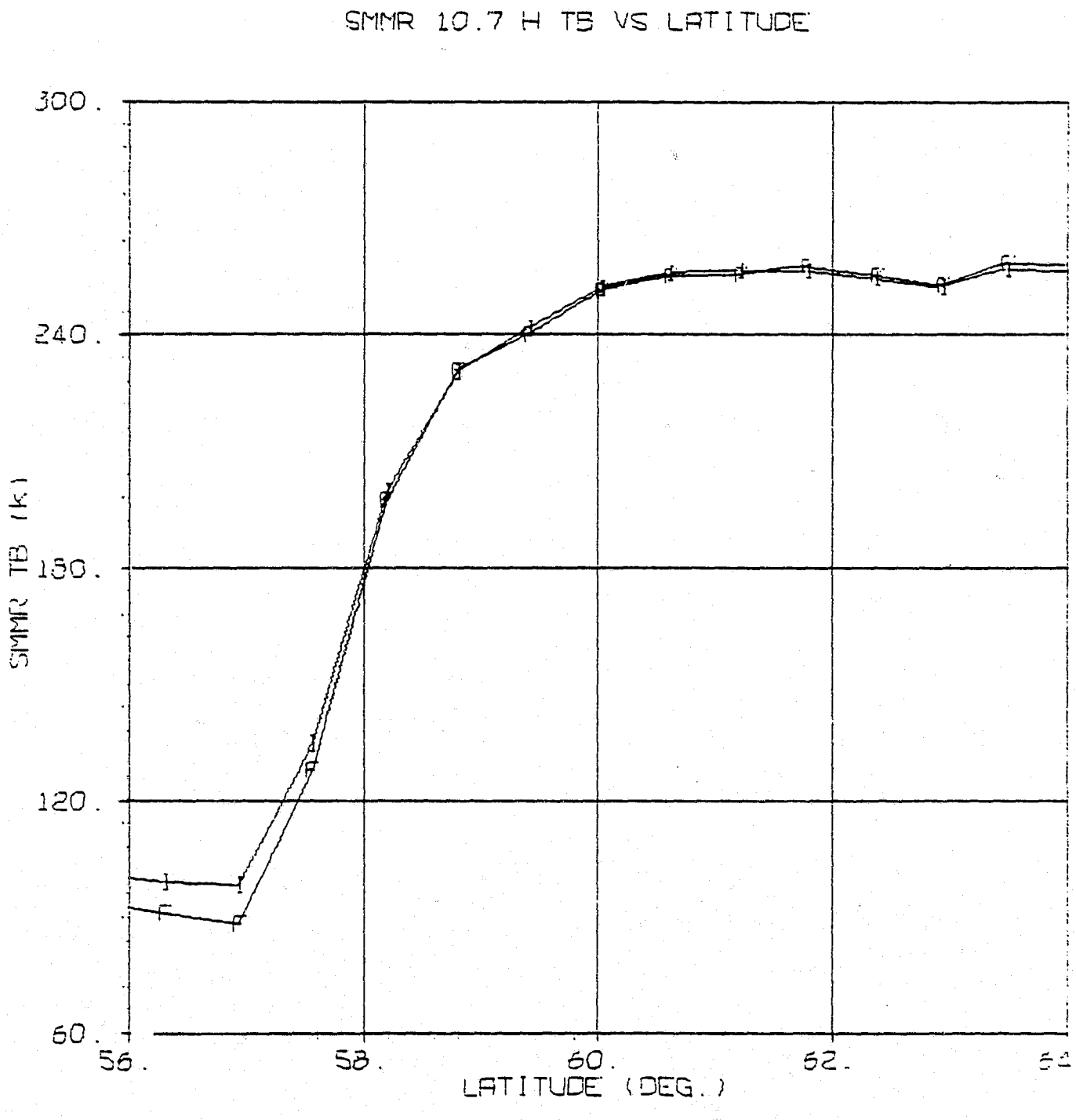

Orbit 1178, Grid 2, Column 1

Figure 4.5. Coastline Crossing, Cross and Interim

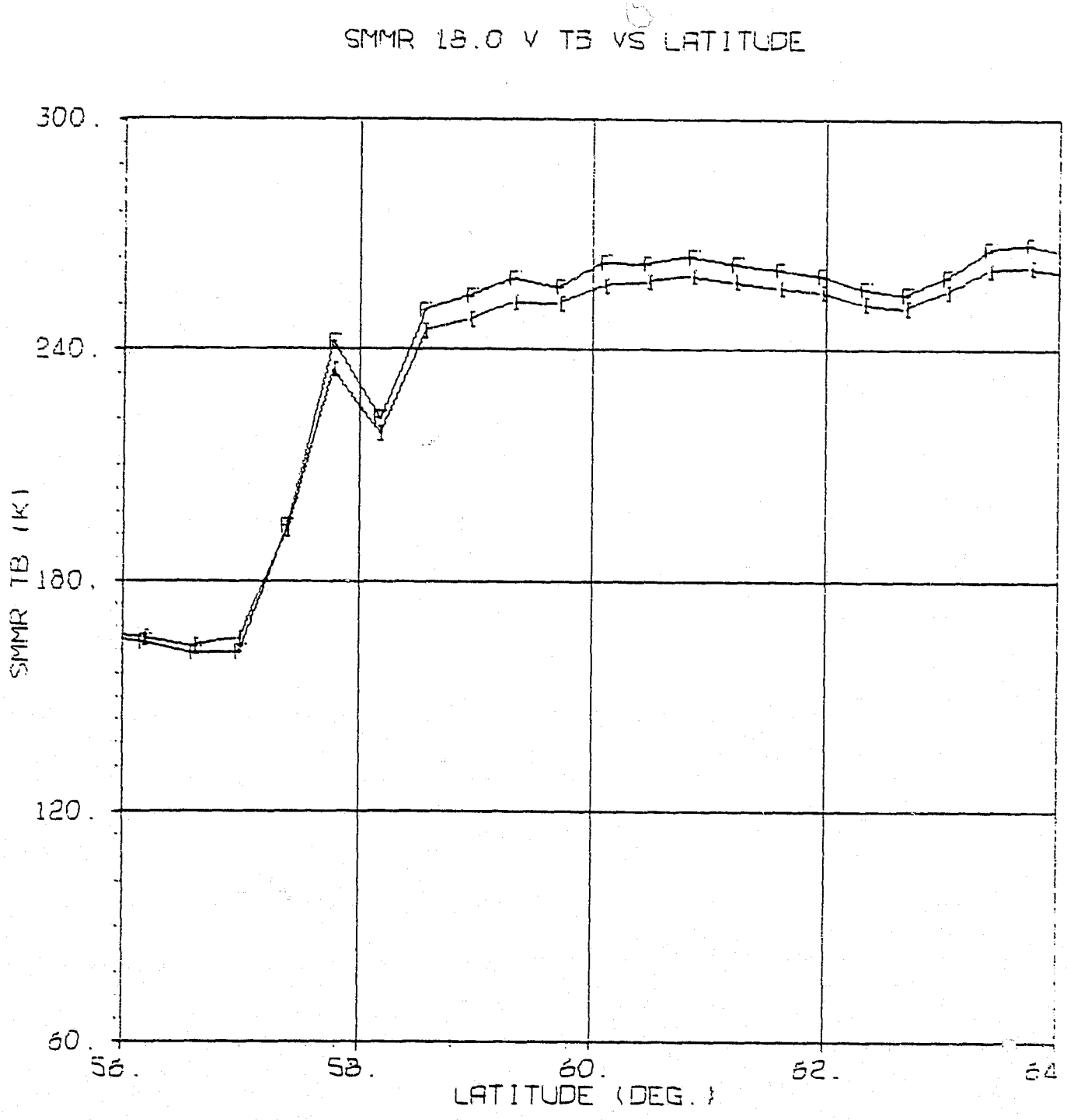

Orbit 1178, Grid 3, Column 1

Figure 4.6. Coastline Crossing, Cross and Interim

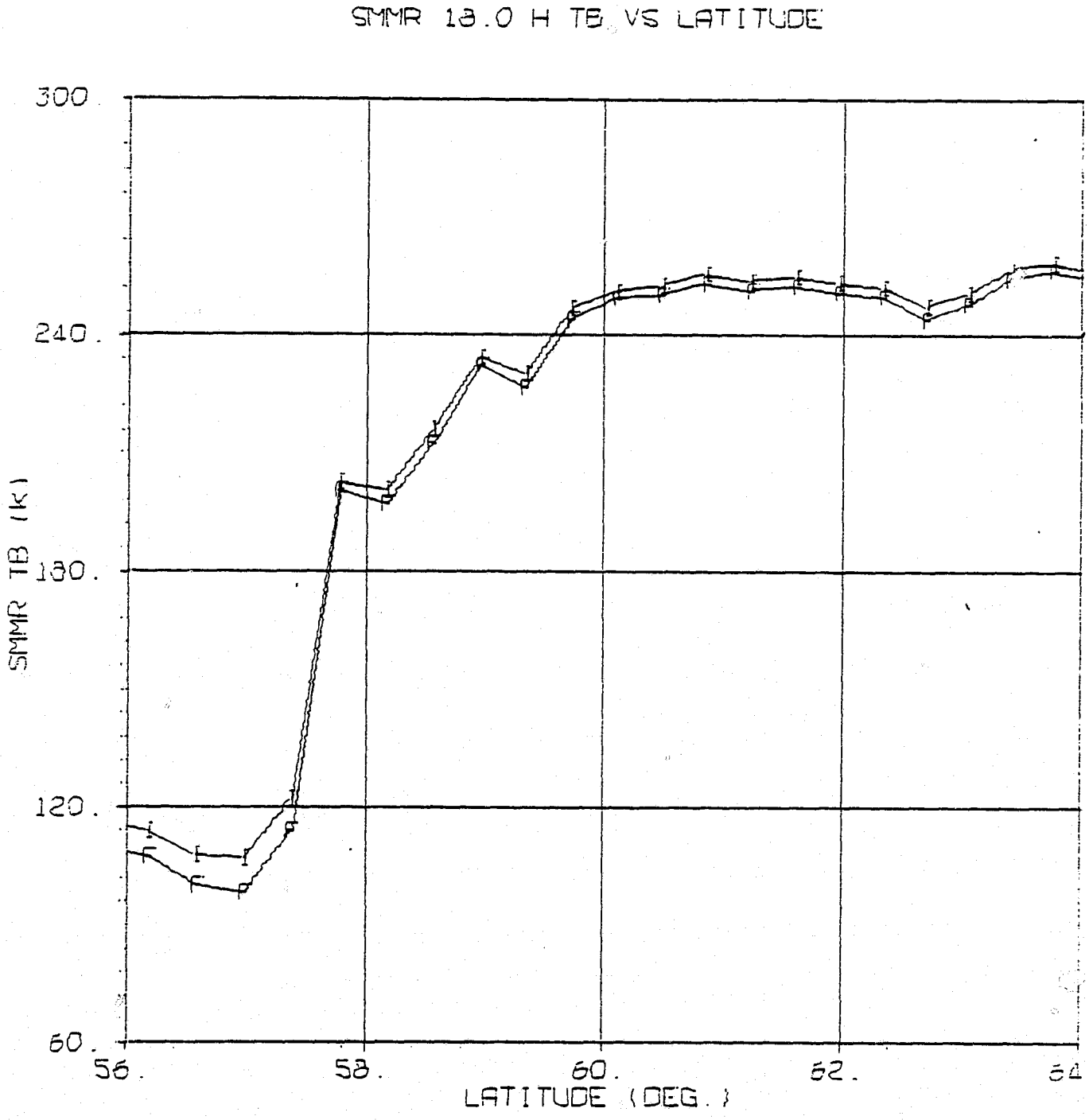

Orbit 1178, Grid 3, Column 1

Figure 4.7. Coastline Crossing, Cross and Interim

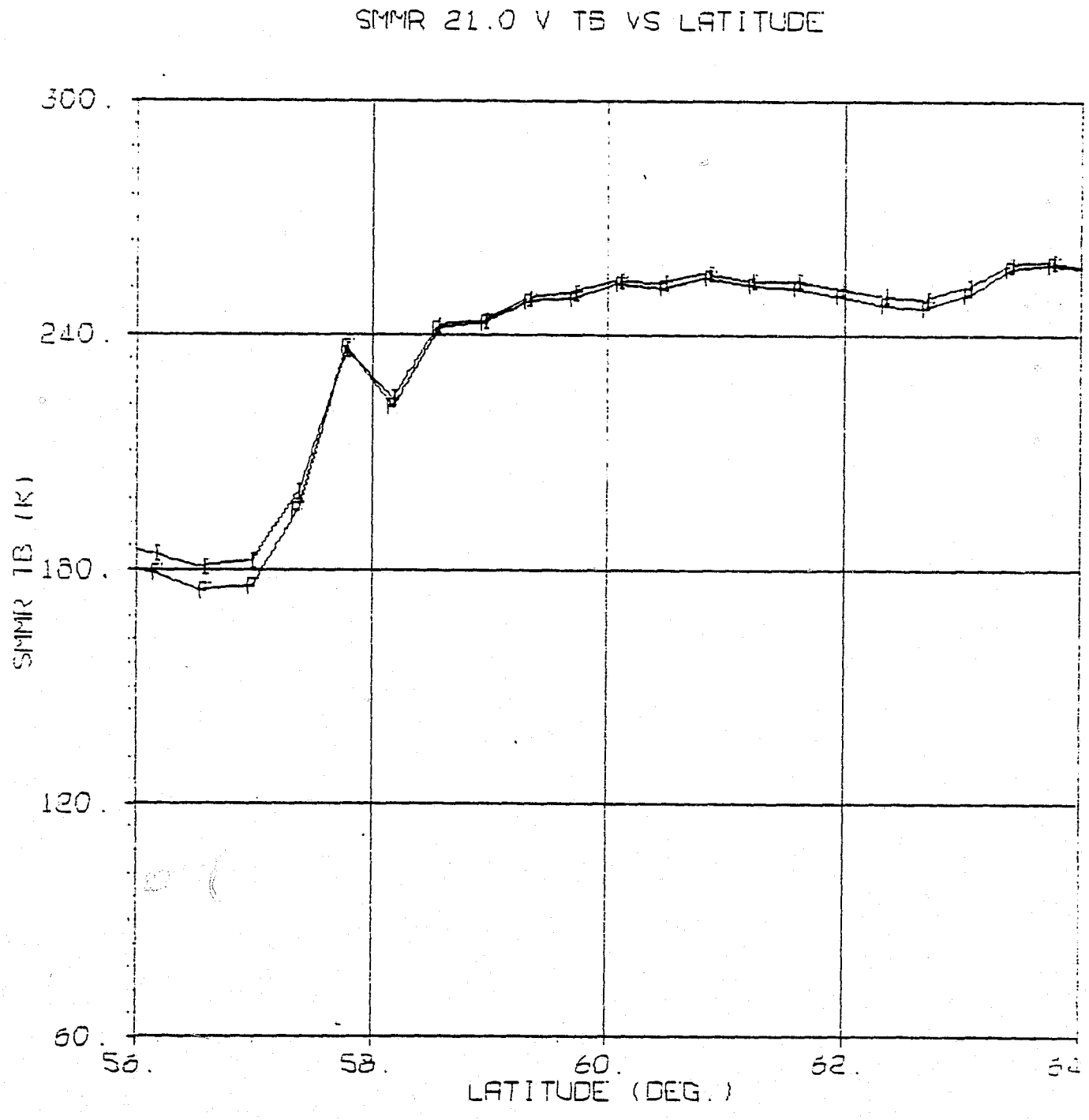

Orbit 1178, Grid 3, Column 1

Figure 4.8. Coastline Crossing, Cross and Interim

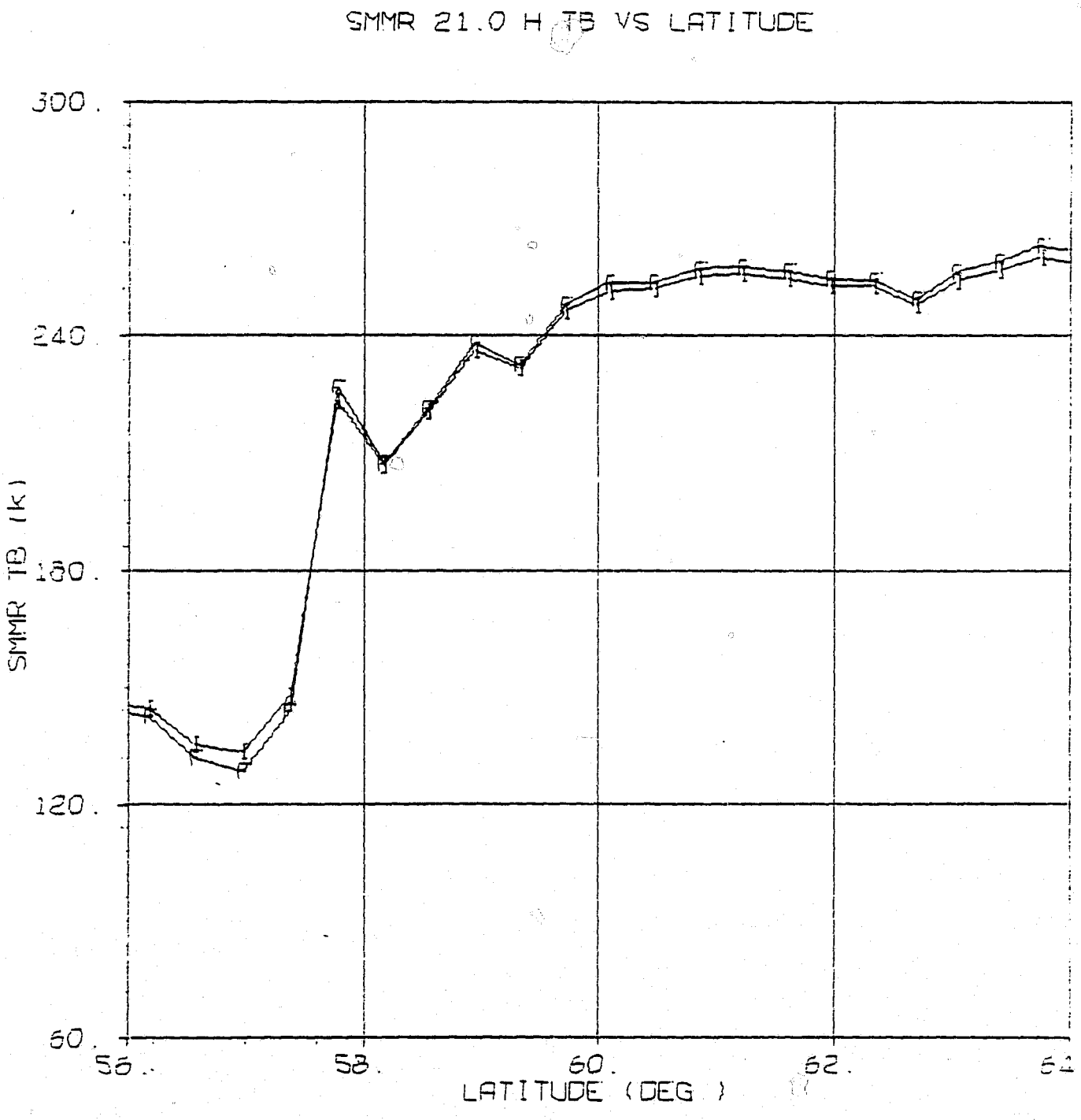

Orbit 1178, Grid 3, Column 1

Figure 4.9. Coastline Crossing, Cross and Interim

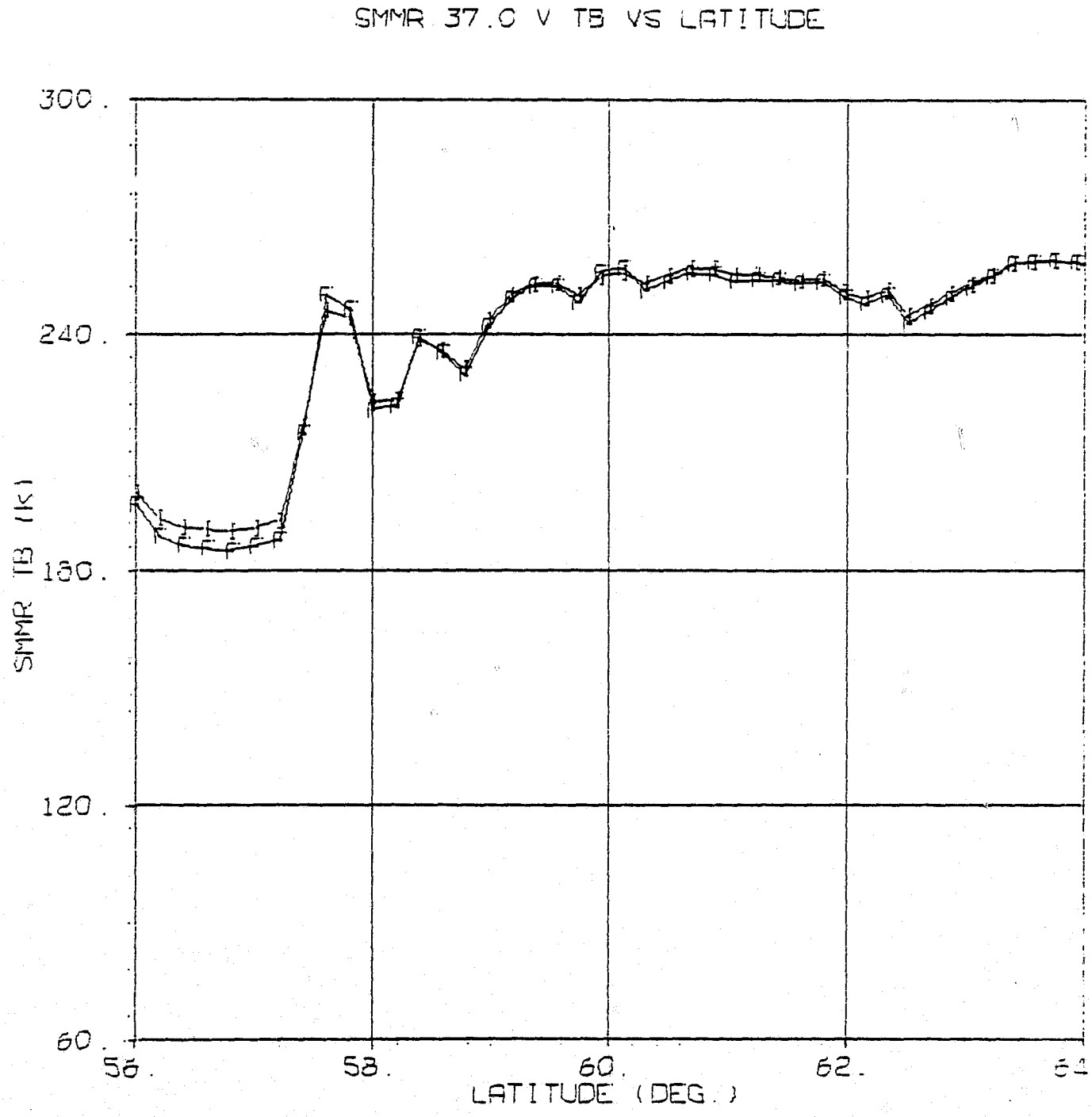

Orbit 1178, Grid 4, Column 1

Figure 4.10. Coastline Crossing, Cross and Interim

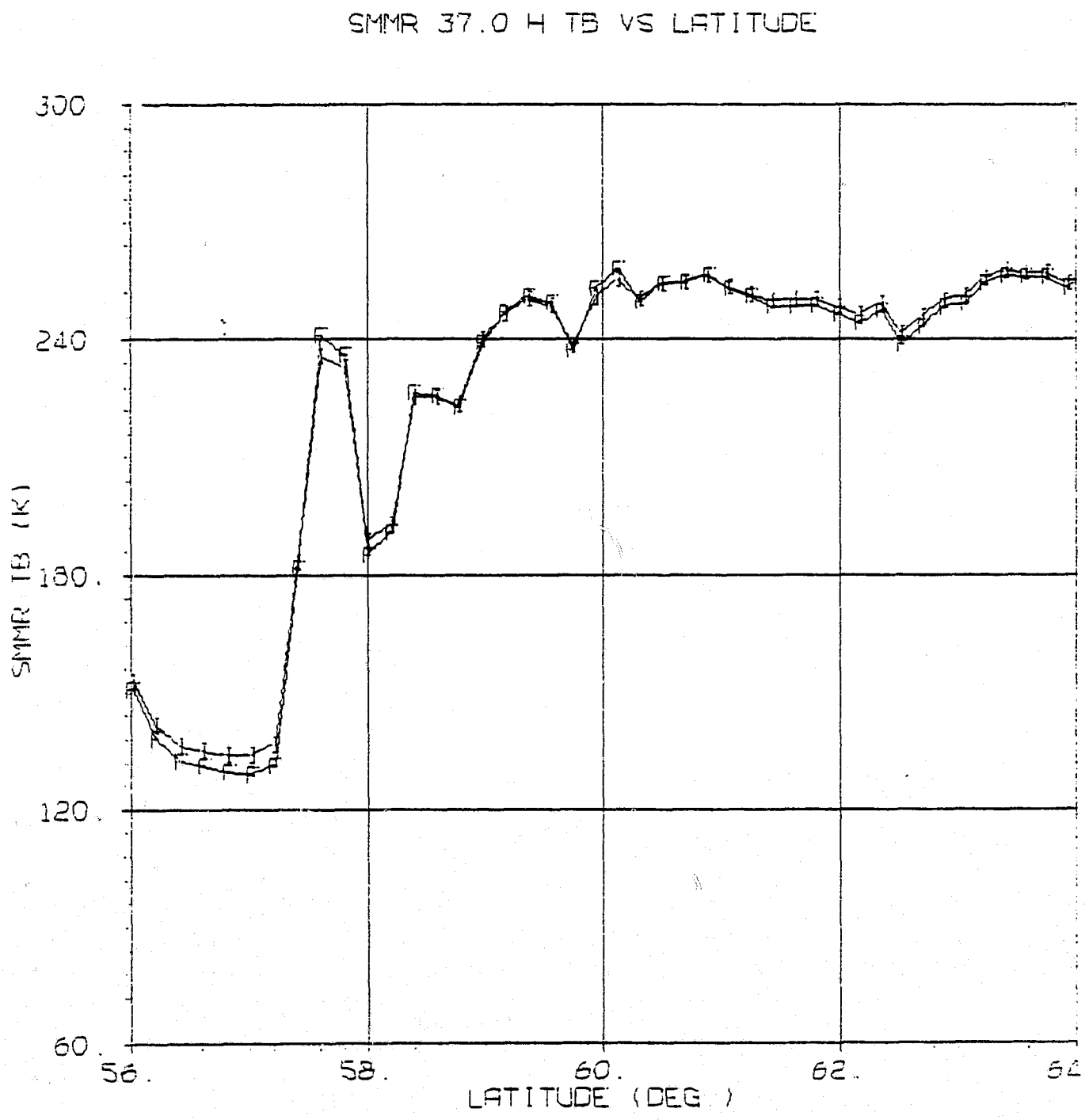

Orbit 1178, Grid 4, Column 1

Figure 5.1. Paralleling Coastline, Nominal and Interim

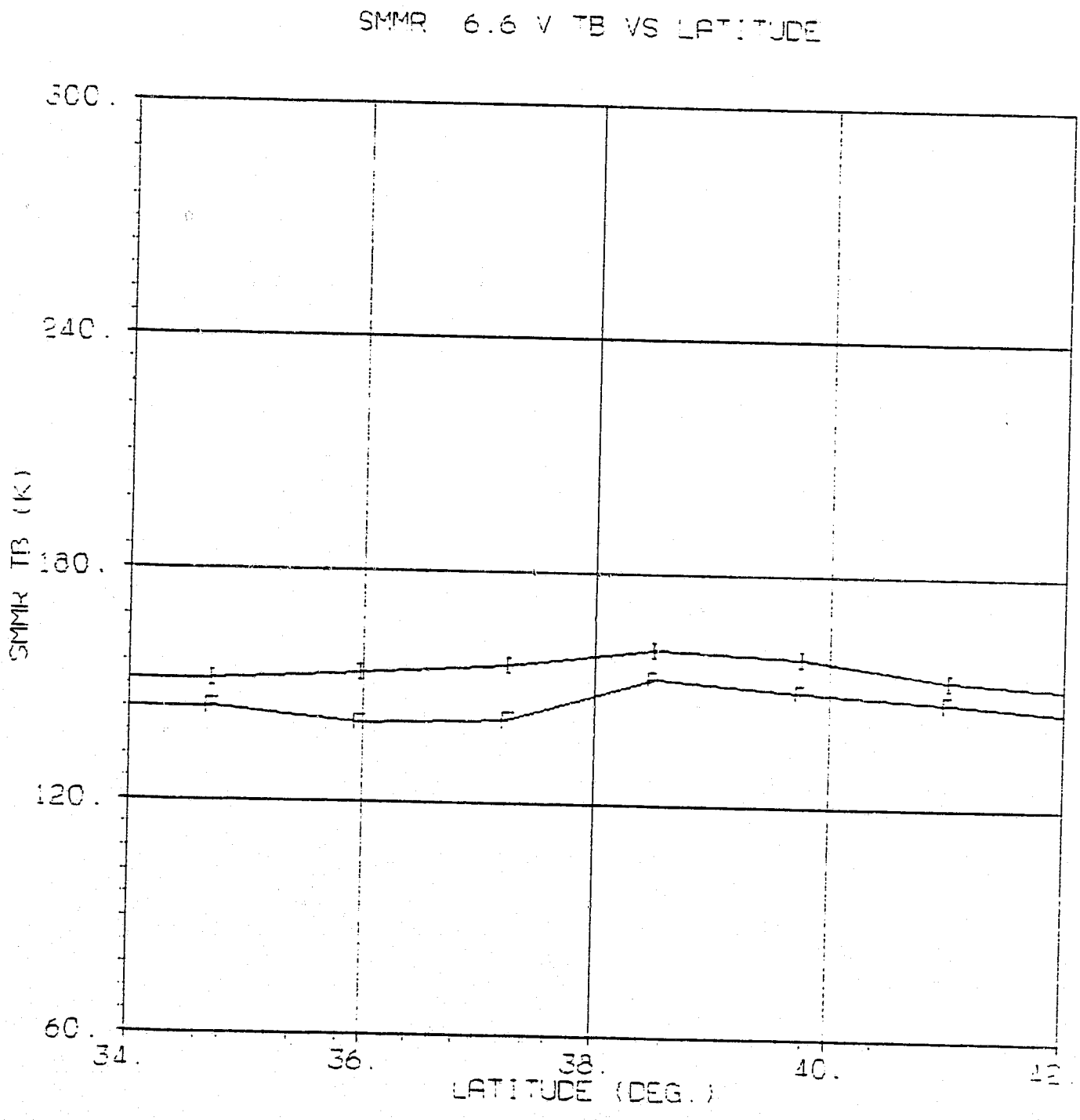

Orbit 1212, Grid 1, Column 4

Figure 5.2. Paralleling Coastline, Nominal and Interim

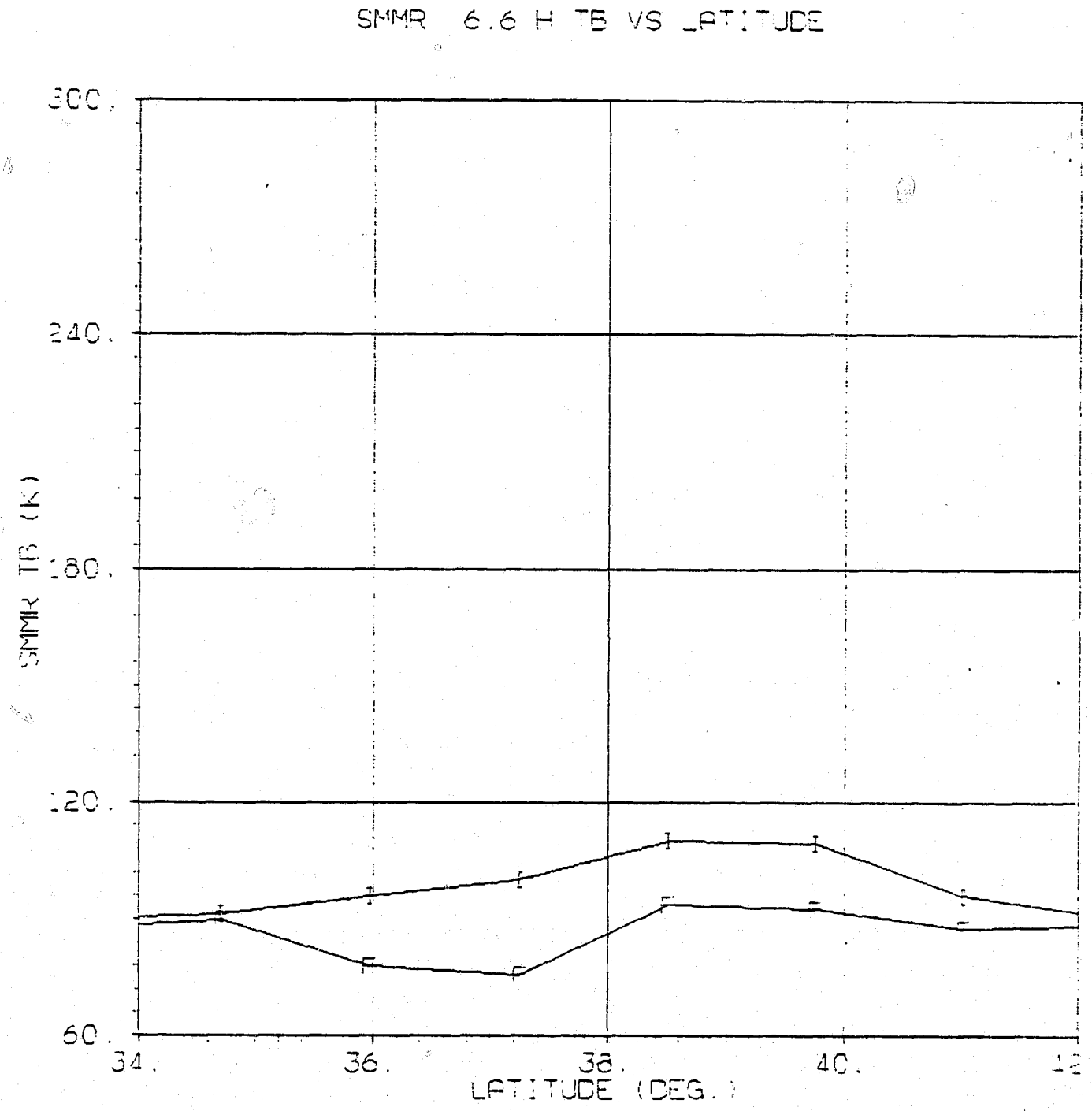

Orbit 1212, Grid 1, Column 4

Figure 5.3. Paralleling Coastline, Nominal and Interim

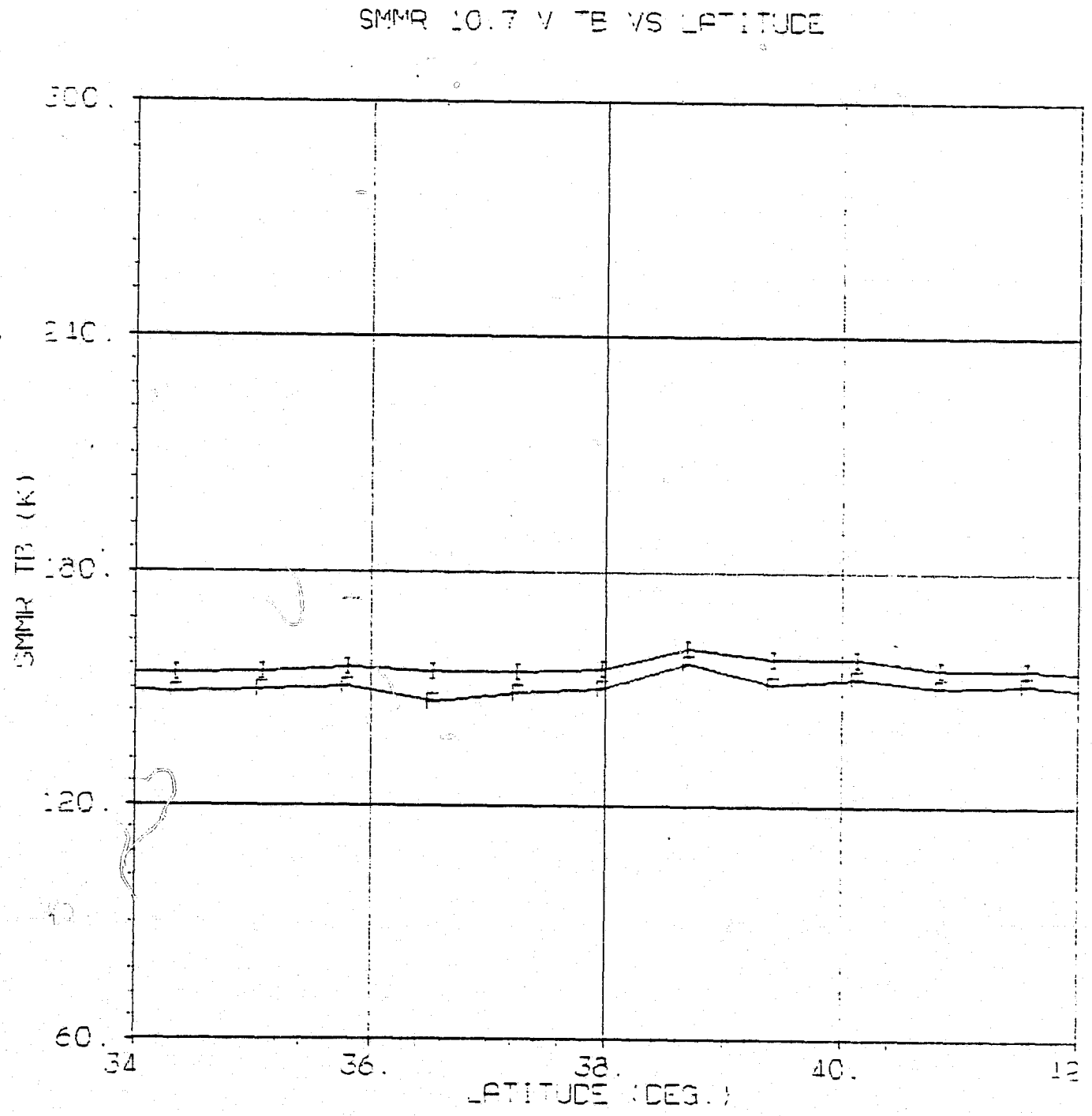

Orbit 1212, Grid 2, Column 7

Figure 5.4. Paralleling Coastline, Nominal and Interim

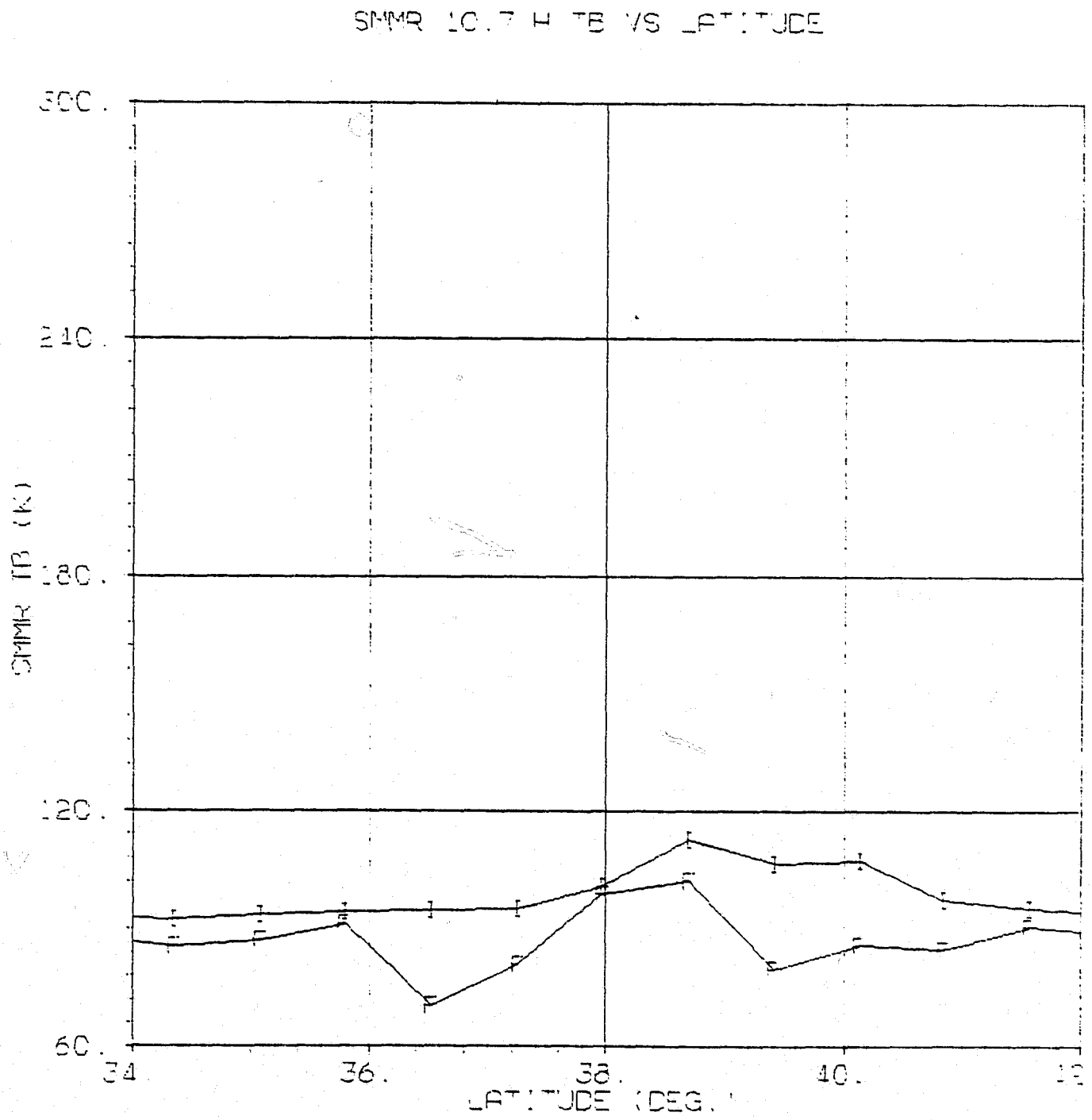

Orbit 1212, Grid 2, Column 7

Figure 5.5. Paralleling Coastline, Nominal and Interim

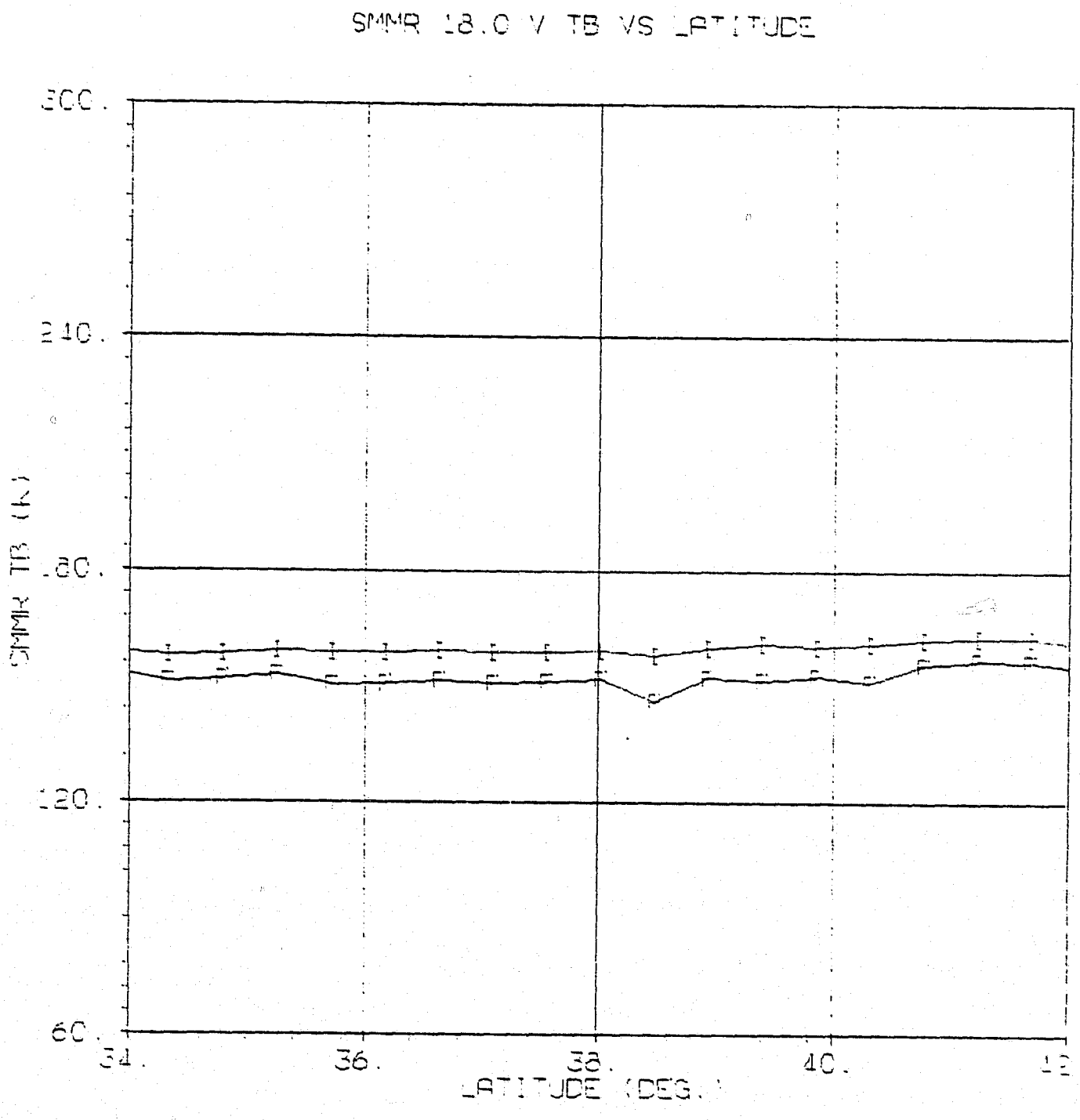

Orbit 1212, Grid 3, Column 11

Figure 5.6. Paralleling Coastline, Nominal and Interim

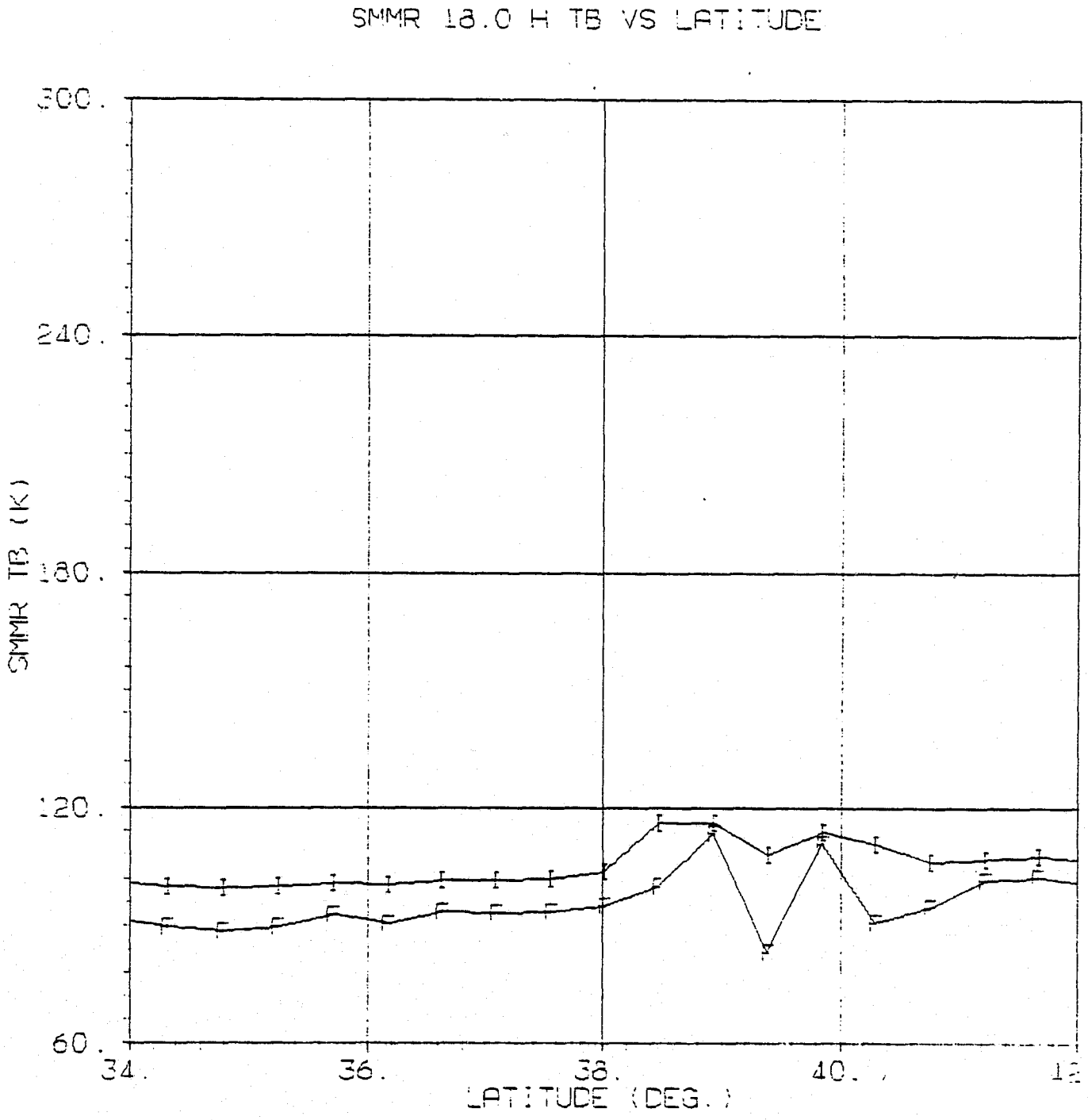

Orbit 1212, Grid 3, Column 11

Figure 5.7. Paralleling Coastline, Nominal and Interim

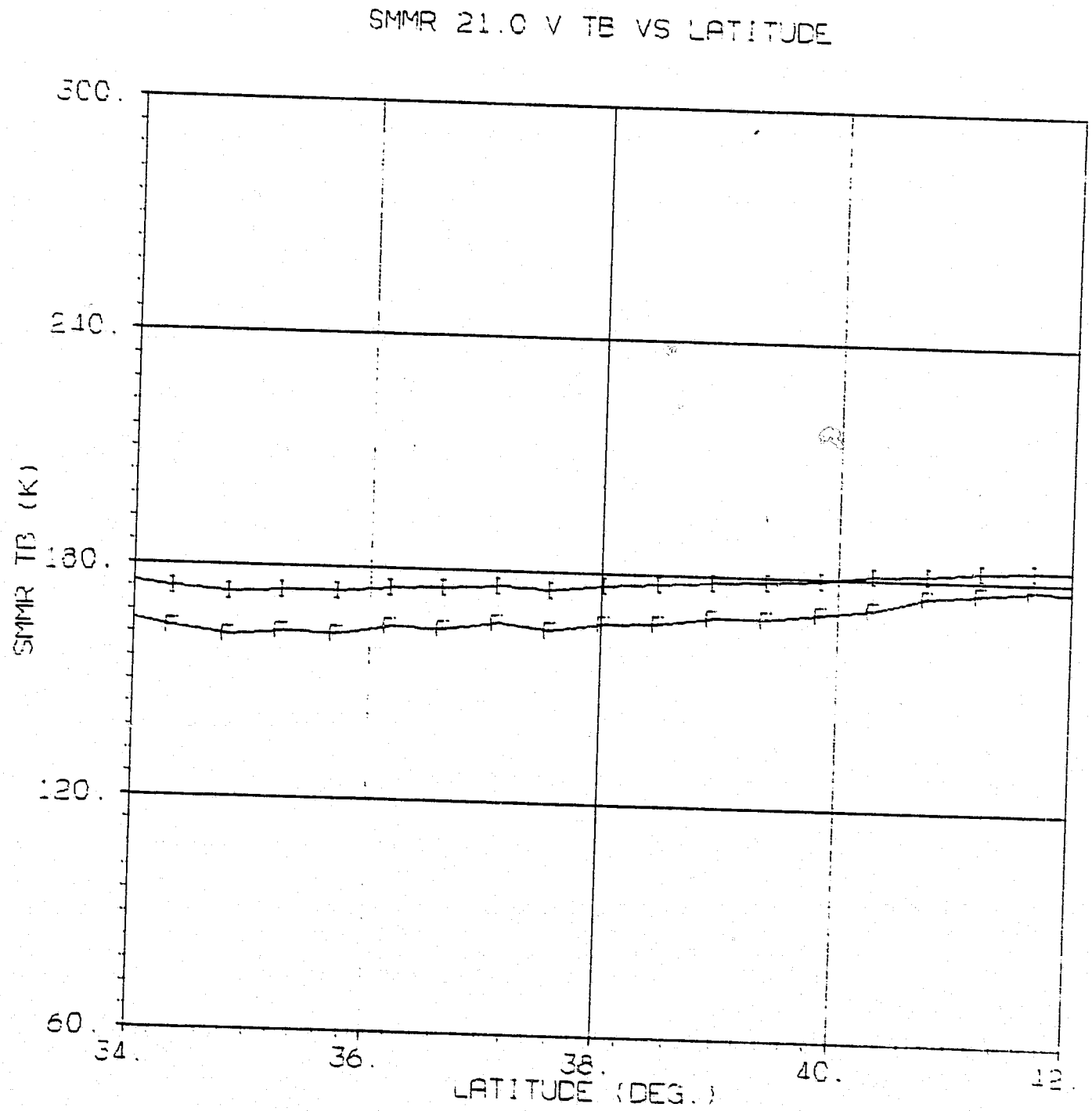

Orbit 1212, Grid 3, Column 11

Figure 5.8. Paralleling Coastline, Nominal and Interim

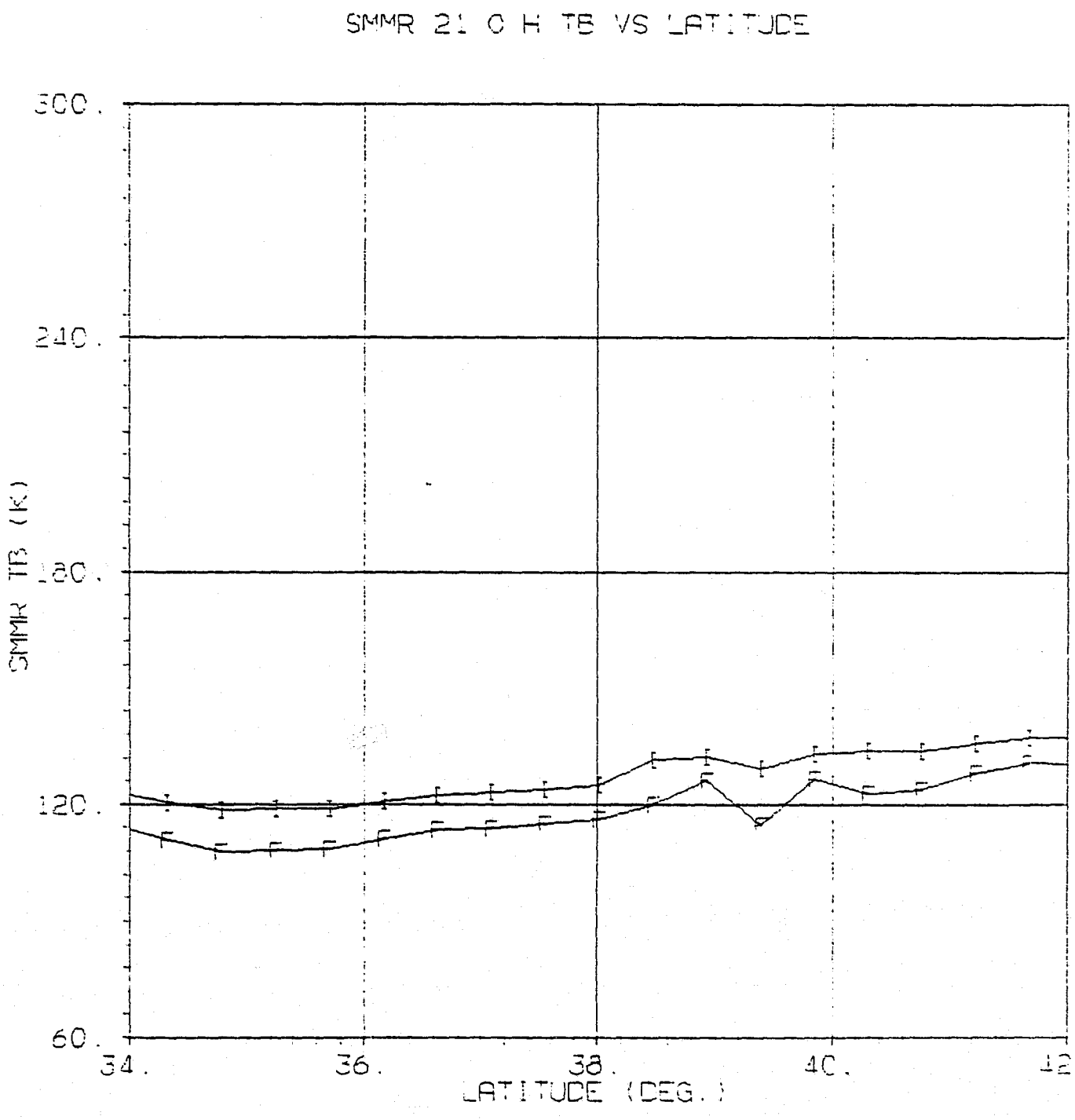

Orbit 1212, Grid 3, Column 11

Figure 5.9. Paralleling Coastline, Nominal and Interim

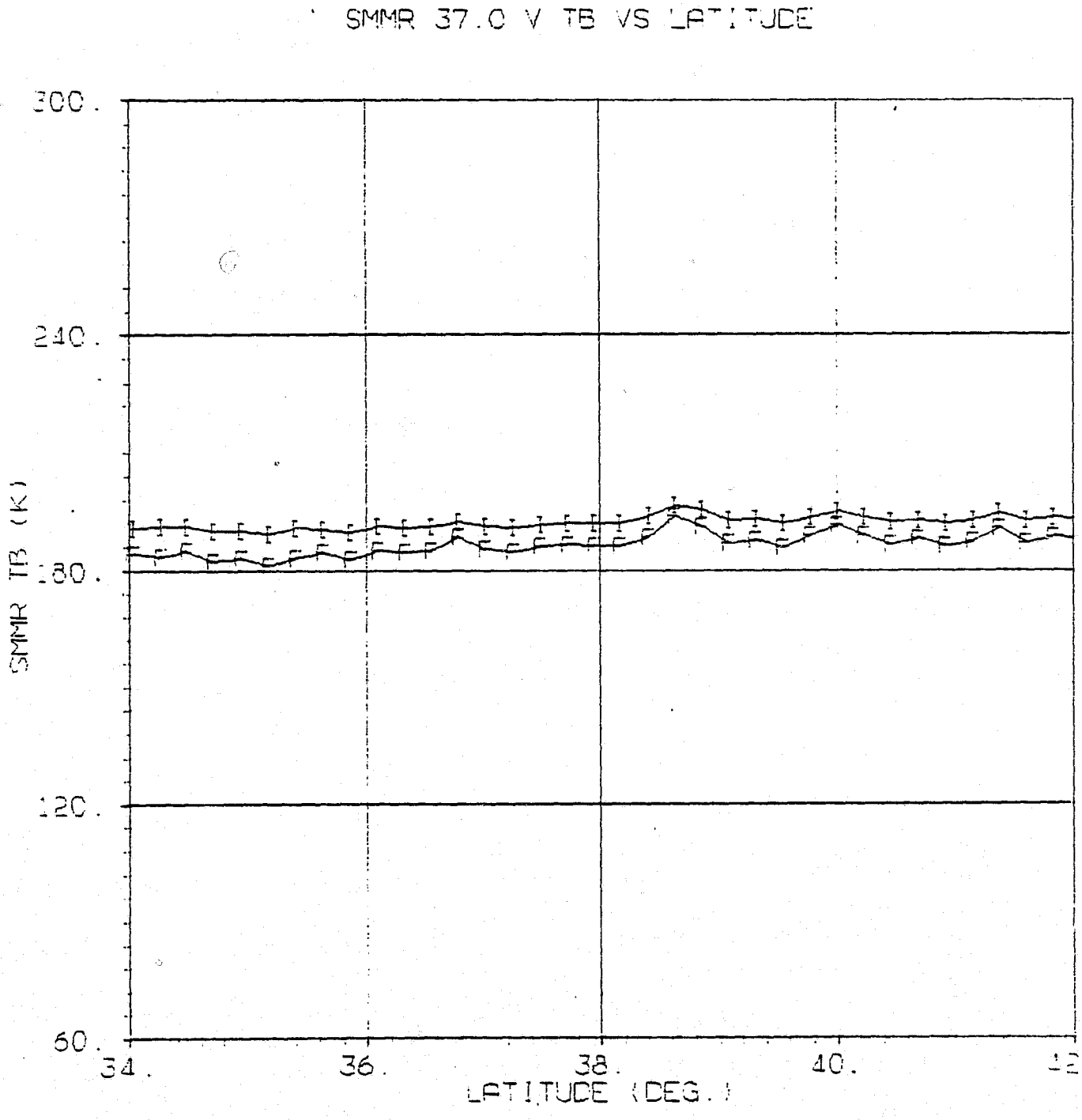

Orbit 1212, Grid 4, Column 22

Figure 5.10. Paralleling Coastline, Nominal and Interim

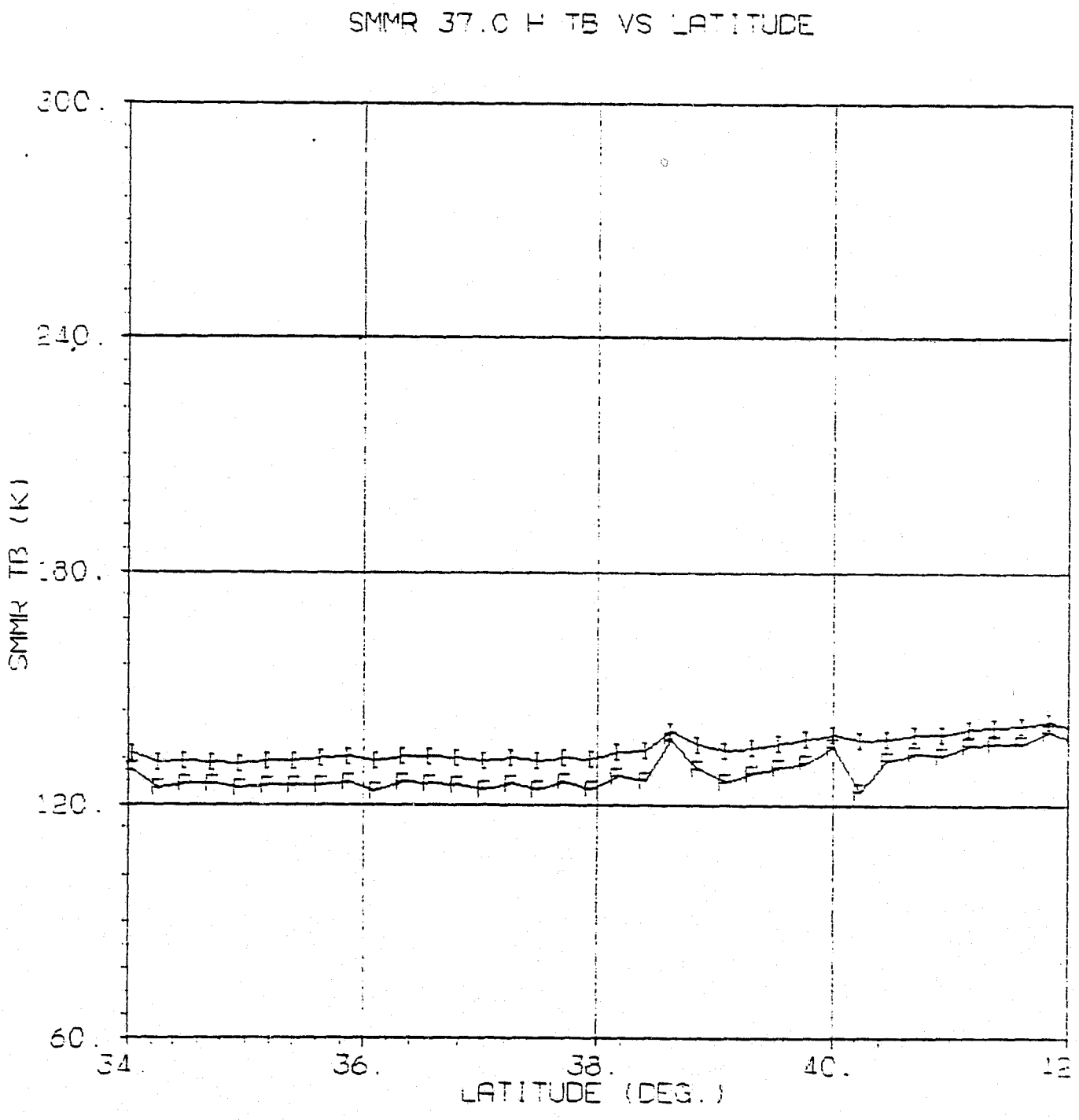

Orbit 1212, Grid 4, Column 22

Figure 6.1. Paralleling Coastline, Cross and Interim

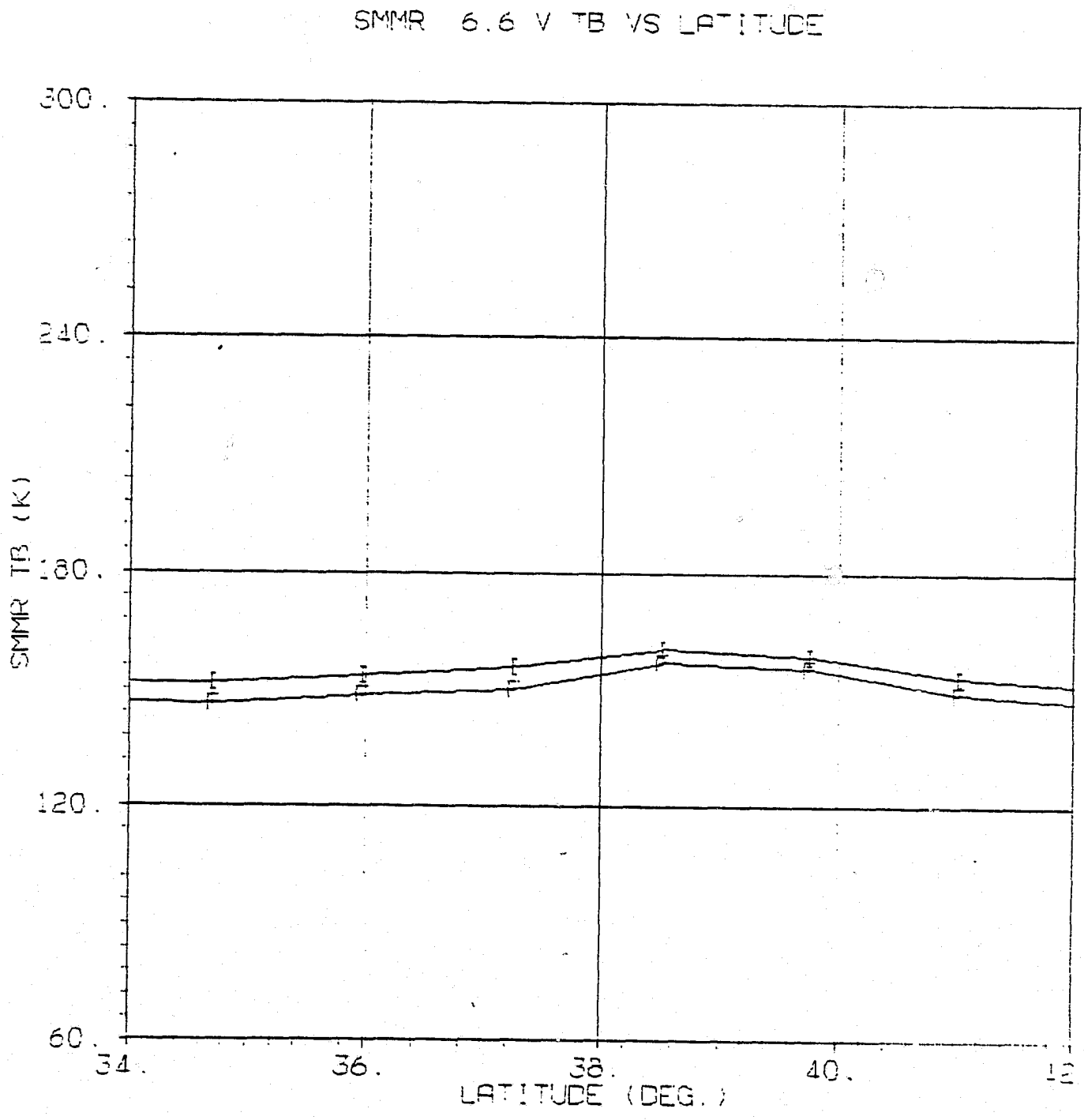

Orbit 1212, Grid 1, Column 4

Figure 6.2. Paralleling Coastline, Cross and Interim

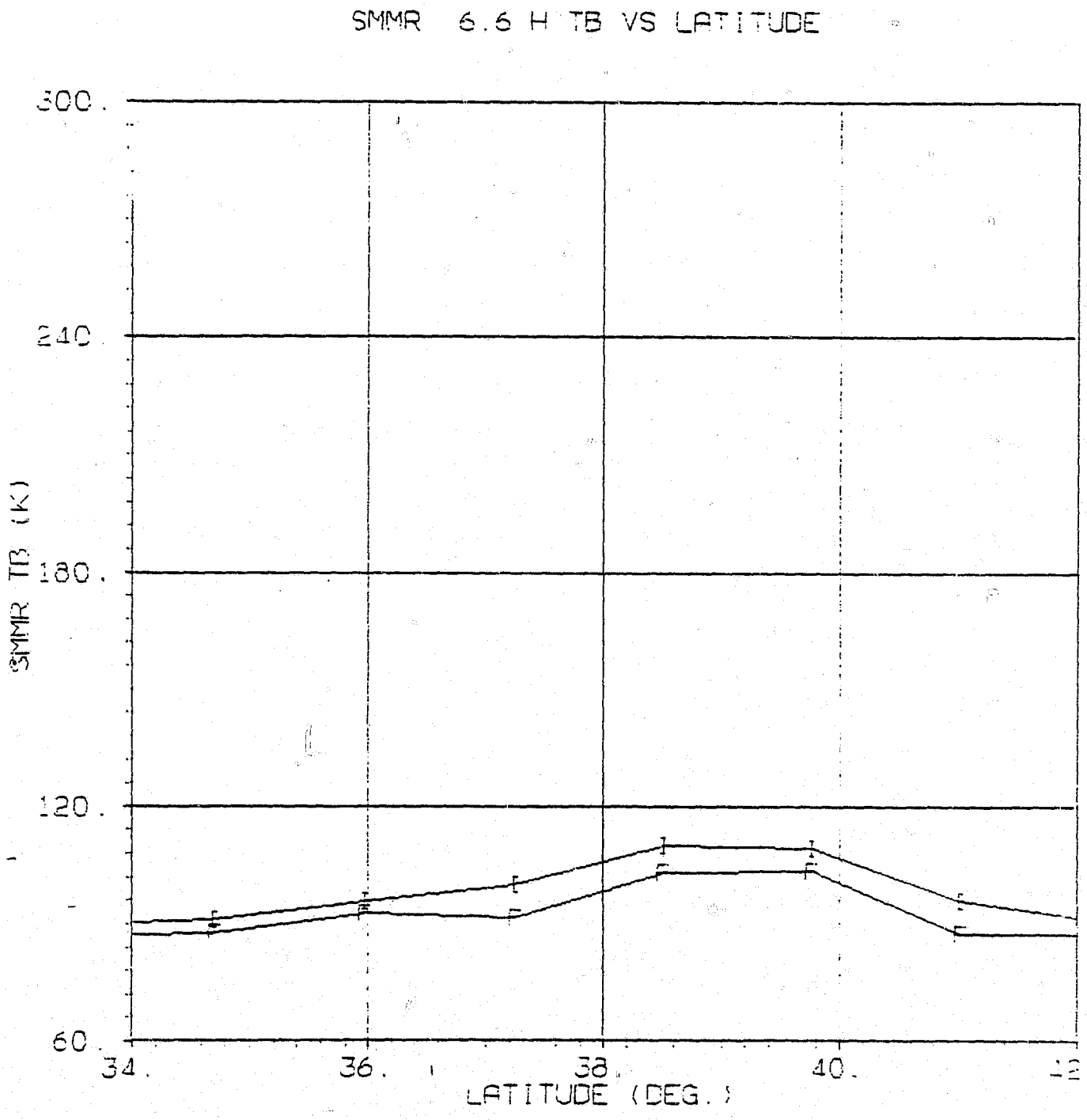

Orbit 1212, Grid 1, Column 4

Figure 6.3. Paralleling Coastline, Cross and Interim

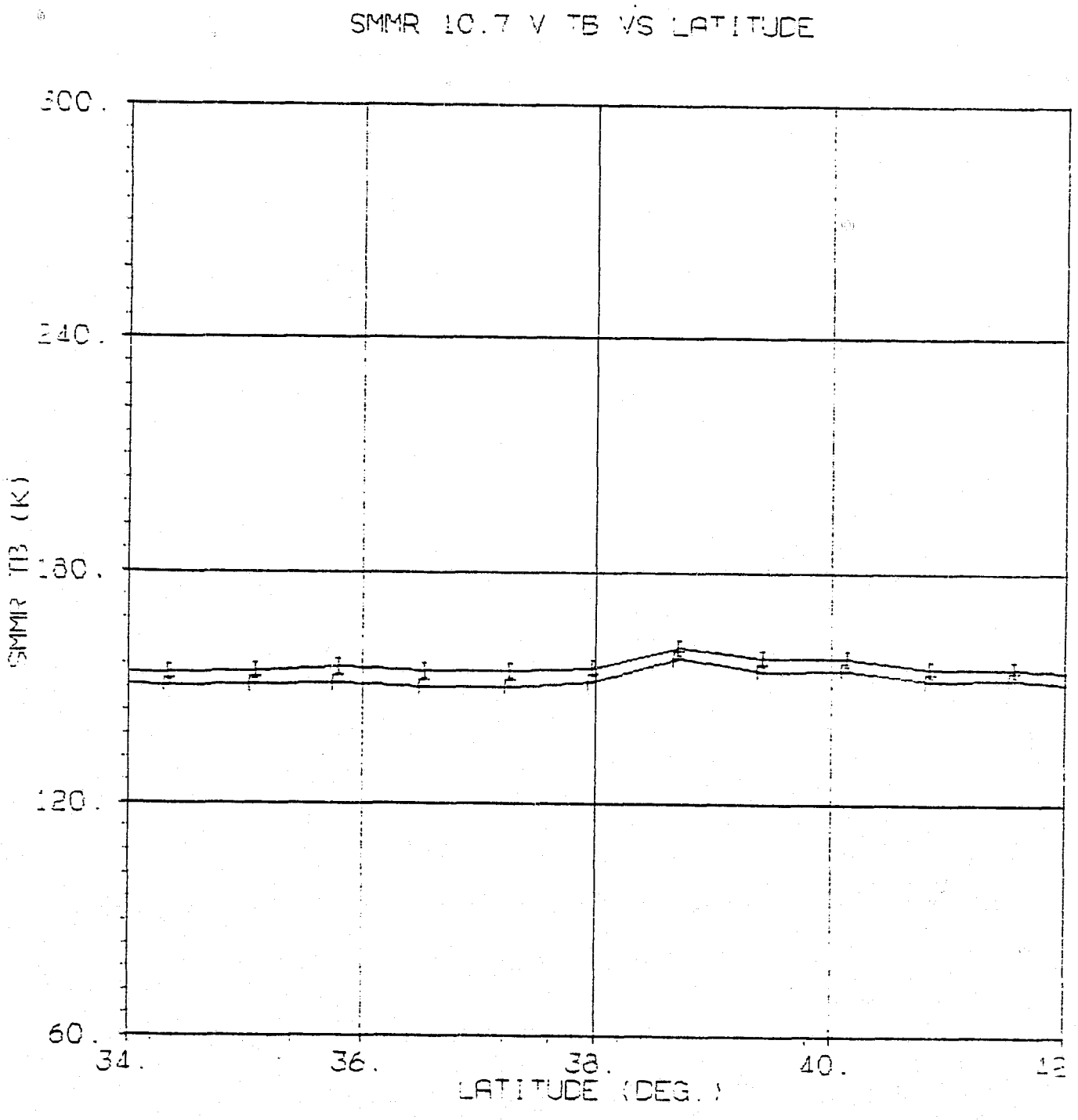

Orbit 1212, Grid 2, Column 7

Figure 6.4. Paralleling Coastline, Cross and Interim

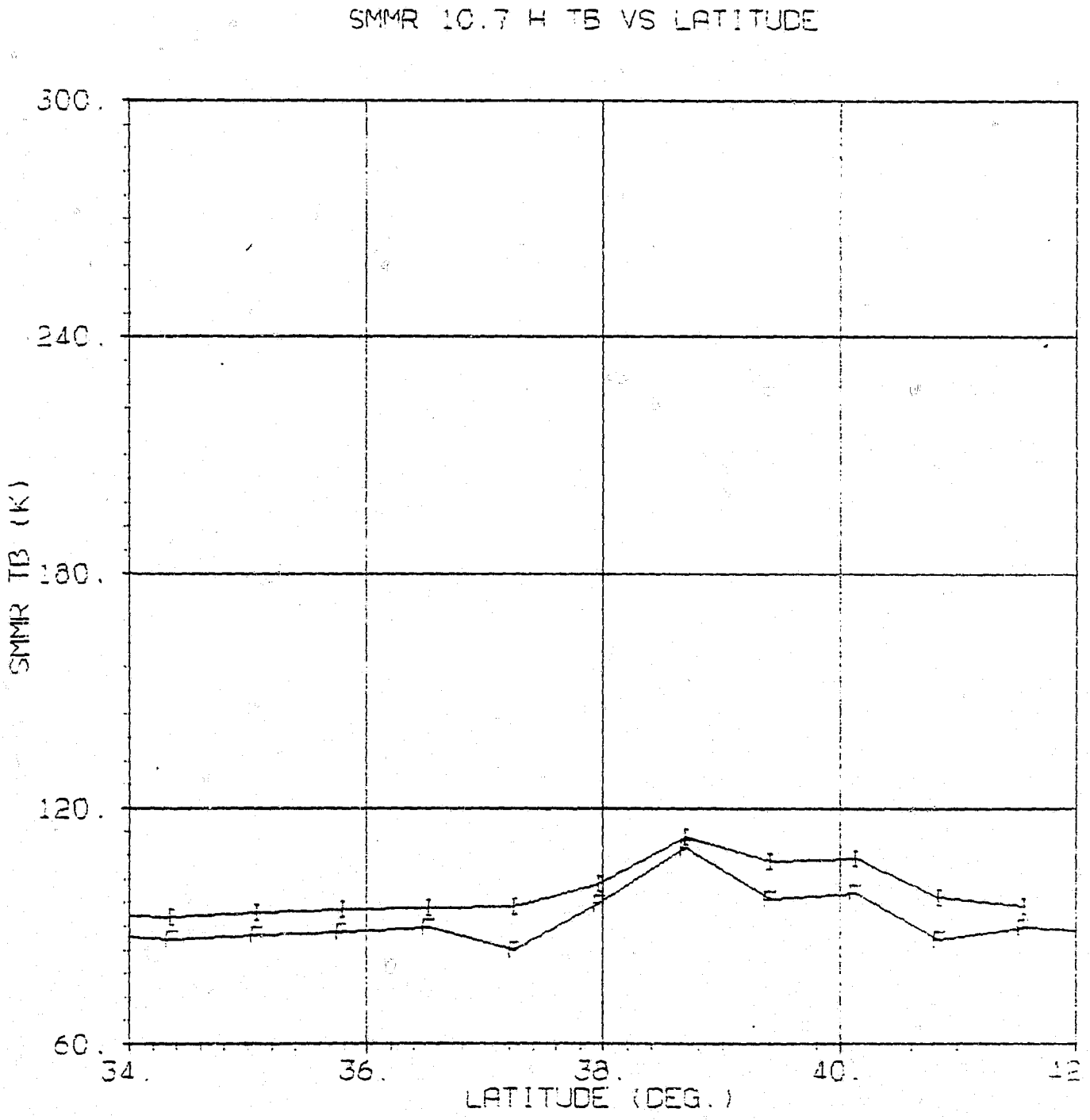

Orbit 1212, Grid 2, Column 7

Figure 6.5. Paralleling Coastline, Cross and Interim

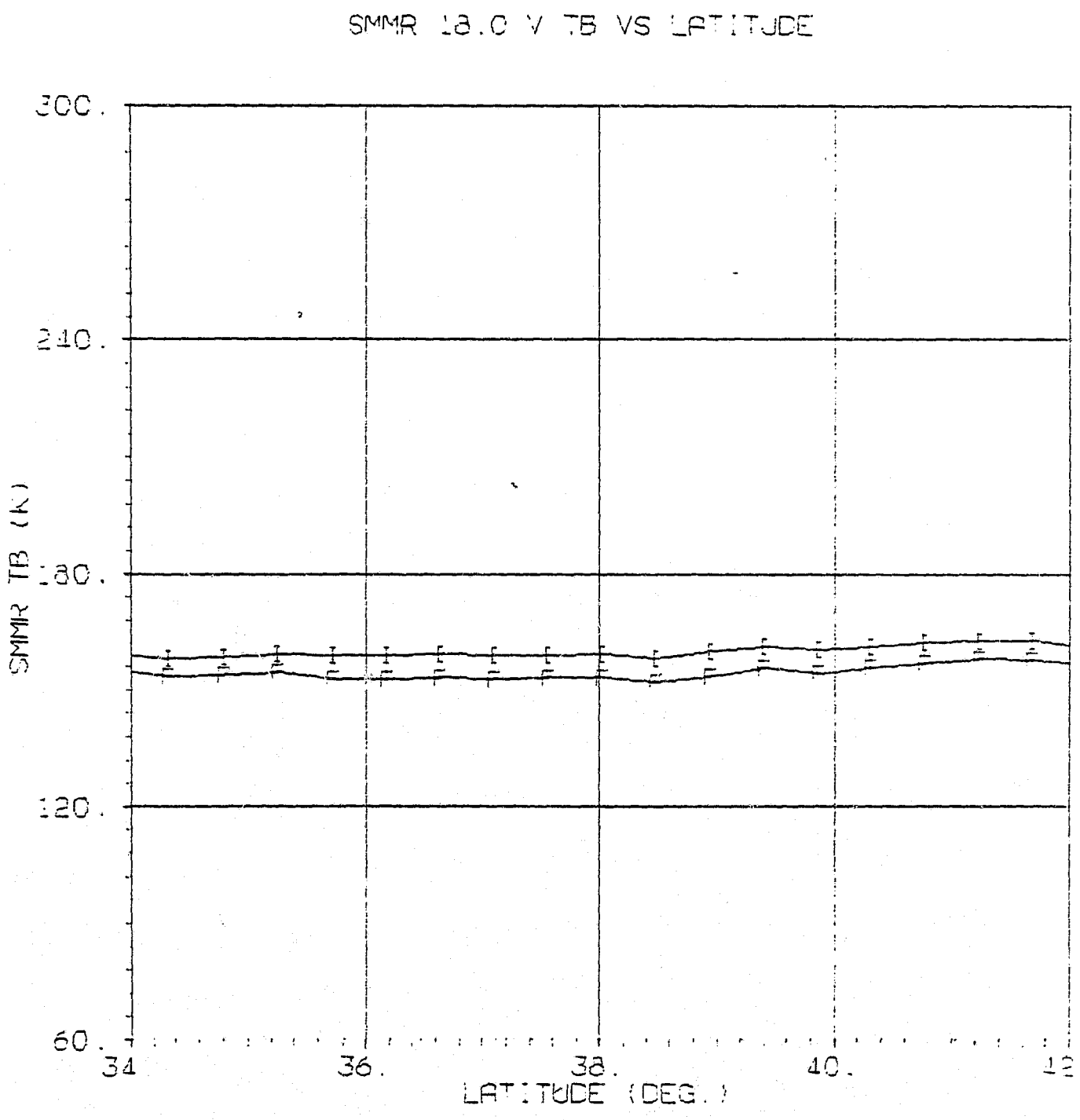

Orbit 1212, Grid 3, Column 11

Figure 6.6. Paralleling Coastline, Cross and Interim

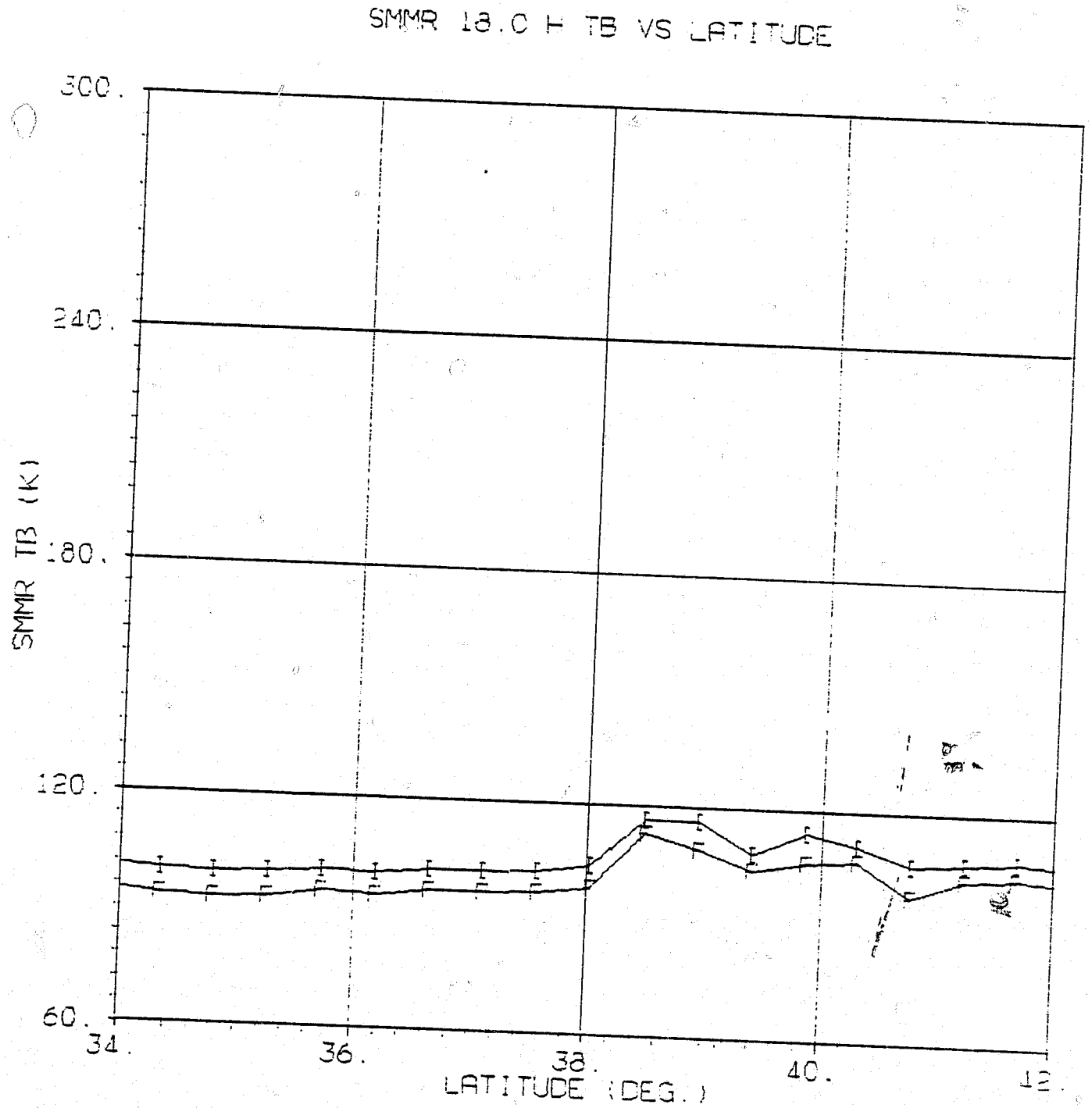

Orbit 1212, Grid 3, Column 11

Figure 6.7. Paralleling Coastline, Cross and Interim

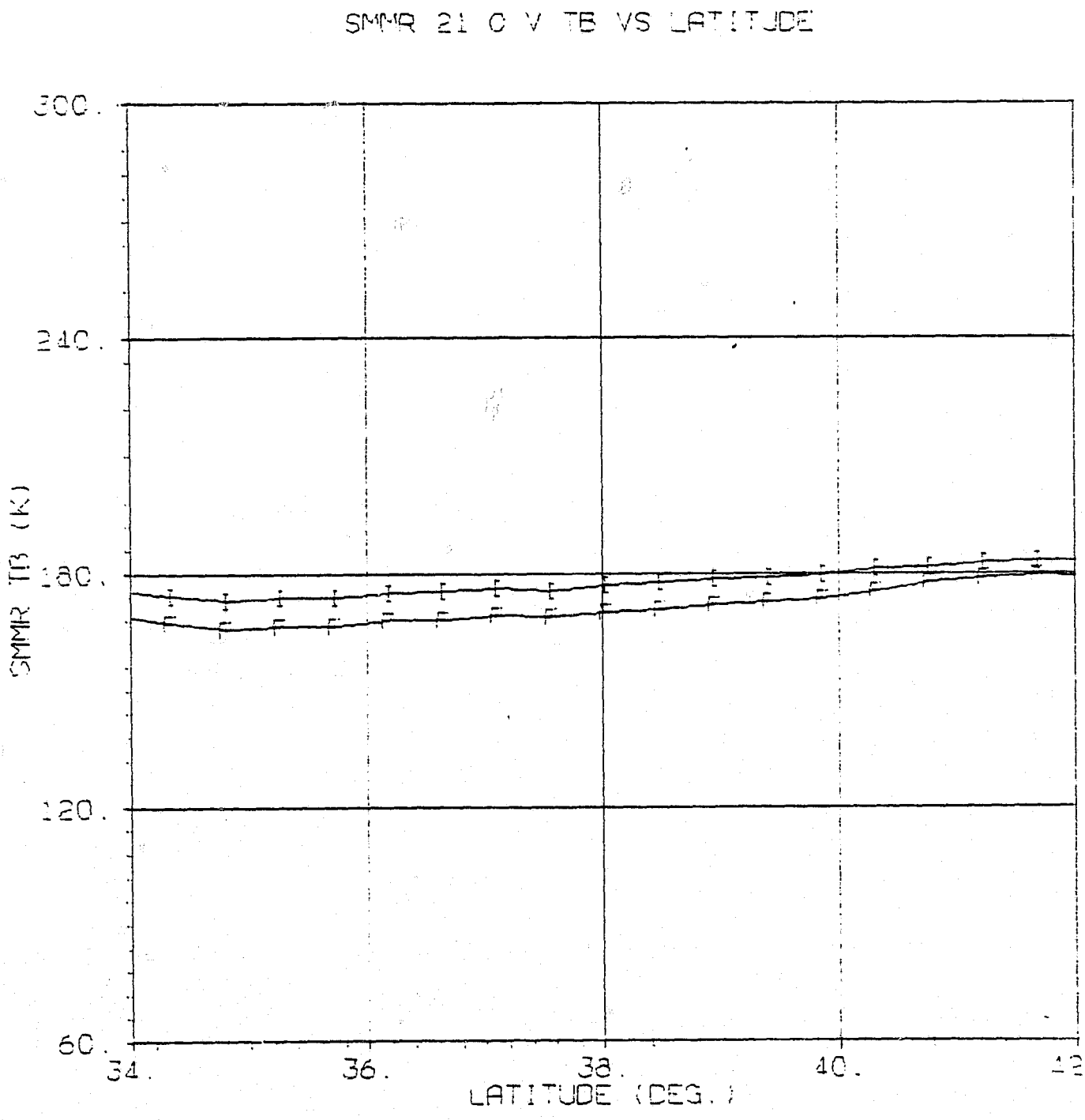

Orbit 1212, Grid 3, Column 11

Figure 6.8. Paralleling Coastline, Cross and Interim

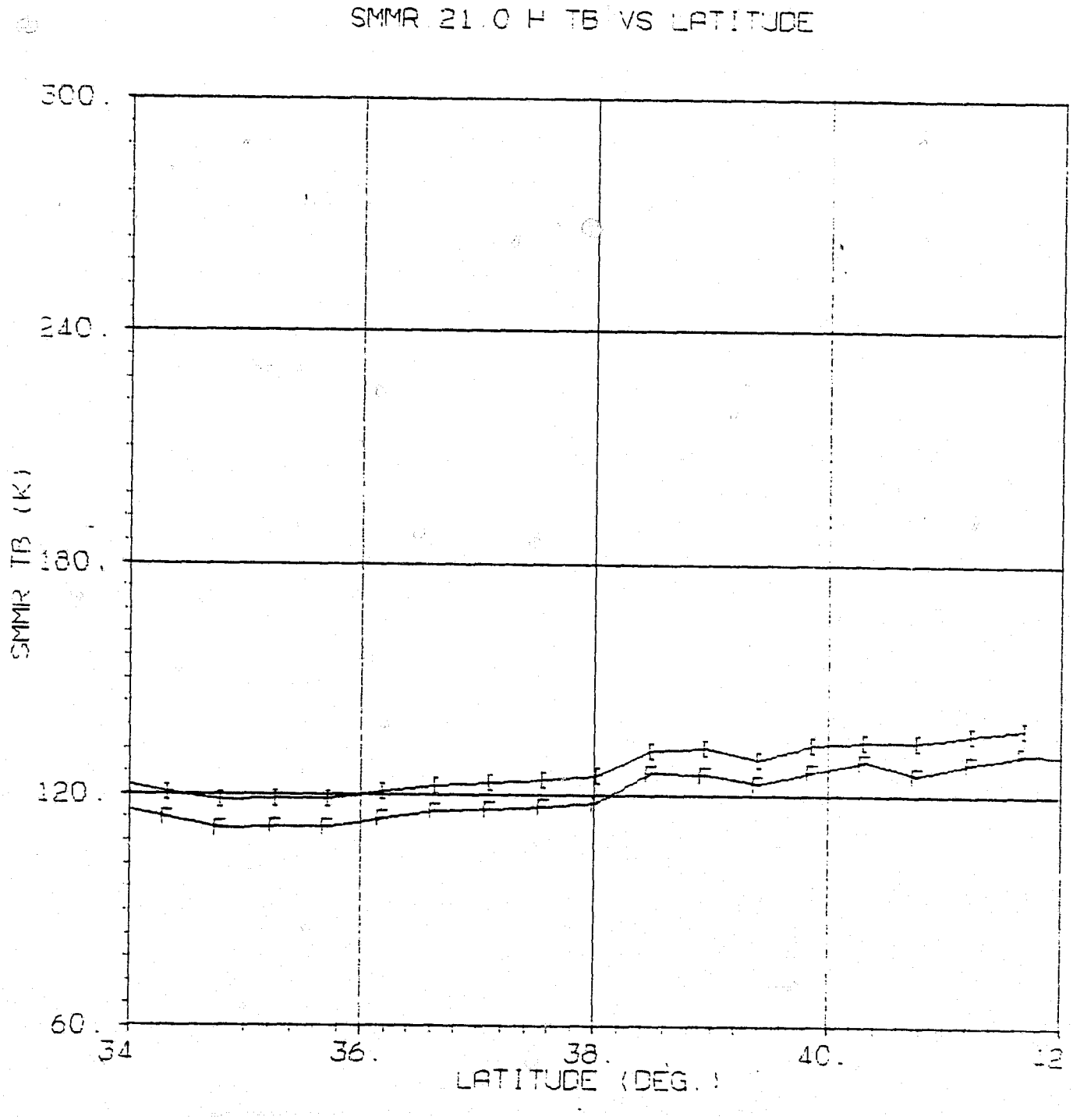

Orbit 1212, Grid 3, Column 11

Figure 6.9. Paralleling Coastline, Cross and Interim

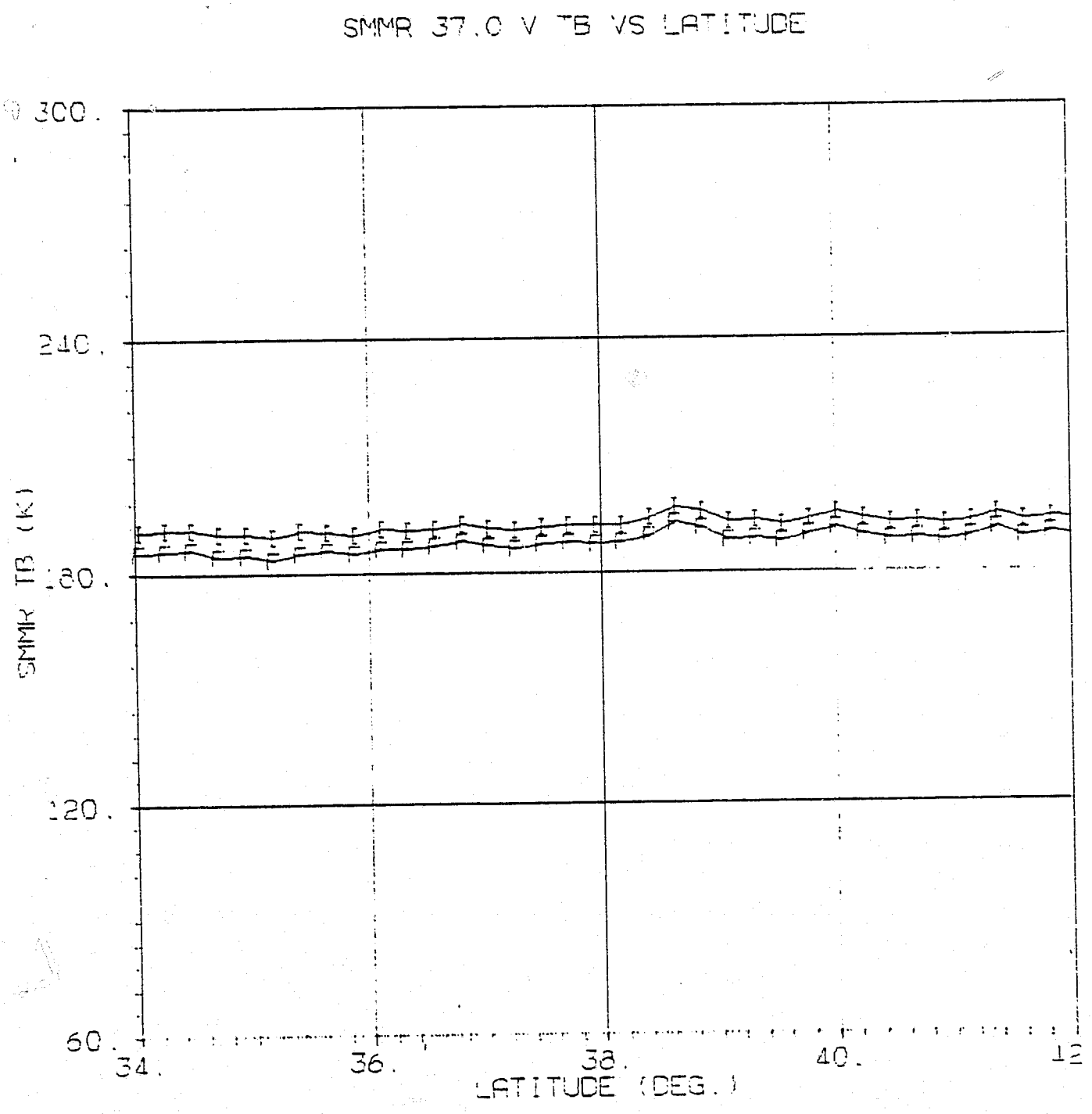

Orbit 1212, Grid 4, Column 22

Figure 6.10. Paralleling Coastline, Cross and Interim

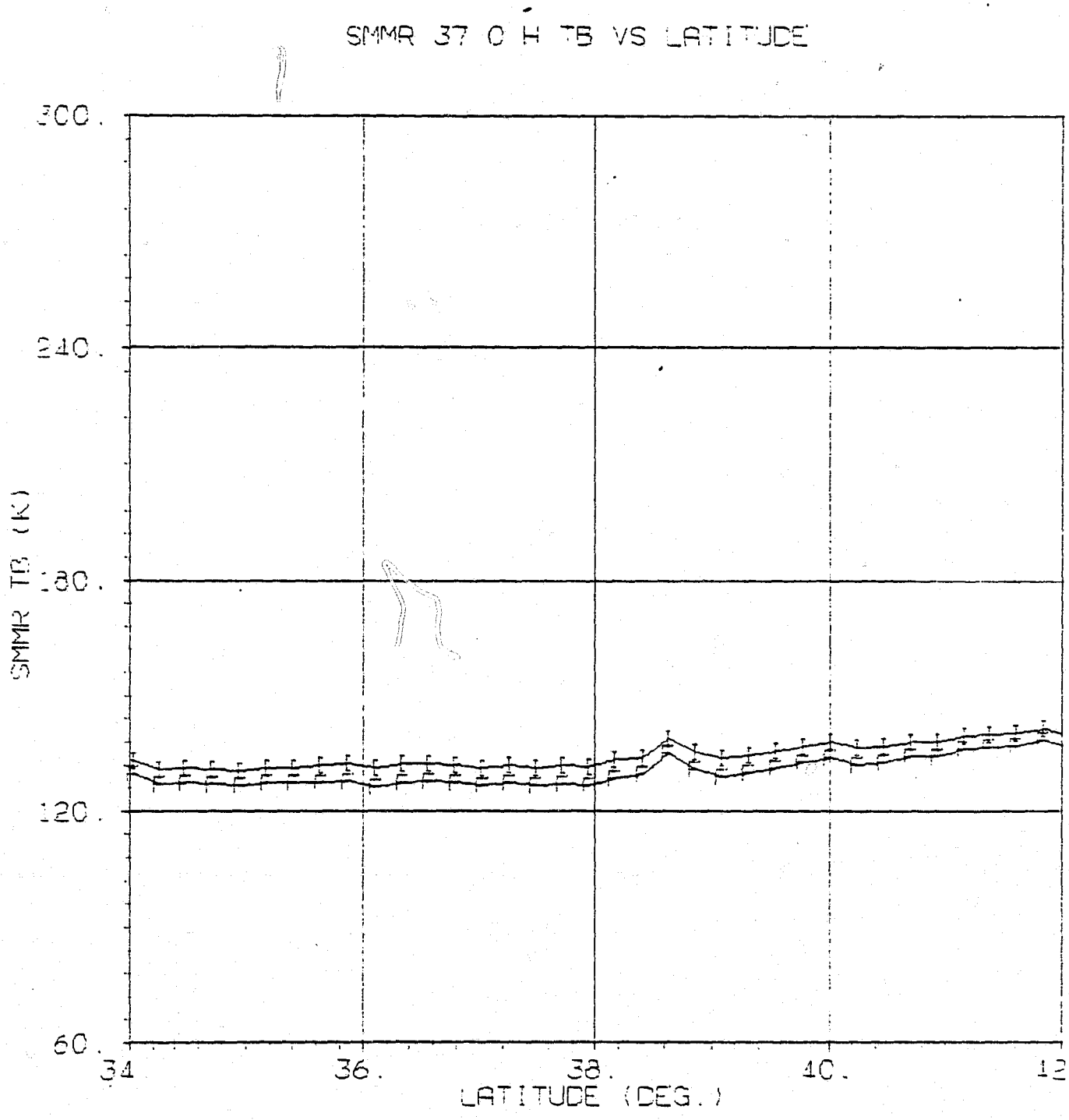

Orbit 1212, Grid 4, Column 22

Figure 7.1. Interim Mode

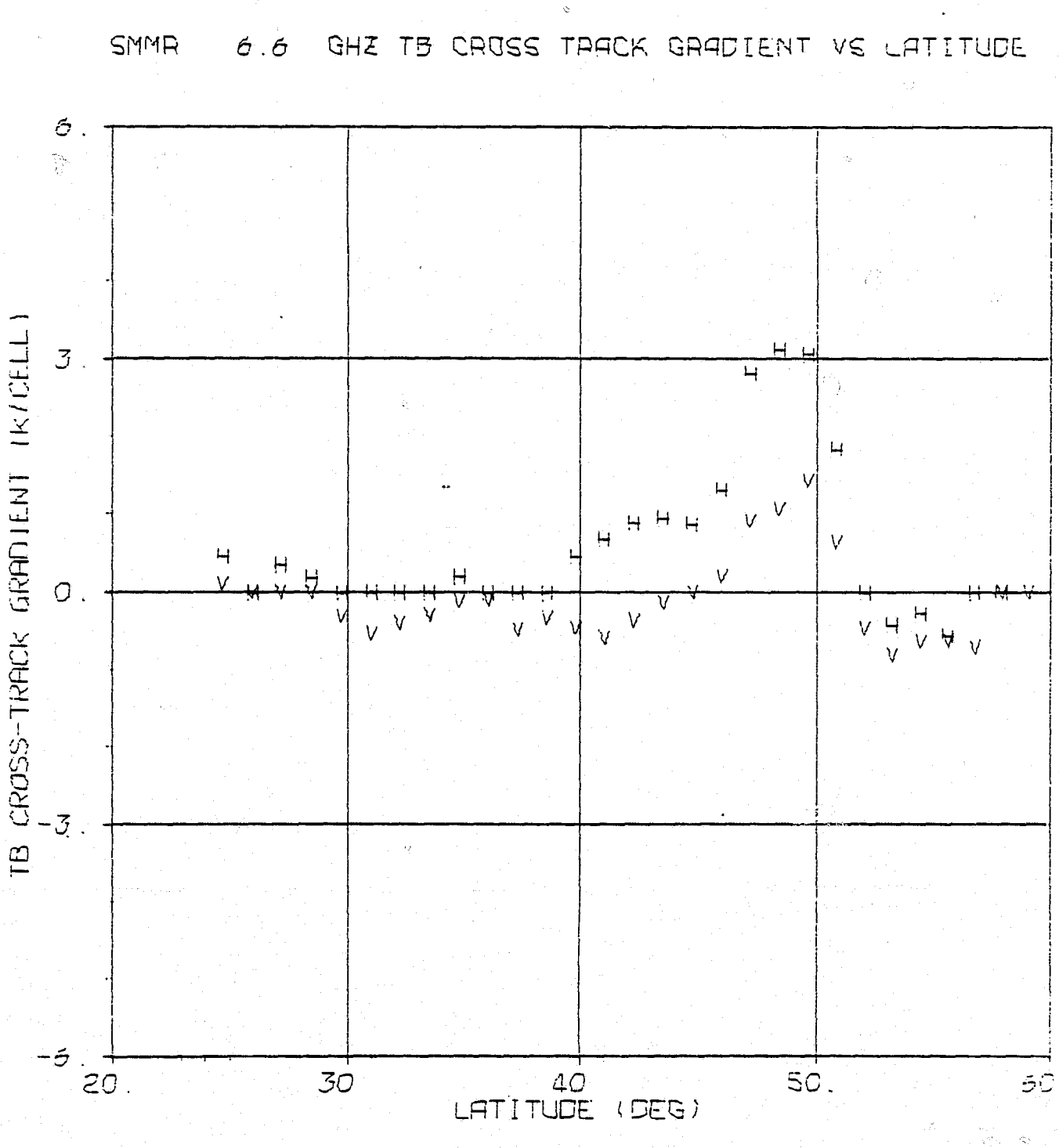

Orbit 1178

Figure 7.2. Interim Mode

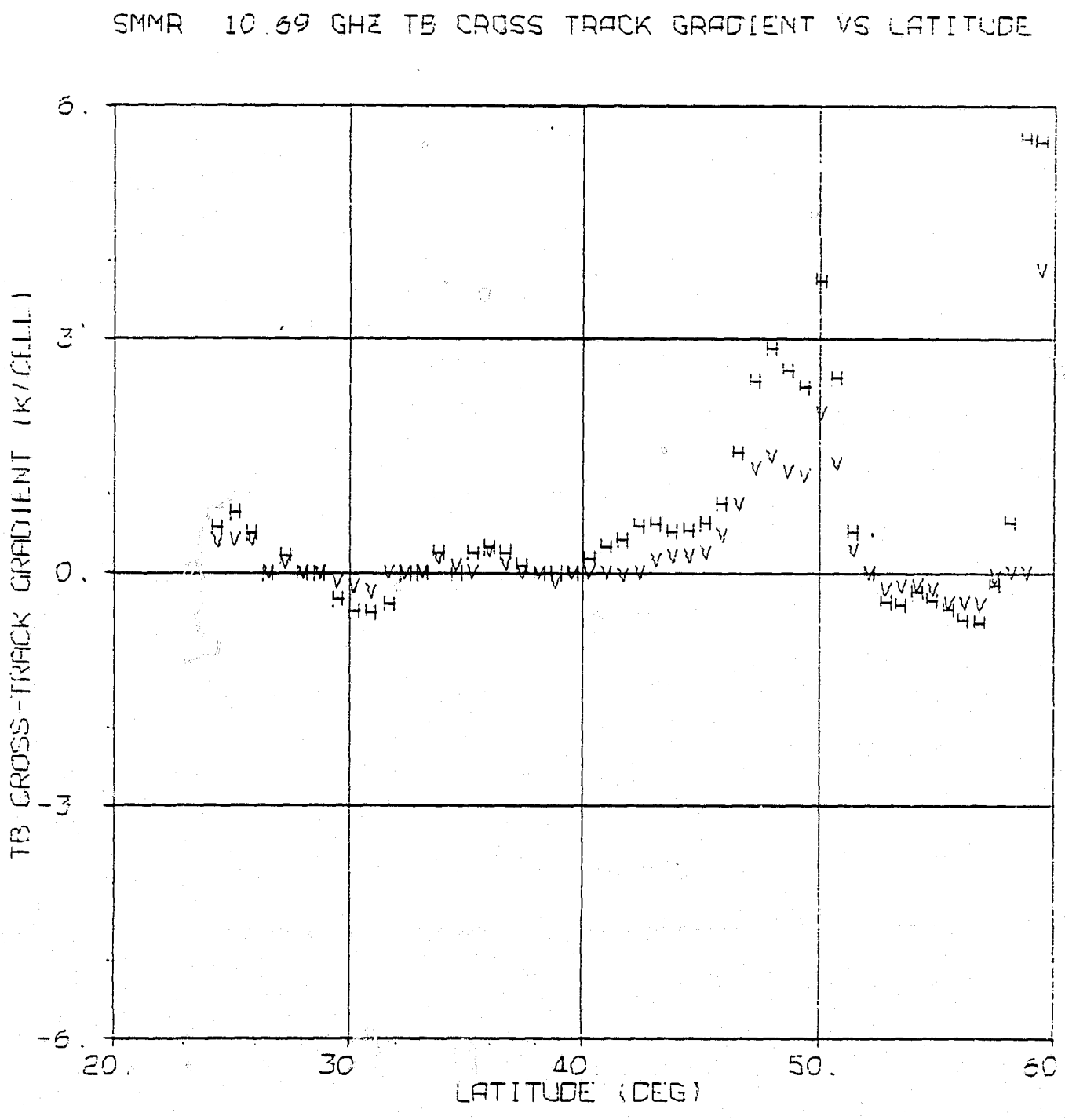

Orbit 1178

Figure 7.3. Interim Mode

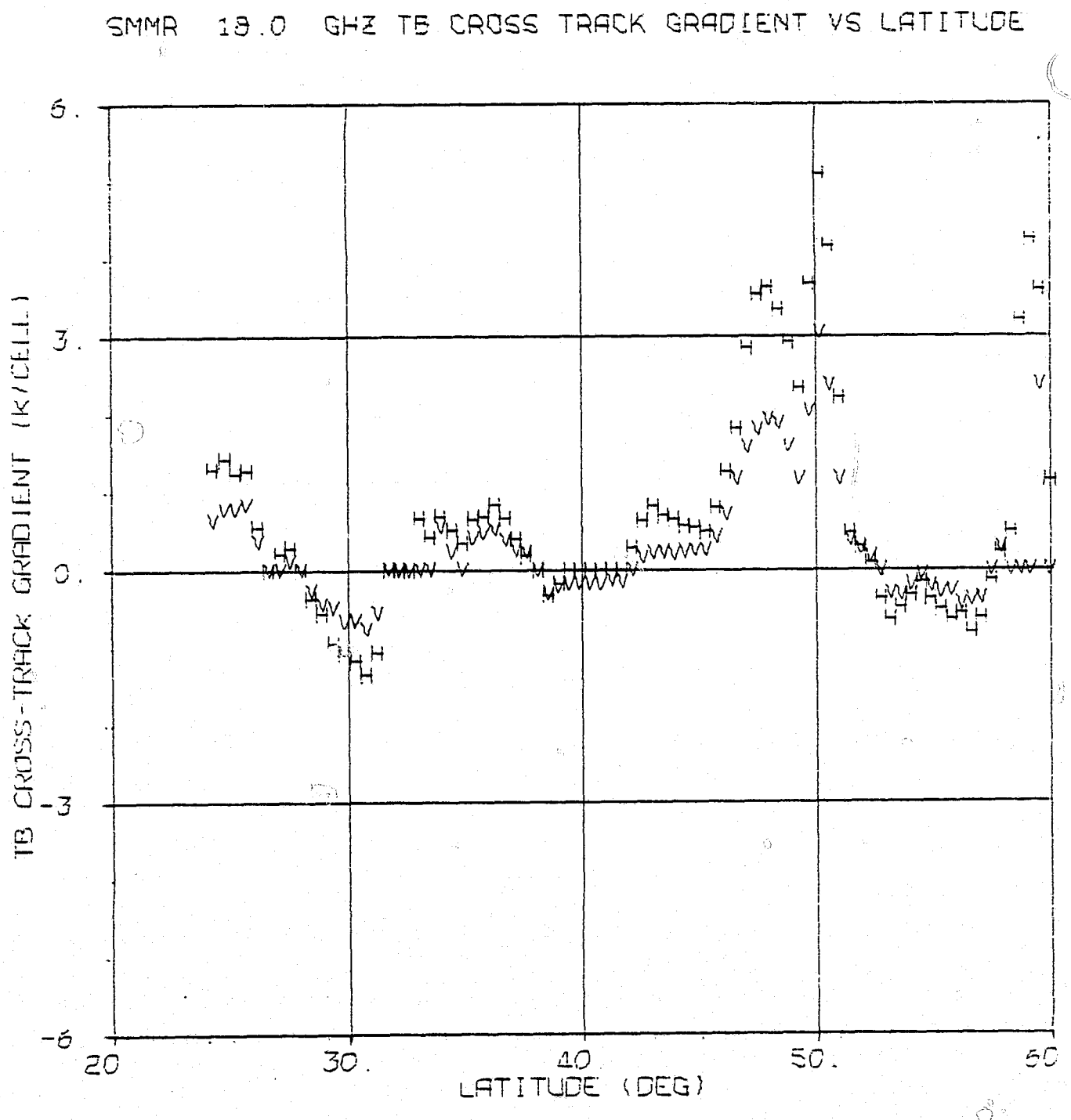

Orbit 1178

Figure 7.4. Interim Mode

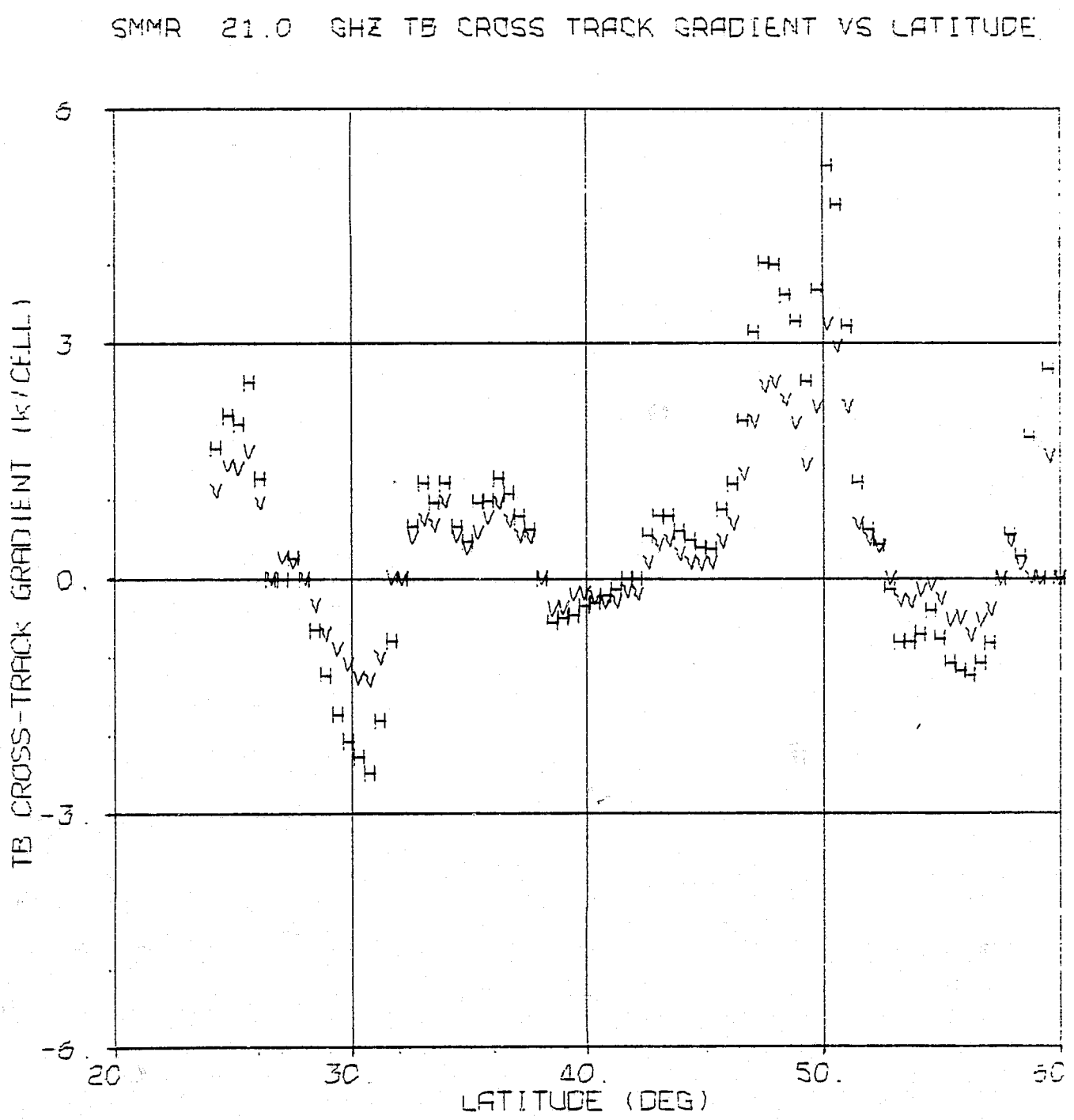

Orbit 1178

Figure 7.5. Interim Mode

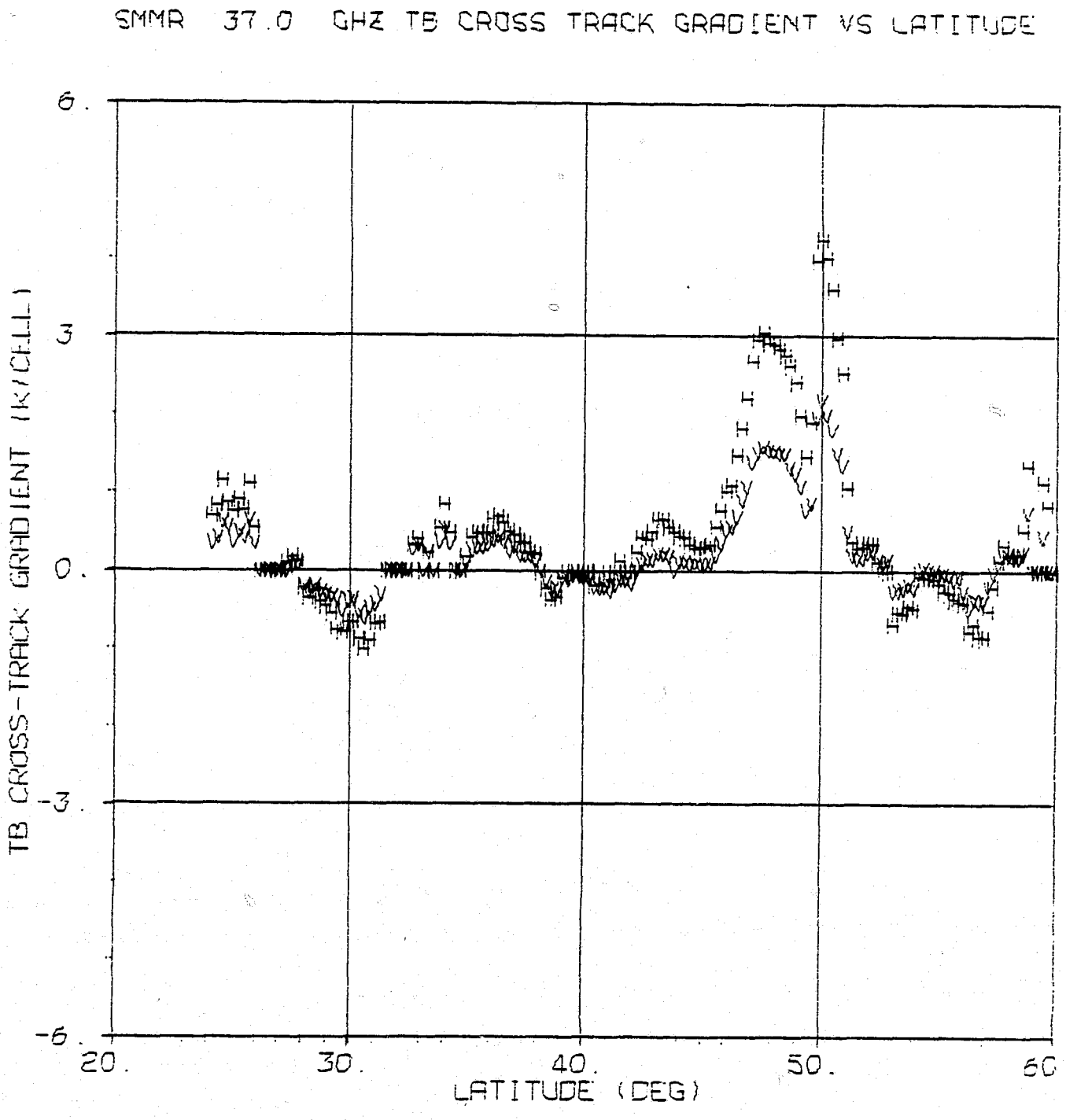

Orbit 1178

Figure 8.1. Cross Mode

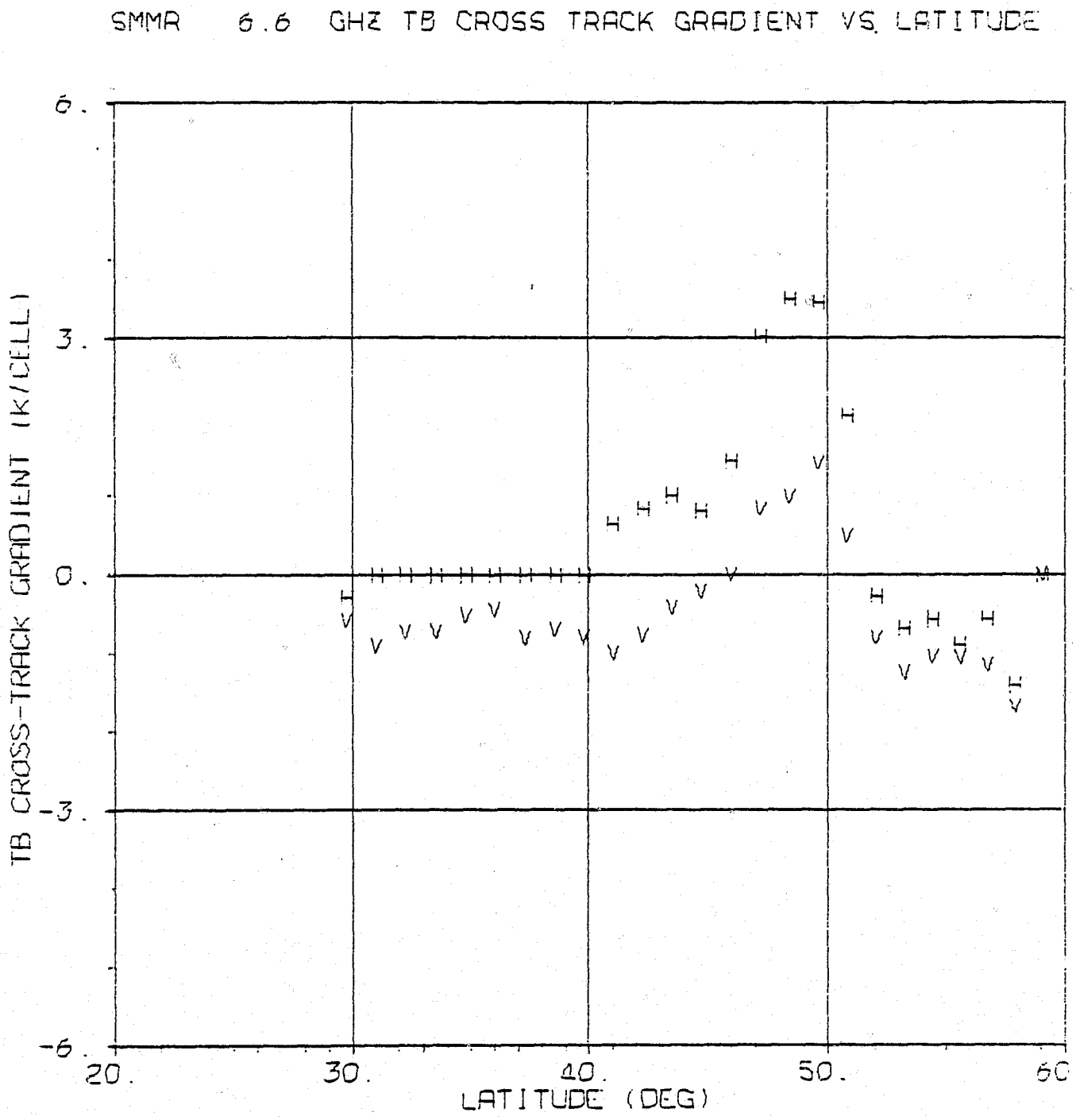

Orbit 1178

Figure 8.2. Cross Mode

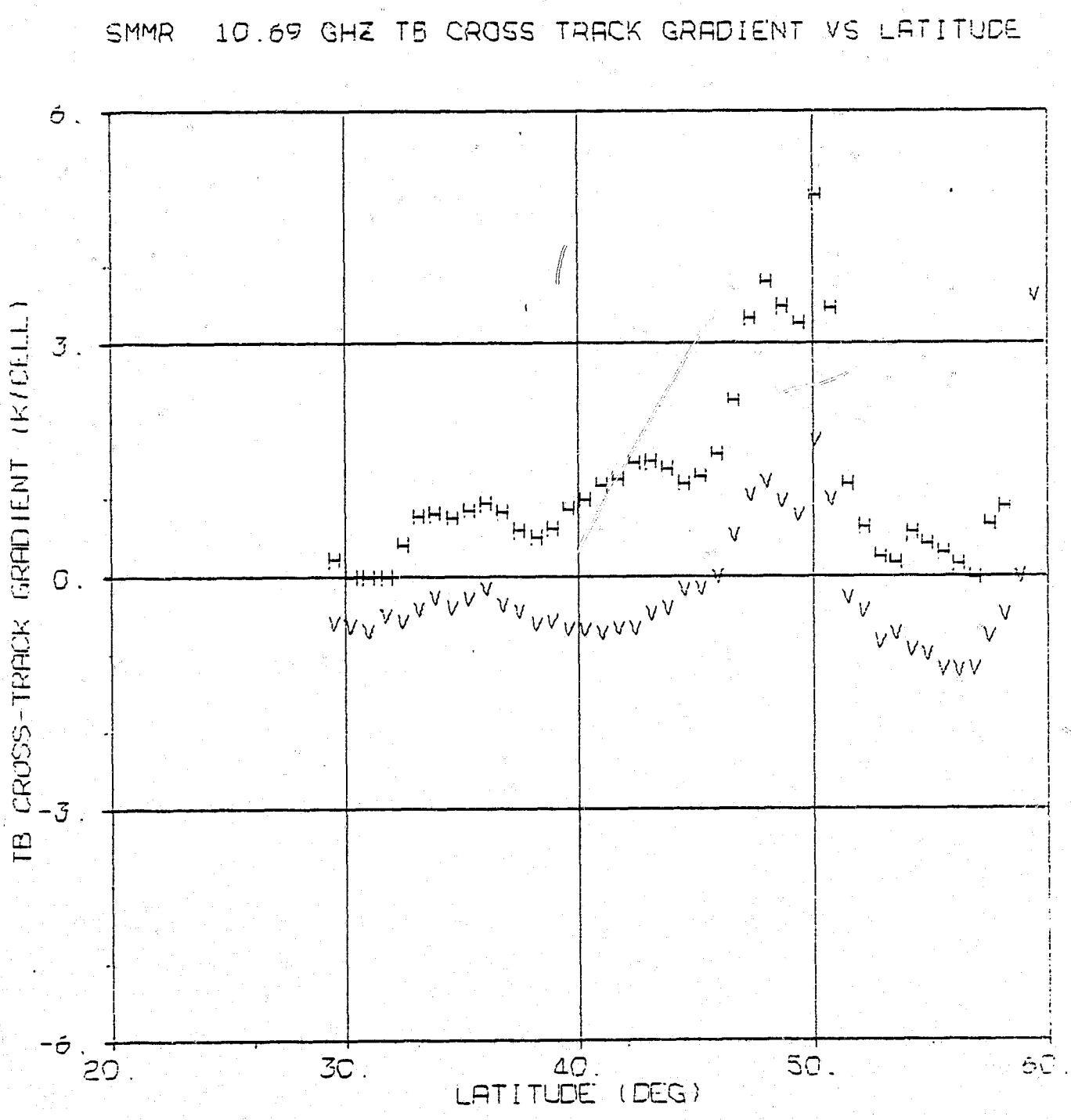

Orbit 1178

Figure 8.3. Cross Mode

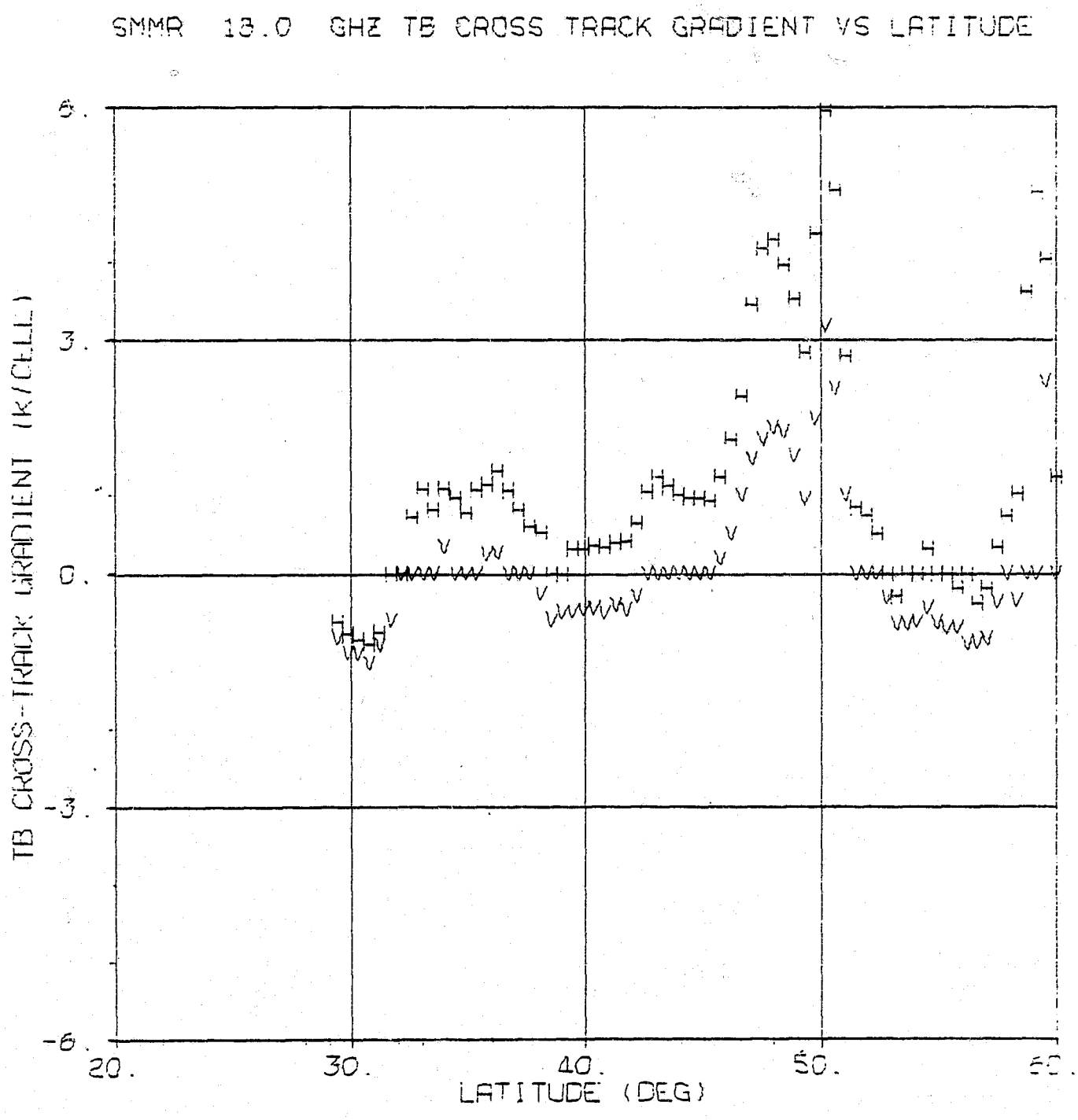

Orbit 1178

Figure 8.4. Cross Mode

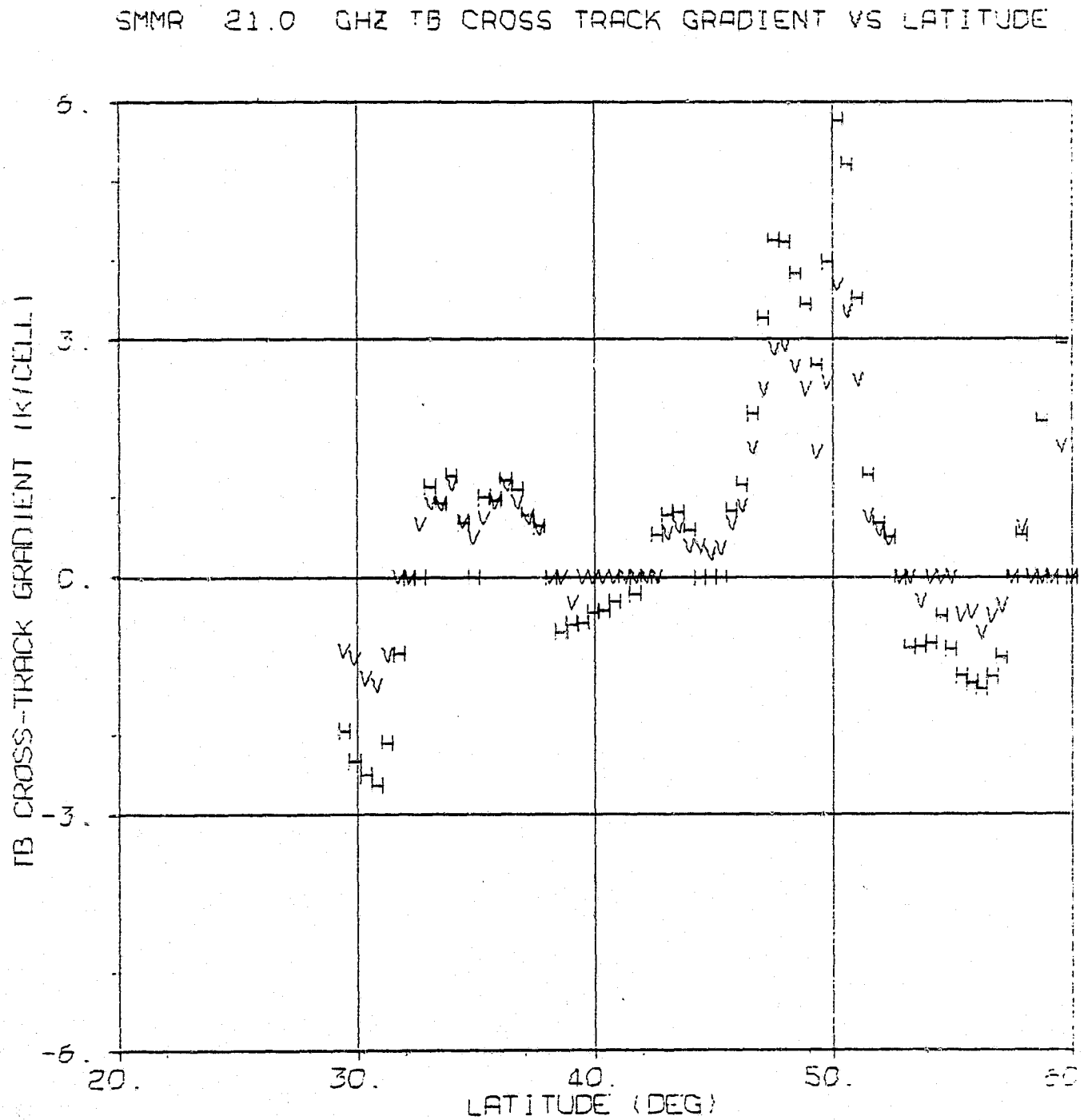

Orbit 1178

Figure 8.5. Cross Mode

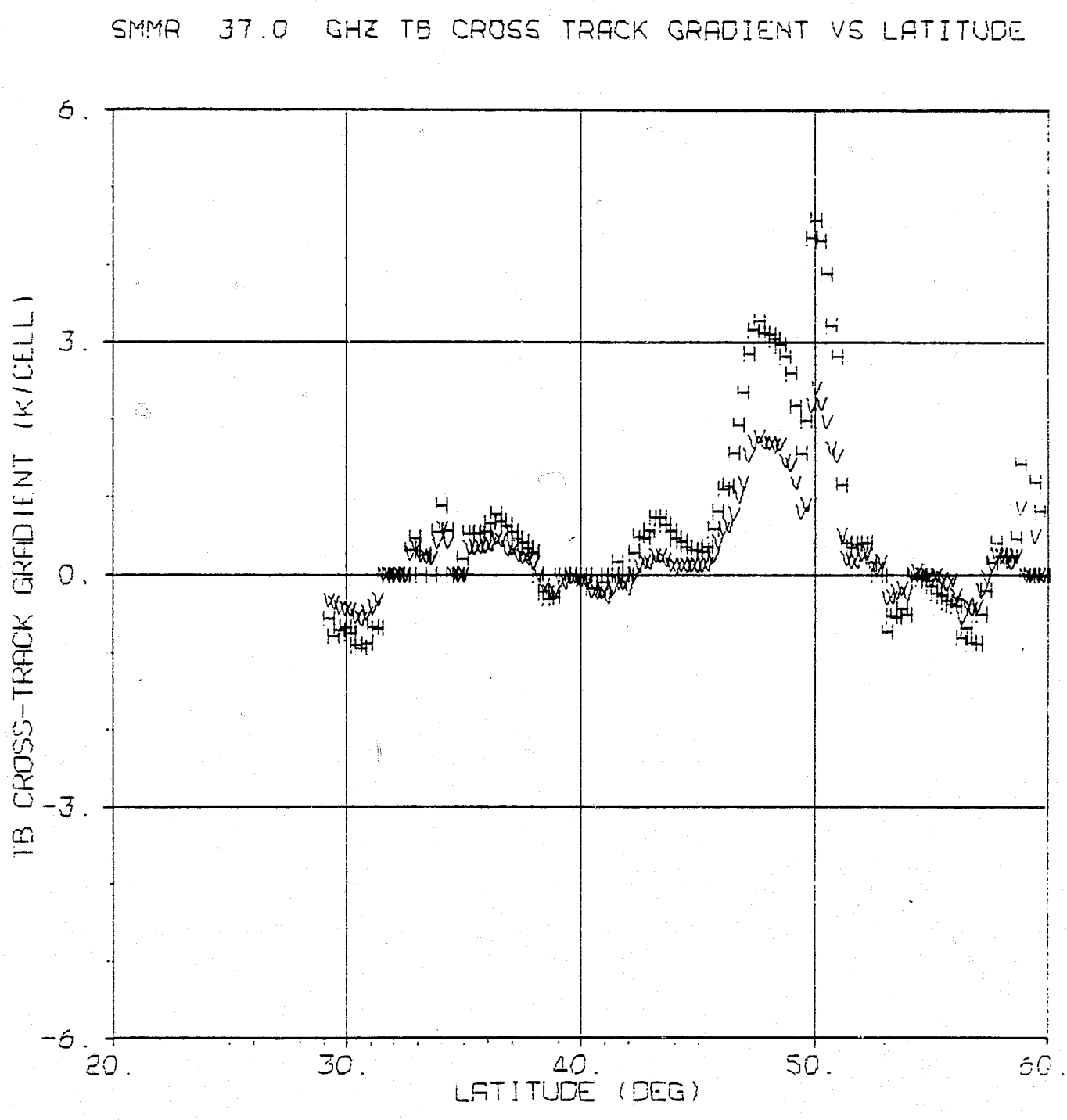

Orbit 1178

C-2

Figure 9.1. Nominal Mode

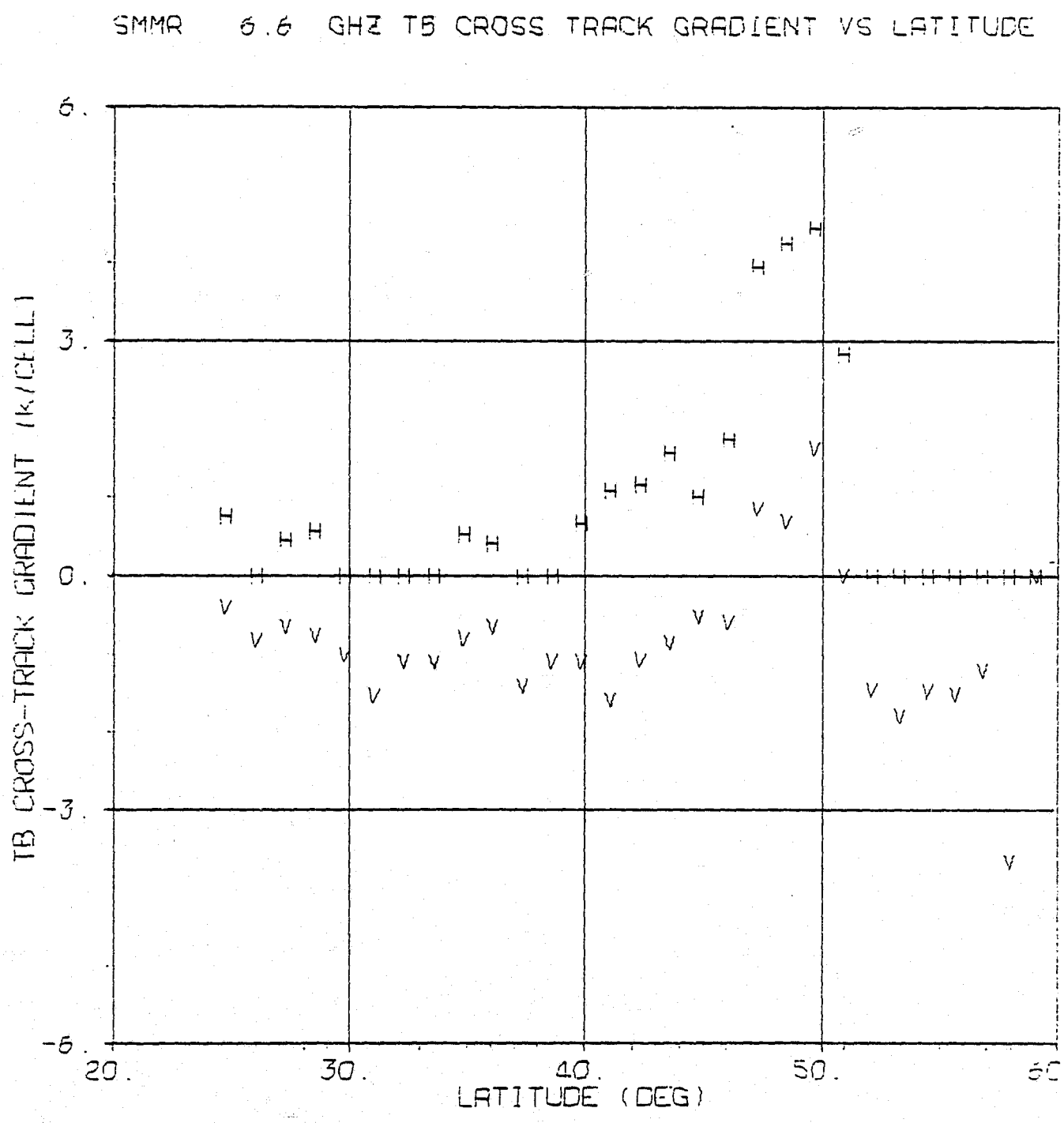

Orbit 1178

Figure 9.2. Nominal Mode

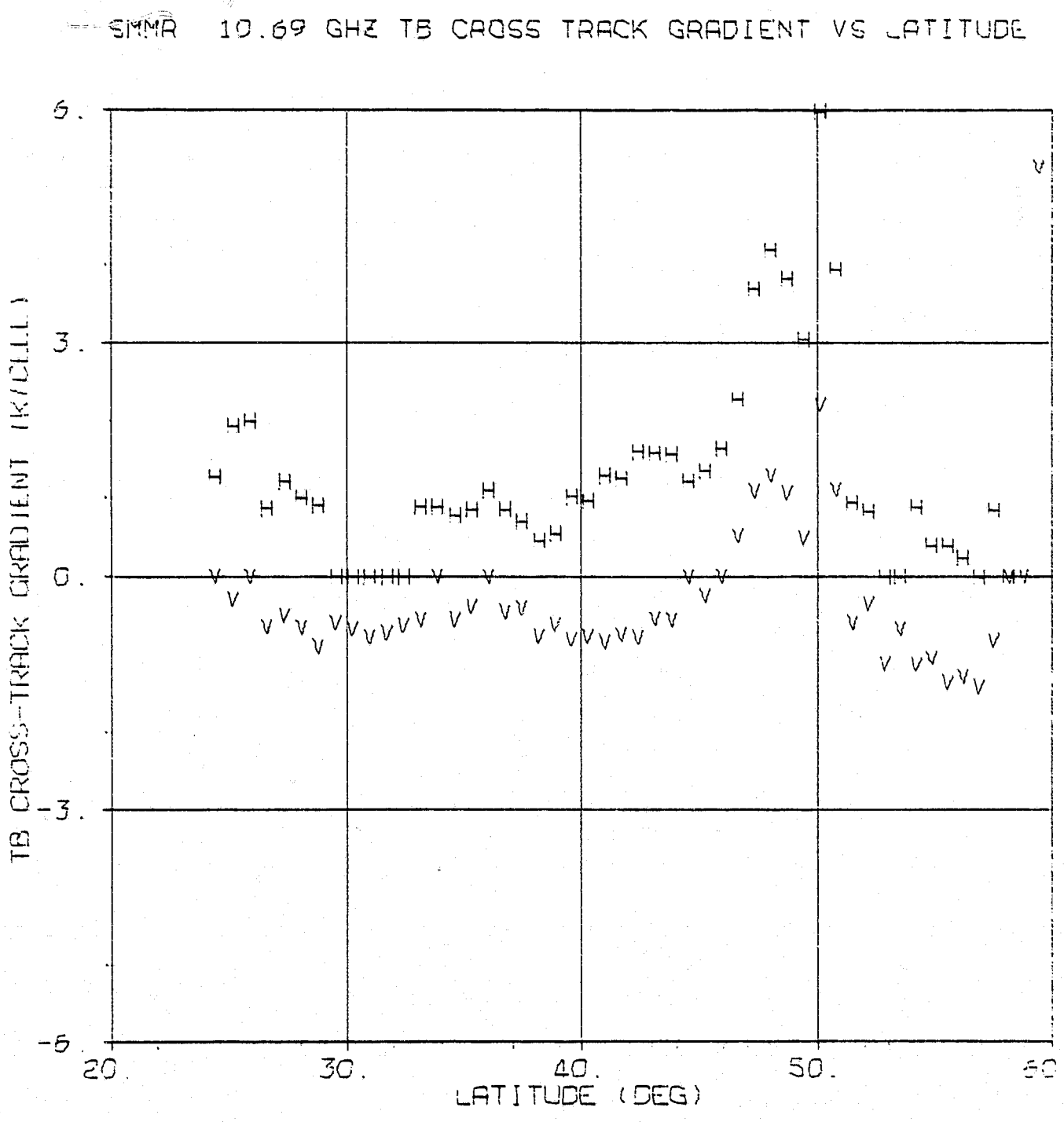

Orbit 1178

Figure 9.3. Nominal Mode

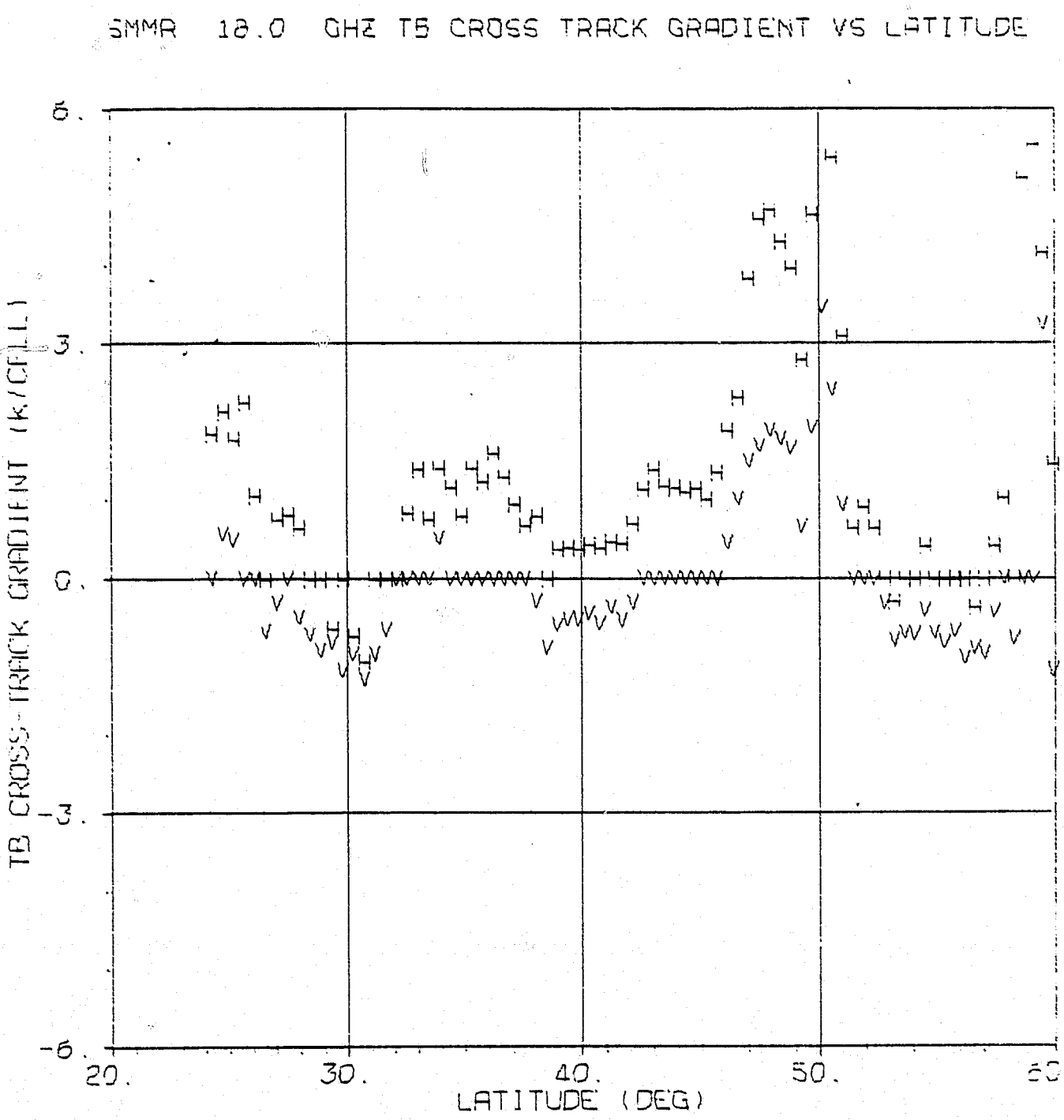

Orbit 1178

Figure 9.4. Nominal Mode

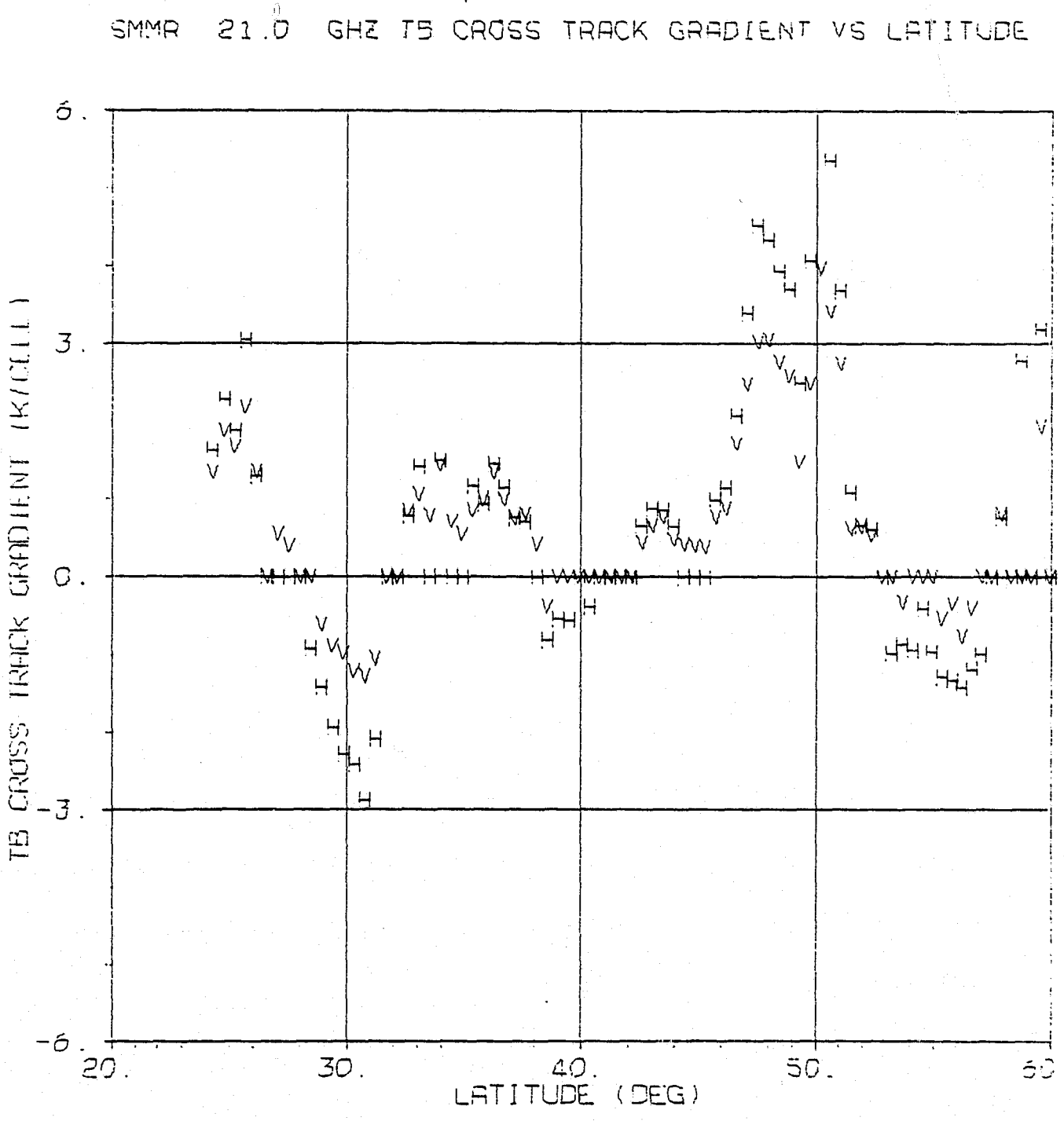

Orbit 1178

Figure 9.5. Nominal Mode

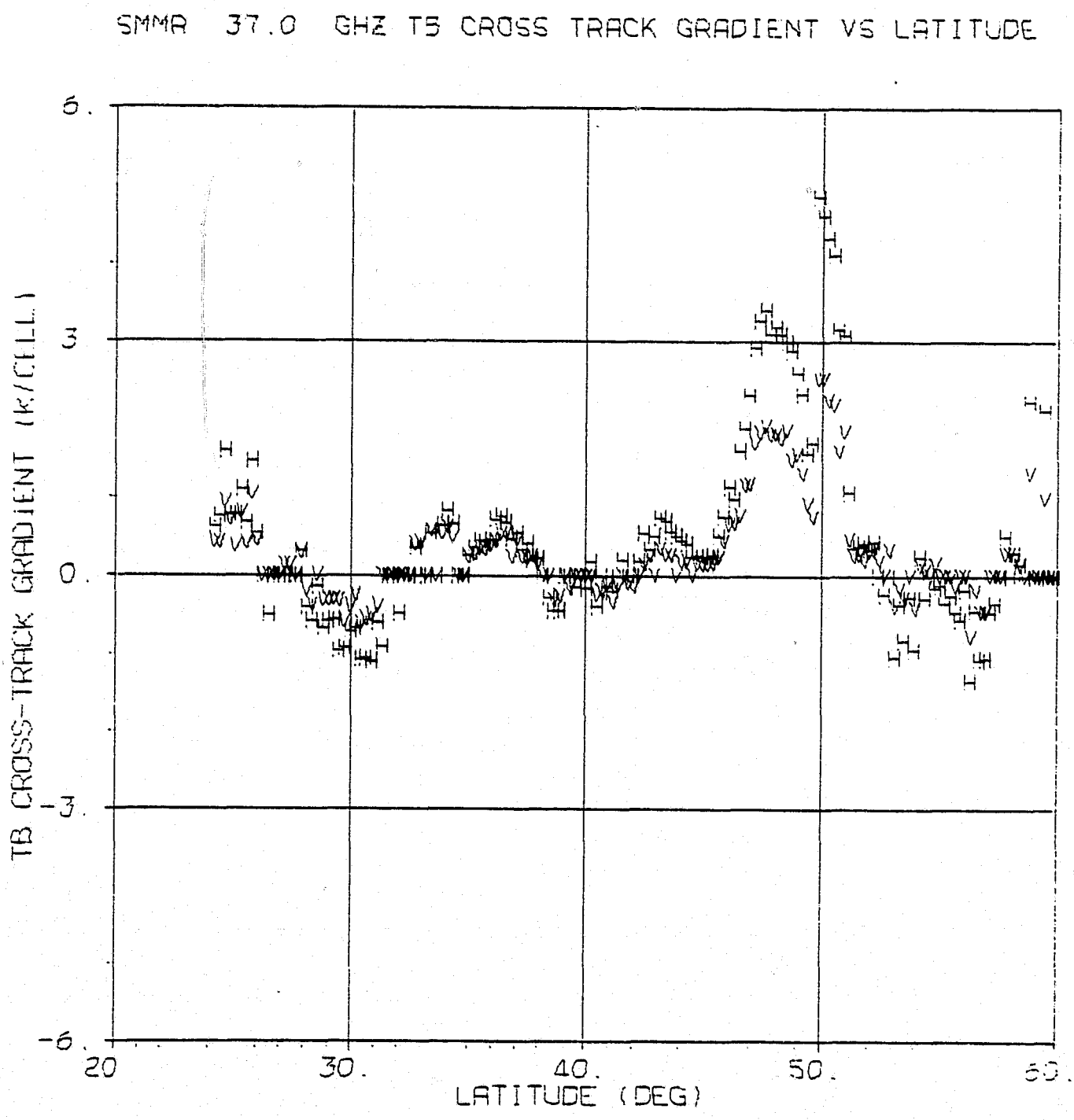

Orbit 1178

Table 3. Cross-Track Gradients for Interim, Cross, and Nominal Modes

1. Orbit 1178, 25°N to 45°N

	Mean Slope (K/cell)			Mean Slope Differences (K/cell)	
Channel	Interim	Cross	Nominal	Cross - Interim	Nominal - Interim
6.6 V	-0.224	-0.670	-0.984	-0.446	-0.760
6.6 H	0.297	0.231	0.480	-0.066	0.183
10.7 V	0.062	-0.510	-0.532	-0.572	-0.594
10.7 H	0.168	0.782	0.924	0.614	0.756
18 V	0.046	-0.264	-0.274	-0.310	-0.320
18 H	0.202	0.491	0.737	0.289	0.535
21 V	0.157	0.178	0.378	0.021	0.221
21 H	0.189	-0.094	0.144	-0.283	-0.045
37 V	0.027	0.019	0.083	-0.008	0.056
37 H	0.136	0.113	0.106	-0.023	-0.030

2. Orbit 1212, 20°N to 40°N

	Mean Slope (K/cell)			Mean Slope Differences (K/cell)	
Channel	Interim	Cross	Nominal	Cross - Interim	Nominal - Interim
6.6 V	0.492	-0.416	-1.306	-0.908	-1.798
6.6 H	1.704	1.125	0.482	-0.579	-1.222
10.7 V	0.141	-0.238	-0.400	-0.379	-0.541
10.7 H	0.124	0.386	0.258	0.262	0.134
18 V	-0.206	-0.615	-0.609	-0.409	-0.403
18 H	-0.401	0.013	0.088	0.414	0.313
21 V	-0.754	-0.742	-0.749	0.012	0.005
21 H	-1.311	-1.467	-1.554	-0.156	-0.243
37 V	-0.085	-0.084	0.006	0.001	0.091
37 H	-0.210	-0.177	-0.117	0.033	0.093

Table 4. Cross-Track Gradient Differences Averaged Together for Orbits 1178 and 1212

	Average Mean Slope Differences (K/cell)		Average Total Variation Differences (K)*	
Channel	Cross - Interim	Nominal - Interim	Cross - Interim	Nominal - Interim
6.6 V	-0.677	-1.279	-2.71	-5.12
6.6 H	-0.323	-0.520	-1.29	-2.08
10.7 V	-0.476	-0.568	-3.33	-3.98
10.7 H	0.438	0.445	3.07	3.12
18 V	-0.360	-0.362	-3.96	-3.98
18 H	0.352	0.424	3.87	4.66
21 V	0.017	0.113	0.19	1.24
21 H	-0.220	-0.144	-2.42	-1.58
37 V	-0.004	0.074	-0.09	1.63
37 H	0.005	0.032	0.11	0.70

*These are the mean slope differences multiplied by the appropriate number of cells per grid row, yielding differences in total variation across the swath.

Table 5. Cross-Track Gradients for Simulated Data

1. Nominal Mode, using Gaussian antenna pattern approximation.

Channel	Correlation (R^2)	Intercept (K)	Slope (K/cell)	Total Variation (K)*
6.6 V	0.86	155.41	-0.93	-3.72
6.6 H	0.82	82.36	0.87	3.48
10.7 V	0.51	158.45	-0.43	-3.01
10.7 H	0.58	85.74	0.55	3.85
18 V	0.79	178.58	-0.72	-7.92
18 H	0.73	105.35	0.88	9.68
21 V	0.00	198.76	0.04	0.44
21 H	0.02	142.84	0.13	1.43
37 V	0.54	199.95	0.08	1.76
37 H	0.37	139.10	0.10	2.20

2. Interim Mode

Channel	Correlation (R^2)	Intercept (K)	Slope (K/cell)	Total Variation (K)*
6.6 V	0.96	154.16	-0.24	-0.96
6.6 H	1.00	82.94	0.60	2.40
10.7 V	0.74	158.24	0.03	0.21
10.7 H	0.89	89.62	0.03	0.21
18 V	0.99	176.91	-0.11	-1.21
18 H	0.99	113.09	0.09	0.99
21 V	0.95	200.22	-0.04	-0.44
21 H	1.00	148.55	0.11	1.21
37 V	1.00	202.58	0.05	1.10
37 H	0.99	142.83	0.02	0.44

*These are the slopes multiplied by the appropriate number of cells per grid row, yielding total variations across the swath.

Table 6. Simulation and Spacecraft Gradient Differences

Frequency	Spacecraft Data			Simulation
	Mean V Slope (K/cell)	Mean H Slope (K/cell)	H Slope - V Slope (K/cell)	H Slope - V Slope (K/cell)
6.6	-1.15	0.48	1.63	1.80
10.7	-0.47	0.59	1.06	0.98
18	-0.44	0.32	0.76	1.60
21	-0.19	-0.71	-0.52	0.09
37	0.04	-0.01	-0.05	0.02

Notes:

1. Spacecraft data entries are nominal mode values averaged together for orbits 1178 and 1212.
2. Simulation data entries are for the nominal mode, using Gaussian antenna pattern approximation.

Table 7. Refinement of cosβ Estimates

Channel	Initial Values	Faraday Update	Final Values	cosβ 1σ Uncertainty	T_B Cross-Track Variation 1σ Uncertainty (°K)
6.6 V	0.03	-0.06	-0.04	0.02	0.4
6.6 H	0.21	0.24	0.23	0.02	0.4
10.7 V	0.06	0.06	0.06	0.02	0.4
10.7 H	0.04	0.04	0.03	0.02	0.4
18 V	-0.23	-0.23	-0.24	0.06	0.7
18 H	0.23	0.23	0.21	0.06	0.7
21 V	-0.05	-0.05	-0.10	0.08	0.9
21 H	0.31	0.31	0.33	0.07	0.8
37 V	0.19	0.19	0.09	0.03	0.4
37 H	0.16	0.16	0.08	0.03	0.4

Figure 10.1. Before cos β Correction

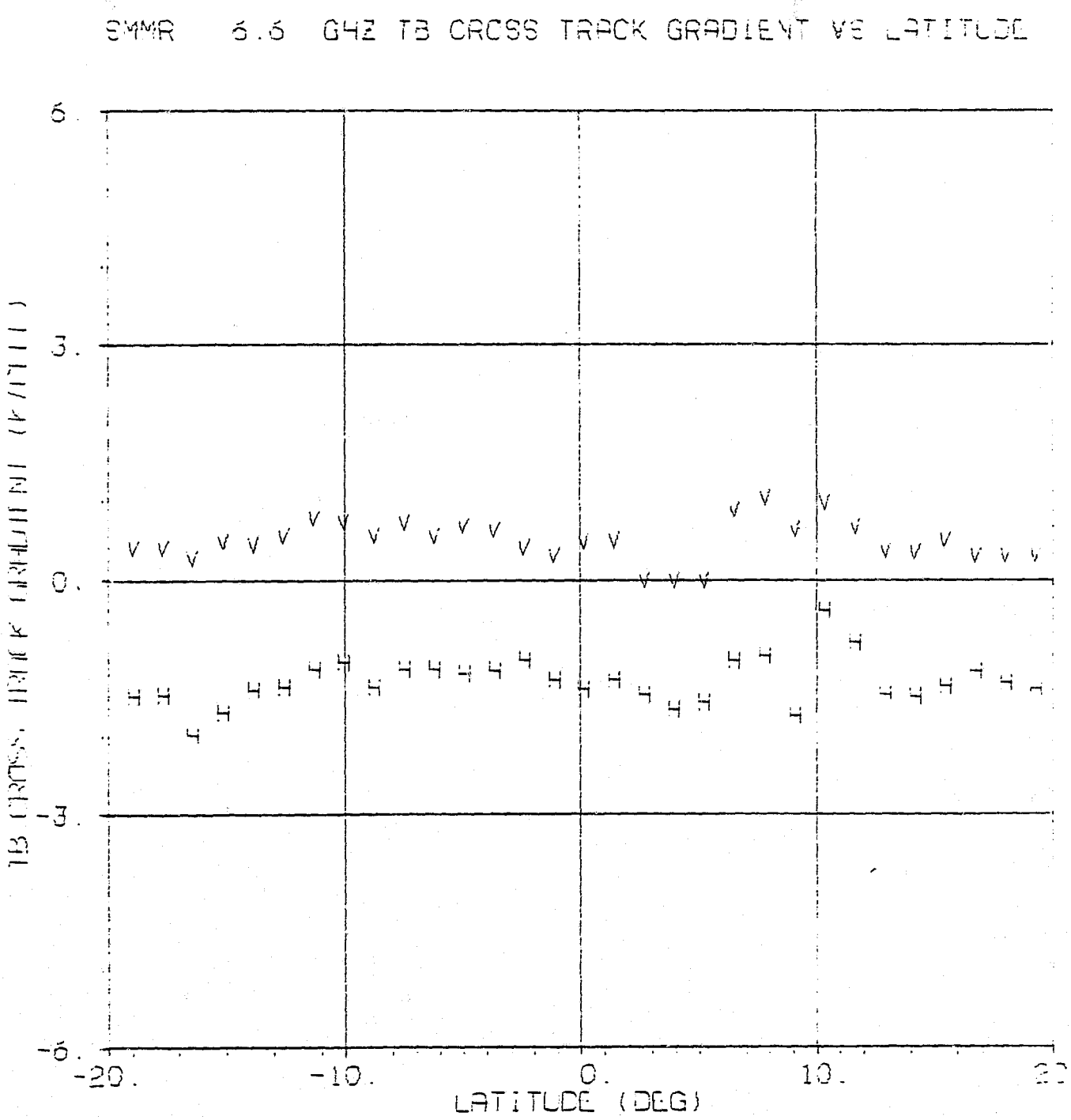

Orbit 1463, Interim Mode

Figure 10.2. Before cos β Correction,

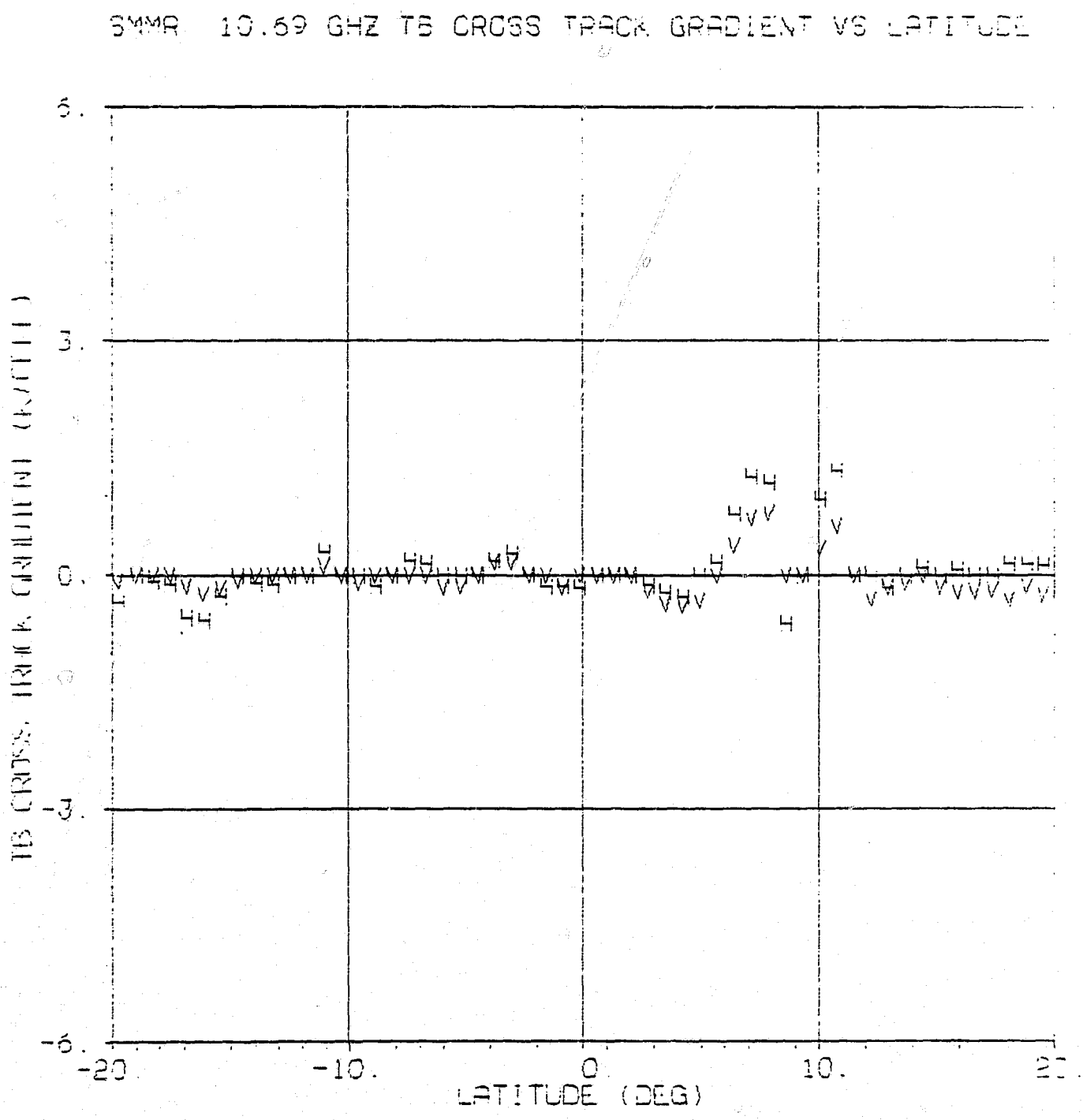

Orbit 1463, Interim Mode

Figure 10.3. Before cos β Correction,

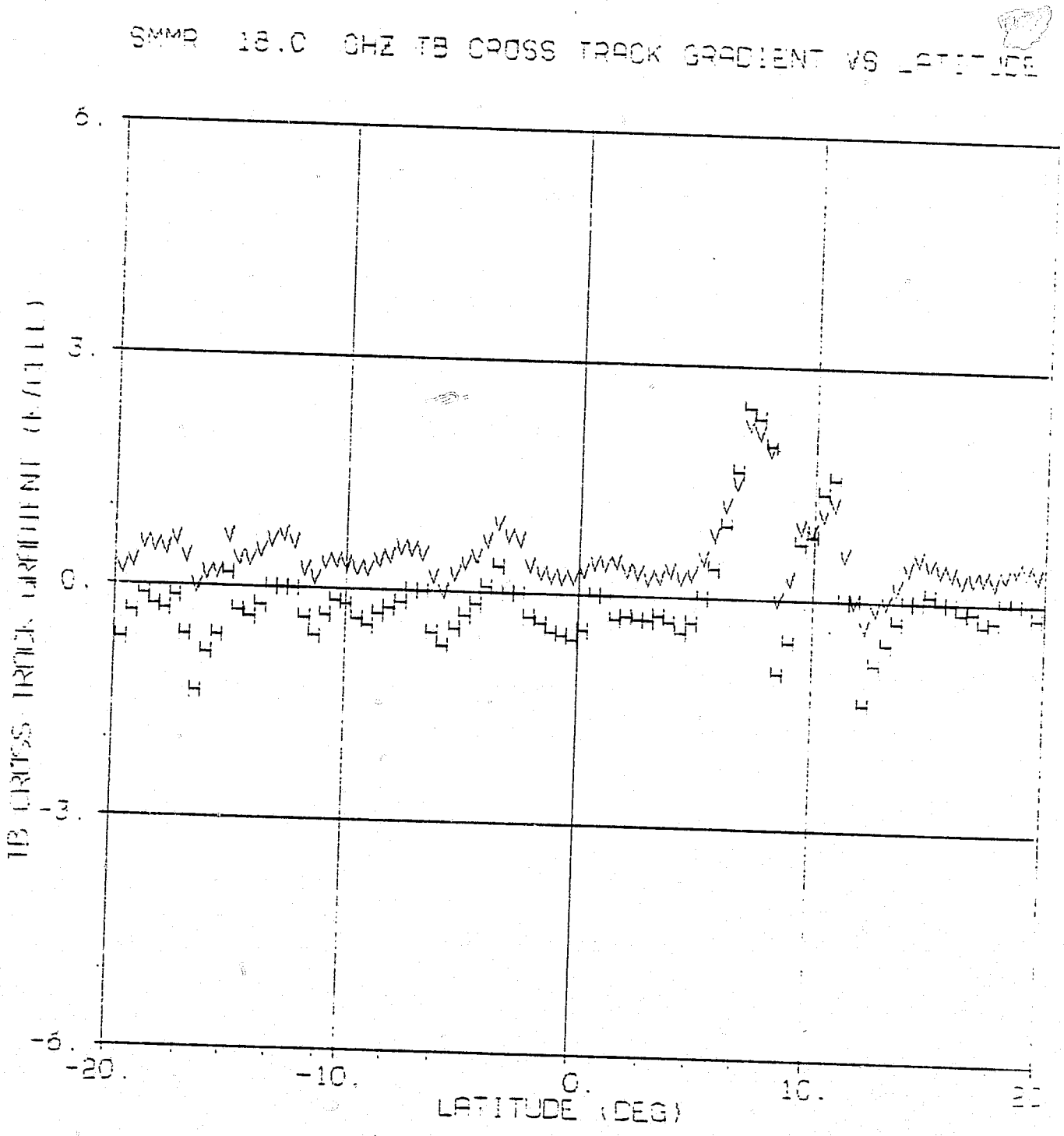

Orbit 1463, Interim Mode

Figure 10.4. Before cos β Correction,

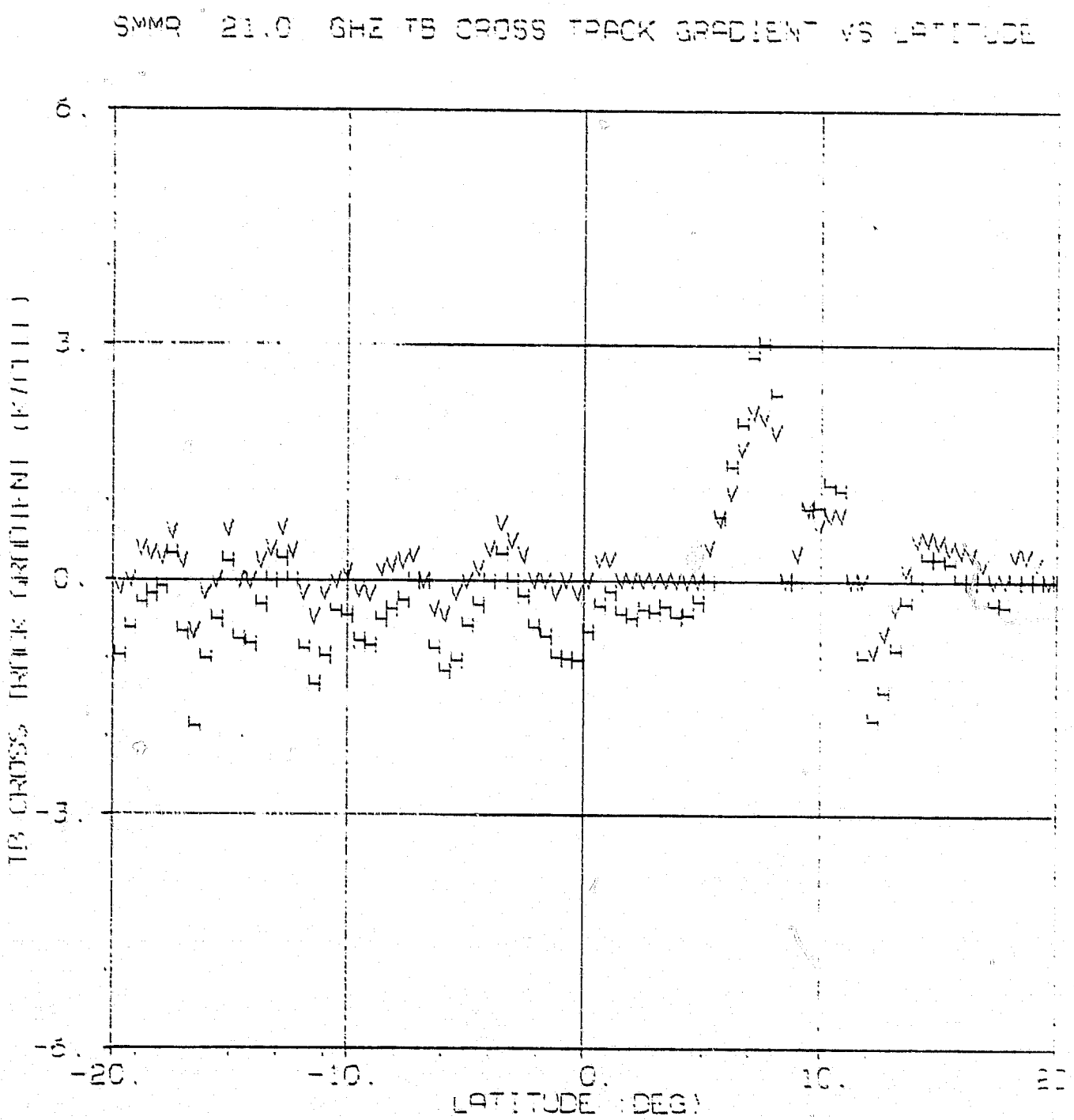

Orbit 1463, Interim Mode

Figure 10.5. Before cos β Correction,

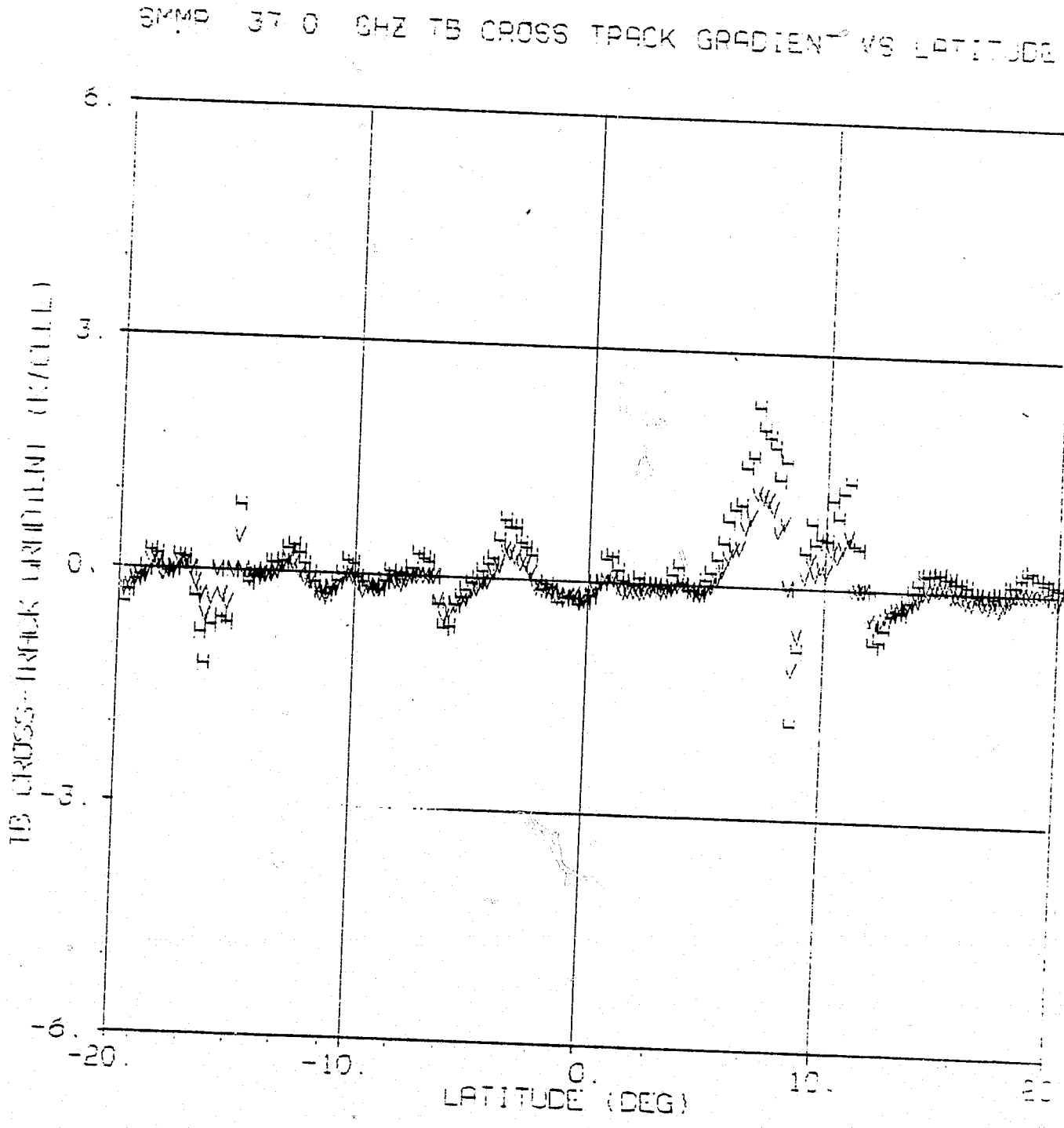

Orbit 1463, Interim Mode

Figure 11.1. After cos β Correction,

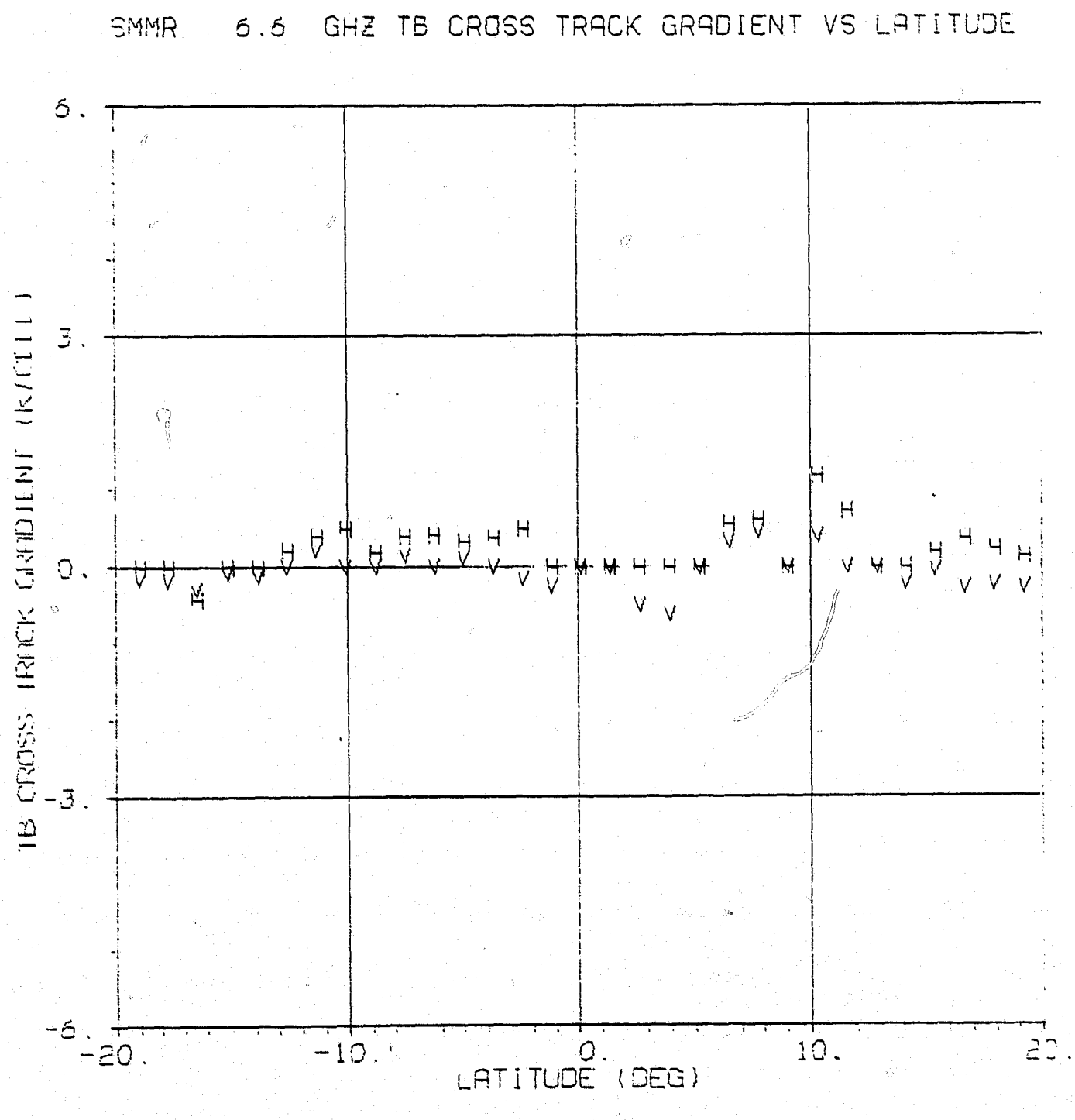

Orbit 1463, Interim Mode

Figure 11.2. After cos β Correction,

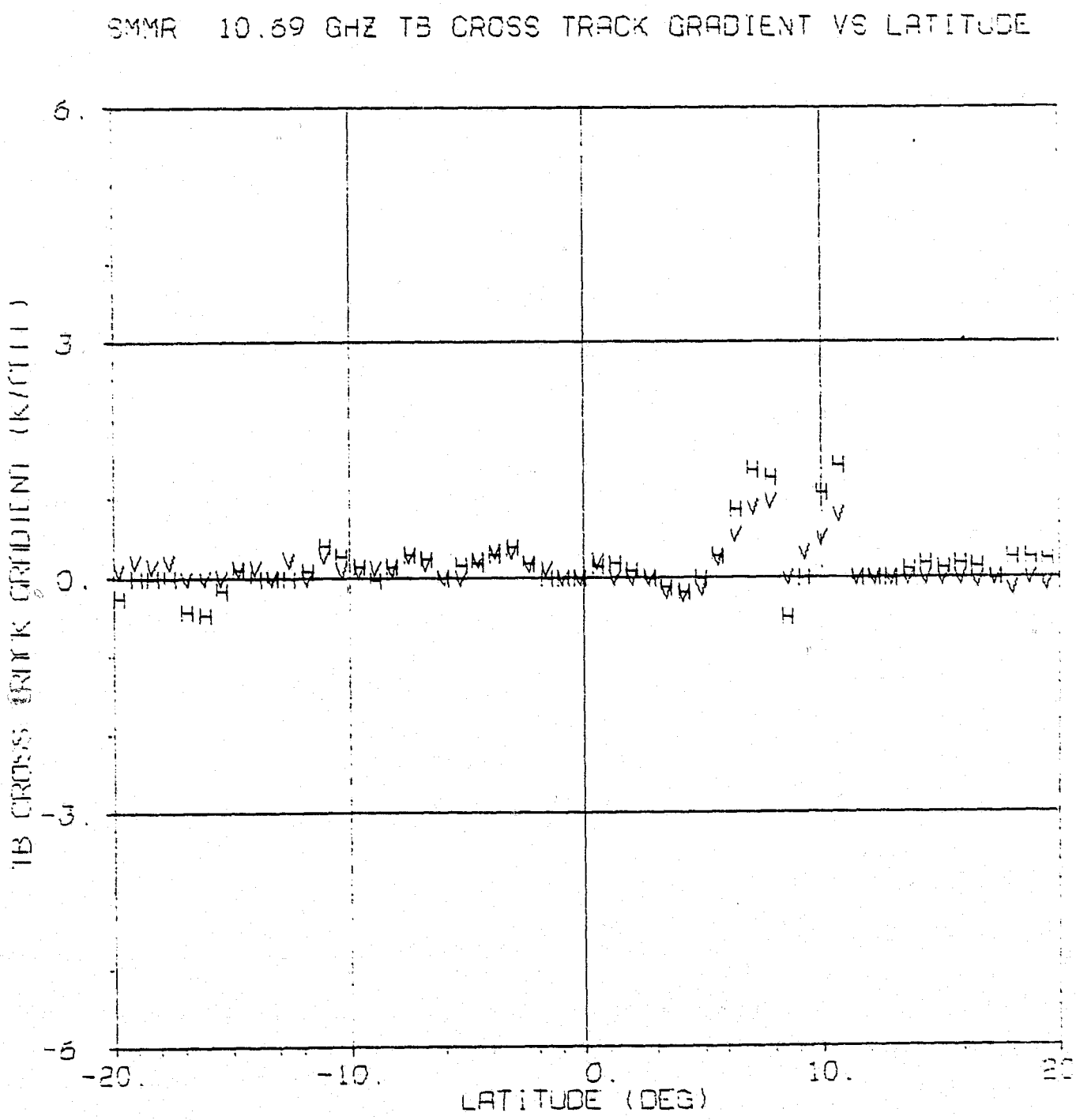

Orbit 1463, Interim Mode

Figure 11.3. After cos β Correction,

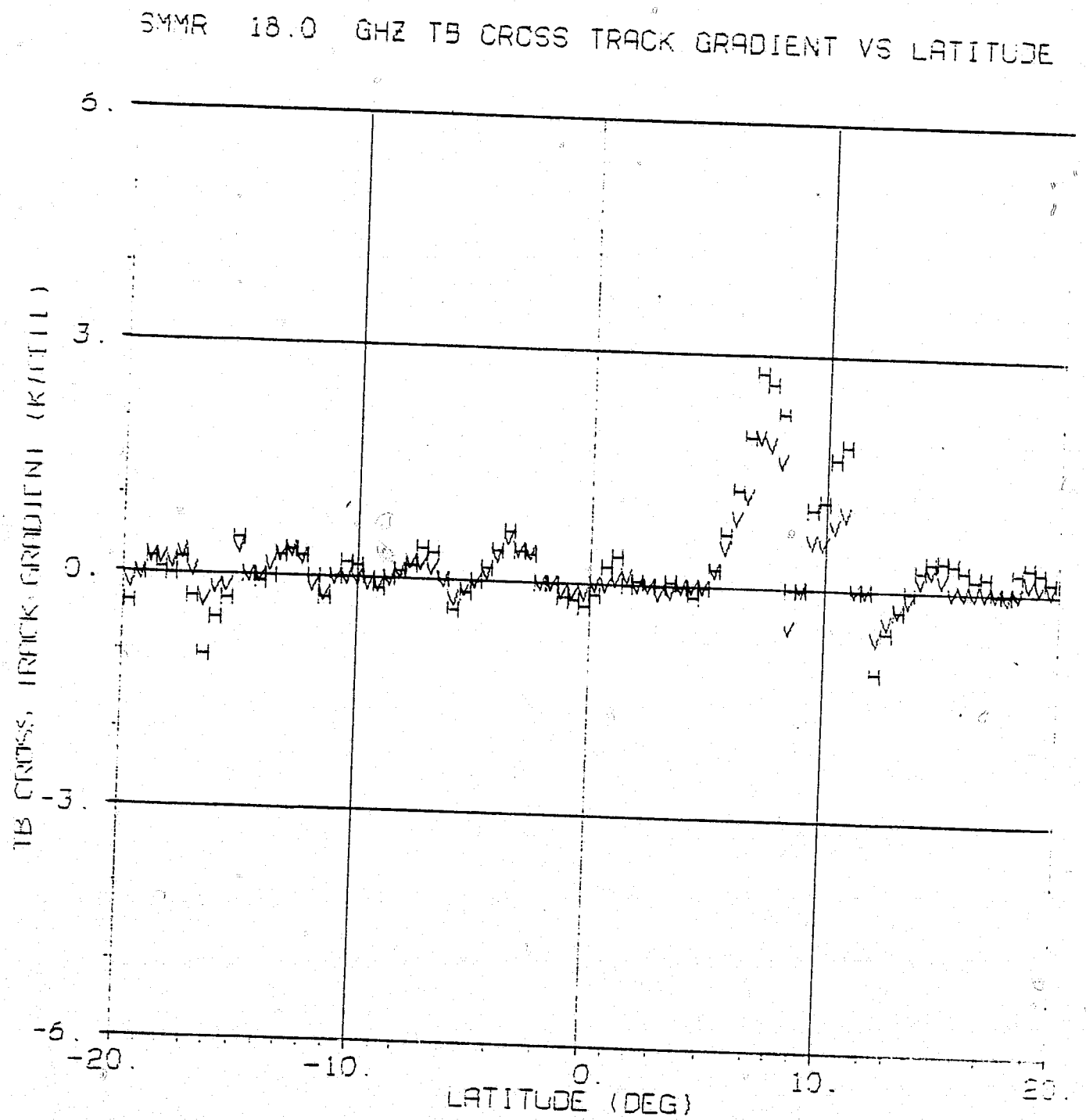

Orbit 1463, Interim Mode

Figure 11.4. After cos β Correction,

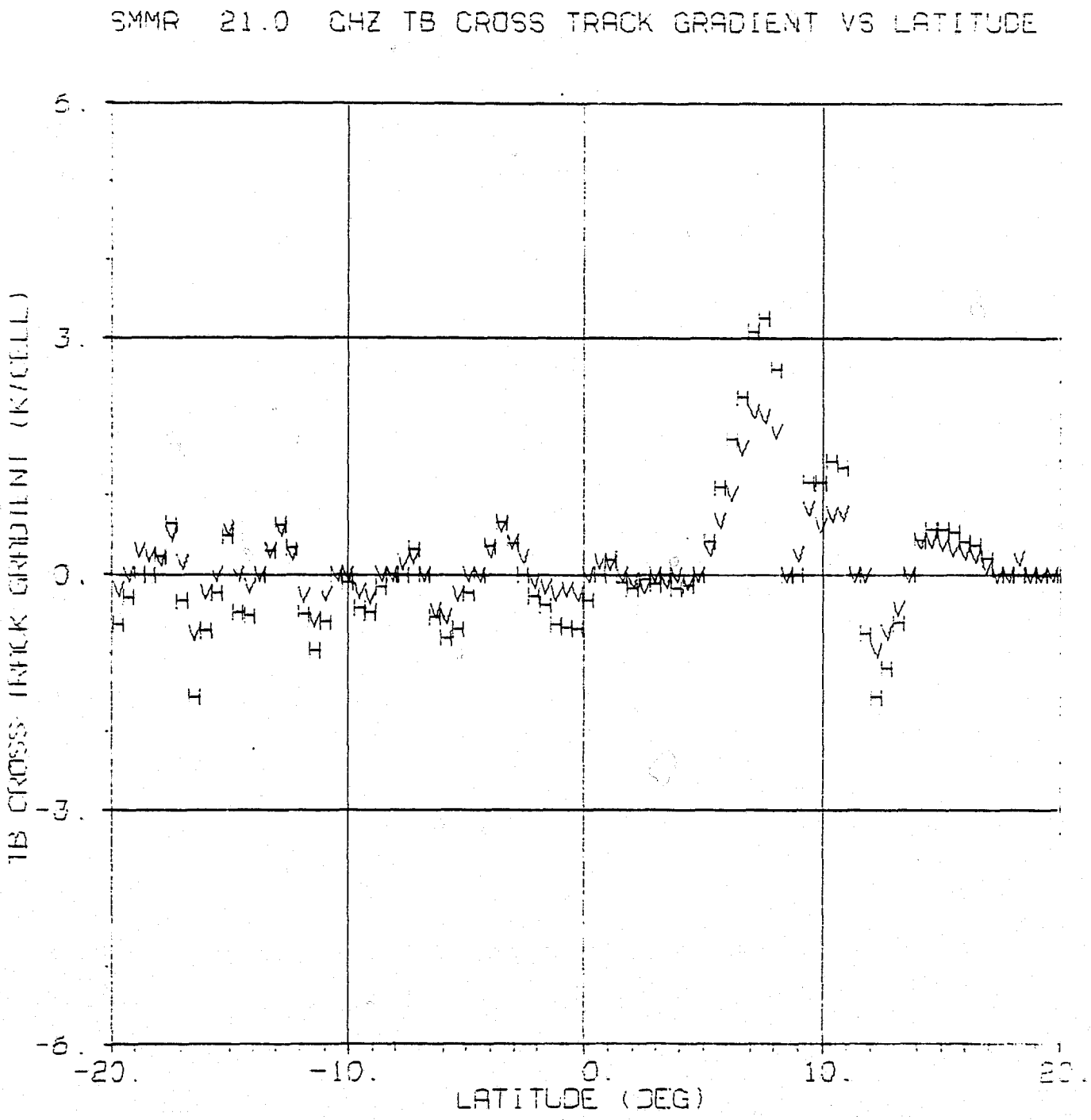

Orbit 1463, Interim Mode

Figure 11.5. After cos β Correction,

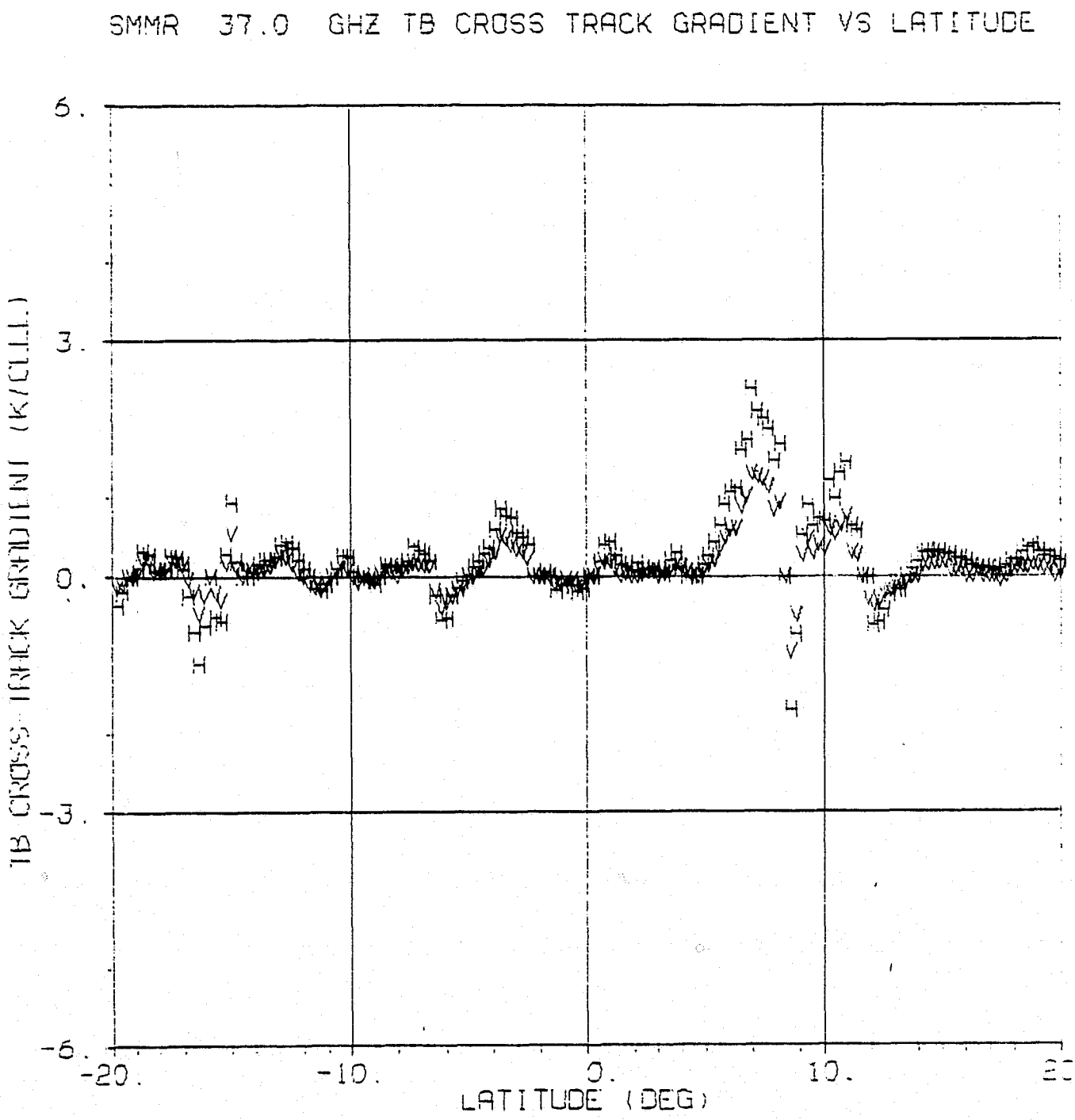

Orbit 1463, Interim Mode

Table 8.1. Mean Clear Weather SMMR Brightness Temperatures

Channel	-5° to 5°	5° to 15°	20° to 30°	30° to 40°	40° to 50°	50° to 60°	Land
6.6 V	155	155	152	150	147	144	250
6.6 H	87	88	88	86	86	84	245
10.7 V	158	159	159	157	157	154	257
10.7 H	93	93	93	92	92	92	257
18 V	169	169	165	160	160	160	257
18 H	112	112	110	108	108	107	257
21 V	195	195	188	182	182	177	257
21 H	150	150	145	140	140	137	257
37 V	200	200	197	193	193	190	257
37 H	150	150	144	138	138	135	257

Notes:

1. Column headings refer to latitude ranges given in degrees north of the equator.
2. Table entries are in degrees Kelvin, and are interim mode measurements.
3. Land entries were measured for mainland Alaska.

Table 8.2. World Brightness Temperature Map Values

Channel	0°	10°	25°	35°	45°	55°	Land
6.6 V	157	156	154	151	148	145	260
6.6 H	88	87	85	84	82	80	260
10.7 V	164	163	159	156	153	149	260
10.7 H	96	94	91	88	86	84	260
18 V	192	188	179	173	166	161	265
18 H	134	128	117	109	102	96	265
21 V	228	220	205	194	184	174	265
21 H	190	177	156	141	127	116	265
37 V	219	215	206	199	192	186	275
37 H	167	160	148	138	130	123	275

Notes:

1. Column headings refer to north latitudes.
2. Table entries are in degrees Kelvin.

Table 8.3. World T_B Map Minus SMMR Clear Weather T_B Values

Channel	0°	10°	25°	35°	45°	55°	Land
6.6 V	2	1	2	1	1	1	10
6.6 H	1	-1	-3	-2	-4	-4	15
10.7 V	6	4	0	-1	-4	-5	3
10.7 H	3	1	-2	-4	-6	-8	3
18 V	23	19	14	13	6	1	8
18 H	22	16	7	1	-6	-11	8
21 V	33	25	17	12	2	-3	8
21 H	40	27	11	1	-13	-21	8
37 V	19	15	9	6	-1	-4	18
37 H	17	10	4	0	-8	-12	18

Notes:

1. Column headings refer to north latitudes.
2. Table entries are in degrees Kelvin.
3. Land entries were measured for mainland Alaska.

Table 9. SMMR T_B Variations Due to Weather

Channel	Variation (°K)*
6.6 V	8
6.6 H	8
10.7 V	15
10.7 H	25
18 V	40
18 H	65
21 V	50
21 H	75
37 V	55
37 H	100

*These variations from baseline ocean values were measured for interim mode APC output from 45°N of orbit 1212.